



Republic of Iraq

Ministry of Higher Education & Scientific Research

University of Kerbala

College of Engineering

Civil Engineering Department

Behavior of Concrete Filled Double Web Steel Beams

A Thesis Submitted to the Council of the Faculty of the College of the Engineering/University Of Kerbala in Partial Fulfillment of the Requirements for the Master Degree in Civil Engineering

Abbas Jalal Kaishesh

(B. Sc. in Civil Engineering-2019)

Supervised By:

Prof. Dr. Sadjad Amir Hemzah

Assist prof. Dr. Bahaa Hussain Mohammed

February 2023

Rajab 1444

بِسْمِ اللَّهِ الرَّحْمَنِ الرَّحِيمِ
(قَالُوا سُبْحَانَكَ لَا عِلْمَ لَنَا إِلَّا مَا عَلَّمْتَنَا
إِنَّكَ أَنْتَ الْعَلِيمُ الْحَكِيمُ)

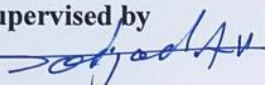
صَدَقَ اللَّهُ الْعَلِيُّ الْعَظِيمُ

(البقرة - 32)

Examination committee certification

We certify that we had read the thesis entitled "**Behavior of Concrete Filled Double Web Steel Beams** " and as an examining committee, we examined the student "**Abbas Jalal kaishesh**" in its content and in what is connected with it and that in our opinion it is adequate as a thesis for the degree of Master of Science in Civil Engineering.

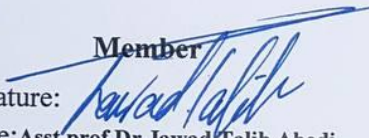
Supervised by

Signature: 
Name: Prof. Dr. Sadjad Amir Hemzah
Date: / / 2023

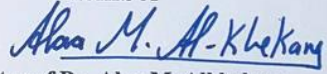
Supervised by

Signature: 
Name: Assist Prof. Dr. Bahaa Hussain Mohammed
Date: / / 2023

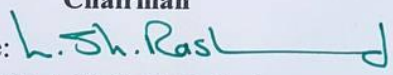
Member

Signature: 
Name: Asst. prof. Dr. Jawad Talib Abodi
Date: / / 2023

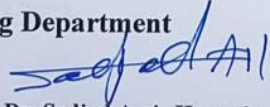
Member

Signature: 
Name: Asst. prof. Dr. Alaa M. Alkhekany
Date: / / 2023

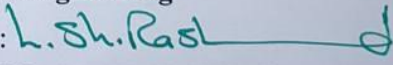
Chairman

Signature: 
Name: Prof. Dr. Laith Shakir Rasheed
Date: / / 2023

Approval of Head of Civil Engineering Department

Signature: 
Name : prof. Dr. Sadjad Amir Hemzah
Date: / / 2023

Approval of Deanery of the College of Engineering

Signature: 
Name: Prof. Dr. Laith Shakir Rasheed
Date: / / 2023


Supervisor Certificate

We certify that the thesis entitled “**Behavior of Concrete Filled Double Web Steel Beams**” was prepared by **Abbas Jalal Kaishesh** under our supervision at the Department of Civil Engineering, Faculty of Engineering, University of Kerbala as a partial of fulfilment of the requirements for the Degree of Master of Science in Civil Engineering.

Signature: 

Prof. Dr. Sadjad Amir Hemzah

Date: / / 2023

Signature: 

Assist Prof. Dr. Bahaa Hussain Mohammed

Date: / / 2023

اقرار المقوم اللغوي

أشهد أنني قد اطلعت على رسالة طالب الماجستير (عباس جلال كعيشيش)
الموسومة ب

Behavior of Steel Double Web Filled Steel Beams

وقد قومتها من الناحية اللغوية والاسلوبية وبذلك تكون صالحة لأغراض المناقشة مع
توصيتنا بالأخذ بنظر الاعتبار تصحيح بعض الملاحظات اللغوية المؤشر عليها
مع التقدير...



التوقيع:

اسم المقوم ولقبه العلمي : أ. م. ضياء جليل شايع

التخصص العام : اللغة الإنكليزية

التخصص الدقيق : الإرادة الإنكليزية

محل العمل : كلية التربية للعلوم الإنسانية

رقم الهاتف النقال : 07804647356

التاريخ : 13.12.2022

Abstract

The current study aims to investigate the structural behavior of a double web beam filled with different concrete made with a combination of Natural Aggregate (NA) and Recycled Concrete Aggregate (RCA). The aim is achieved by implementing experimental and numerical work.

The experimental work involves the manufacture of seven specimens tested under two concentrated and symmetrical loadings with identical properties (i.e., span length, cross-section, and boundary conditions). The thickness and width of the flange plates of the steel beams were 120 mm and 6 mm, respectively, while the thickness of the web plates was 3 mm and depth 188mm. All beam samples had 1100 mm effective span length. The specimens are classified into two groups, in addition to one beam without concrete as a control beam. The first group included three beams filled with normal concrete (the first one filled in middle region, the second beams filled with two side, the third beams filled full region), while the second group contained three double-web beams which were discussed location filled in first group but only different filled with recycled aggregate concrete. The studied parameters were the type and locations of concrete in a double web steel beam.

The experimental result for the first group of specimens revealed that the filled normal concrete in the web zone caused an increase in the ultimate load by (10.19 % to 55.30 %). Further, The max increase was in the ductility index of the specimen (double web steel fully filled normal concrete) around 568% and increase in their stiffness from (2.6 % to 39 %) if compared with the control beam. While the second group of specimens that filled recycled concrete in the web zone caused an increase in the ultimate load by (9.52 % to 42.03 %) .In addition to the max increase in the ductility index of the

specimen (double web steel fully filled recycled concrete) were increased about (380 %) and also increase in their stiffness from (4.5% to 8.03 %) if compared with the control beam.

The numerical work involved using a model non-linear finite element analysis by ABAQUS (2021) software package to conduct the numerical investigation of a double web filled with different types of concrete normal and recycled. There was a good convergence between the experimental and numerical results regarding the ultimate load, maximum deflection, load-deflection curves, and failure mode. The average difference in the ultimate load and the maximum deflection was found to be equal to 5.50 % and 7.90 %, respectively, ensuring the numerical work validity. Two parametric studies of various variables also numerically examined (the effect of concrete compressive strength and steel yield stress). As a result of the parametric studies the increase yield stress for control beam was 310 MPa and 350 MPa, the increase was 5.5 % and 11.11 %, respectively. And the increase compressive strength for beam filled with normal concrete in the sides was 25 MPa and 20 MPa, the increase was 10.33 % and 4.21 %, respectively, if compared with the control beam.

Undertaking

I certify that research work titled “**Behavior of Concrete Filled Double Web Steel Beams**” is my own work. The work has not been presented elsewhere for assessment. Where material has been used from other sources it has been properly acknowledged / referred.

Signature:

Abbas Jalal Kaishesh

Date: / / 2023

Dedication

To the soul of my father who taught me the life meaning

To my mother, the most precious person in my life

To my brothers.

For their endless love,

support and encouragement.

Signature:

Abbas Jalal Kaishesh

Date: / / 2023

Acknowledgements

In the name of ALLAH, the most compassionate the most merciful. Praise be to ALLAH and pray, and peace be on his prophet Mohammed his relatives and companions, and on all those who follow him.

I would like to express my sincere appreciation and deepest gratitude to **Prof. Dr. Sadjad Amir Hemzah** and **Assist Prof. Dr. Bahaa Hussain Mohammed**, whom I had the excellent luck and the honor of being under their supervision, for their continuous encouragement and invaluable guidance throughout this thesis.

Great thanks to University of Kerbala, especially those people who works in Civil Engineering Department, from Deans, Heads, Lecturers, and the staff of the Laboratories at the College of Engineering/University of Kerbala.

I would also like to thank my family, to whom I owe gratitude and appreciation that could never be repaid. Thank you for all the sacrifices you have made and for the support you have constantly given.

Finally, special thanks would be awarded to all friends for their continuous help and encouragement to me, especially my friends Eng. Sajjad Firas, Eng. Ali Fadll Allah ,Eng.Ali Ahmed, Eng. Ali Naser, Eng. Ahmed Wafi and Eng. Assam Yousif.

Signature:

Abbas Jalal Kaishesh

Date: / / 2023

Table of Contents

Examination Committee Certification.....	Error! Bookmark not defined.
Supervisor Certificate	Error! Bookmark not defined.
Linguistic Certificate	Error! Bookmark not defined.
Abstract.....	IV
Undertaking	VI
Dedication.....	VII
Acknowledgements.....	VIII
Table of Contents.....	IX
List of Tables	XIII
List of Figures.....	XV
List of Abbreviations	XIX
List of Symbols.....	XX
Chapter One. INTRODUCTION.....	1
1.1. General.....	2
1.2. Composite Action of Concrete-Filled Steel Tube (CFST).....	3
1.3. Advantages and Disadvantages of Concrete-Filled Steel Tube Beams ..	4
1.4. Failure Modes of CFST Beam under Bending.....	5
1.5. Recycled Concrete Aggregate (RCA)	6
1.6. Classification and Calculation of Section Resistance by the AISC Manual	7
1.6.1. Classification of Shapes For Local Buckling	7
1.6.2. Bending Strength of Compact Shapes	7
1.7. Research Objectives	8
1.8. Search Limitation	8
1.9. Thesis Layout.....	8

Chapter Two. LITERATURE REVIEW	10
2.1. Introduction.....	11
2.2. Overview of Concrete-Filled Steel Tubes (CFSTs)	11
2.3. Previous Studies on Mechanical Properties of (RAC)	14
2.4. Related Theoretical and Experimental Investigations of Steel Beams Filled with Concrete.	16
2.5. Summery and Conclusion	25
Chapter Three. Experimental work.....	26
3.1. Introduction.....	27
3.2. Specimens Description	27
3.2.1. Stiffeners	30
3.2.2. Support Used.....	30
3.3. Double Web Steel Beam Manufacturing Process	31
3.3.1. Preparing of Flanges and Webs	31
3.3.2. The Welding Method	31
3.4. Material Properties	33
3.4.1. Cement	33
3.4.2. Fine Aggregate(F.A).....	34
3.4.3. Coarse Aggregate.....	35
3.4.4. Recycled Coarse Aggregate.....	36
3.4.5. Water.....	38
3.4.6. Steel Plates Properties.....	38
3.5. Concrete Mixes.....	40
3.5.1. Normal Concrete (NC).....	40
3.5.2. Recycled Aggregate Concrete (RAC)	41
3.6. Procedure for Mixing, Preparing, and Casting Double Web Beams ...	41
3.7. Hardened Concrete Testes	43

3.7.1.	Compressive strength test	43
3.7.2.	Splitting Tensile Strength Test	45
3.7.3.	Modulus of Rupture	46
3.8.	Instrumentation and Test Procedure	48
Chapter Four. RESULTS AND DISCUSSION		50
4.1.	Introduction.....	51
4.2.	Properties of Hardened Concrete.....	52
4.2.1.	Cylinder Compressive Strength	52
4.2.2.	Tensile Strength of Splitting	53
4.2.3.	Results of Modulus of Rupture.....	54
4.3.	Experimental Results for Tested Double Web Beams	55
4.3.1.	Control Beam (CB).....	55
4.3.2.	Doble Web Beams Filled with Normal Concrete (N.C) (Group 1).....	57
4.3.3.	Doble Web Beams Filled with Recycled Aggregate Concrete (RAC) (Group 2)	62
4.4.	Discussion of Results.....	69
4.4.1.	Beams Filled with Normal Concrete (N.C).....	70
4.4.2.	Beams Filled with Recycled Aggregate Concrete.....	71
4.5.	Experimental Work Summary	75
Chapter Five. FINITE ELEMENT ANALYSIS		76
5.1.	Introduction.....	77
5.2.	Types of Elements	77
5.3.	Description of Finite Element Modelling.....	79
5.3.1.	Modeling Parts of Specimens	79
5.4.	Materials Properties	80
5.4.1.	Steel Plate Model	80
5.4.2.	Concrete Model.....	80

5.5. Finite Element Modeling Interaction.....	84
5.6. Residual Stresses and Initial Geometric Imperfections.....	85
5.7. Loading and Boundary Conditions.....	86
5.8. Mesh Sensitive.....	87
5.9. Analysis procedure	90
5.10. Comparative Study between FEM and Experimental Results	90
5.10.1. Result of Control Beam (CB)	90
5.10.2. Result of Beam (NMF)	92
5.10.3. Result of Double Web Beam (NEF)	93
5.10.4. Result of Double Web Beam (NFF)	95
5.10.5. Result of Double Web Beam (RMF).	96
5.10.6. Result of Double Web Beam (REF).	98
5.10.7. Result of Double Web Beam (RFF)	99
5.11. Summary of Finite Element Results	101
5.12. Specimens Stress Distribution	102
5.13. Strain Behavior of Composite Double Web Beams	106
5.14. Parametric Study.....	110
5.14.1. Effect of Concrete Compressive Strength	110
5.14.2. Effect of yield strength of steel on the flexural behaviour	111
Chapter Six. CONCLUSIONS AND RECOMMENDATIONS.....	113
6.1. Introduction.....	114
6.2. Conclusions.....	114
6.2.1. Experimental Conclusions	114
6.2.2. Numerical Conclusions.....	116
6.2.3. Recommendations for Future Studies.....	116

List of Tables

Table 3-1: Details of The Tested Samples.	28
Table 3- 2: The Main Components and Chemical Composition of The Cement *	33
Table 3-3: The Physical Properties of the Cement *.....	33
Table 3-4: Grading of The Fine Aggregate.	34
Table 3-5: The Fine Aggregate Physical and Chemical Characteristics *	35
Table 3-6: Grading of The Coarse Aggregate.	35
Table 3-7: The Coarse Aggregate Physical and Chemical Characteristics *.	35
Table 3- 8: Grading of the Recycled Coarse Aggregate.	37
Table 3- 9: Properties of The Steel Coupon.	39
Table 3-10: Quantities of Materials in (Kg/m^3) of (NC) Mix.	41
Table 3-11: Quantities of Materials in (Kg/m^3) of (RAC) Mix.	41
Table 3-12: Results Compressive Strength of Concrete Mixes.	44
Table 3-13: Results Splitting Test of Concrete Mixes.	46
Table 3-14: Results Modulus of Rupture Test of Concrete Mixes.	47
Table 4-1: The Load Capacity for The Tested Beams	72
Table 4-2: The Ductility Index for The Tested Composite Beams.	73
Table 4-3: The Stiffness For The Tested Composite Beams.....	74
Table 5-1: Thicknesses and Types of Elements.	78
Table 5-2: Steel Characteristics Used in The Analysis.	80
Table 5-3: Concrete Damage Plasticity Parameters	84

Table 5-4: Experimental and Numerical Results for Tested Composite Beams
.....101

Table 5-5: Effect of Compressive Strength on Ultimate Load and Maximum
Deflection.111

Table 5- 6: Effect of Yield Stress on Ultimate Load and Maximum Deflection.
.....112

List of Figures

Figure 1-1: Typical Composite Steel Structure (Adluri, 2013).....	2
Figure 1-2: Typical Concrete-Filled Steel Tube Cross Sections (Abdalla, 2012).....	3
Figure 1-3: Failure Modes of CFST, Reinforced Concrete and Hollow Steel Members under Bending (Han et al., 2014).....	5
Figure 1-4: Recycling Process of RAC (Behera et al., 2014).....	6
Figure 2-1: Confining pressure engaged by the dilation of concrete (Harries and Kharel, 2003).....	12
Figure 2-2: The Confinement Effect in Circular and Square Sections (De Oliveira et al., 2009).....	13
Figure 2-3: Mander’s Model for Confined Concrete (Mander et al., 1988).....	14
Figure 2-4: Test Machine (Ghannam, 2016).....	16
Figure 2-5: Boundary Conditions and Mesh Used for Square and Rectangular (Javed et al., 2017).....	18
Figure 2-6: Samples Composite During Test Process (Shallal, 2018).....	19
Figure 2-7: Failure Pattern of Composite Specimens (Al-Obaidi et al., 2018).....	20
Figure 2-8: Typical Failure Modes:(a) unfilled specimen (HB); (b) filled specimen (FB-RC30); (c) all filled specimens after testing (Al Zand et al., 2021).....	22
Figure 2-9: Composite Beams Sections: (a) steel sheet detailing. (b) composite cross-section. (c) Longitudinal section (Al Zand et al., 2021).....	23

Figure 4-1: Results of The Mixtures Cylinder Compressive Strength.....	52
Figure 4-2: Failure Modes of Different Mixtures in Compression.	53
Figure 4-3: Results of Splitting Tensile Strength.	53
Figure 4-4: Failure Modes of Mixtures in Splitting.	54
Figure 4-5: Modulus of Rupture Results for Concrete mixs	54
Figure 4- 6: Failure Modes of Mixtures in Flexure.....	55
Figure 4-7: Load-Deflection Curve for CB.	56
Figure 4-8: CB During the Lab Testing.	56
Figure 4-9: Failure Mode for CB.....	57
Figure 4-10: Load-Deflection Curve for NMF.....	58
Figure 4-11: NMF During the Laboratory Examination.....	58
Figure 4- 12: Failure Mode for NMF.	59
Figure 4-13: Load-Deflection Curve For NEF.....	60
Figure 4-14: NEF During the Laboratory Examination.	60
Figure 4-15: Failure Mode for NEF.	61
Figure 4-16: Load-Deflection Curve For NEF.....	62
Figure 4-17: Failure Mode for NFF.....	62
Figure 4-18: Load-Deflection Curve For RMF.....	63
Figure 4-19: Specimen RMF During the Laboratory Examination.	64
Figure 4-20: Failure Mode for RMF.	64
Figure 4-21: Load-Deflection Curve For REF.	65
Figure 4-22: Specimen REF During the Laboratory Examination.	66
Figure 4-23: Failure Mode for REF Specimen.....	66
Figure 4-24: Load-Deflection Curve For RFF.	67
Figure 4-25: Specimen RFF During the Laboratory Examination.....	68
Figure 4-26: Failure Mode for RFF Specimen.....	68

Figure 4- 27: A Comparison in Load Capacity for Tested Beams.....	72
Figure 4- 28: A Comparison in Ductility Factor for Tested Beams.....	73
Figure 4- 29:A Comparison in Stiffness Criteria for Tested Beams.....	74
Figure 5-1: Node Solid Element (Ellobody, 2013).....	77
Figure 5-2: Node Shell Element (Ellobody, 2013).....	78
Figure 5-3:Assembling The Over All Parts of Compsite Double Web Specimen.....	79
Figure 5-4: Equivalent Uniaxial Stress-Strain Curve for Concrete (Hu et al., 2003).	83
Figure 5-5: Contact type Between The Steel Section and Concrete.	85
Figure 5-6: Residual Stress Distribution of Welded I-Type Cross-Section (Truong et al., 2019).	86
Figure 5-7: Residual Stress Distribution Of Welded I-Double Web.	86
Figure 5- 8: Applied Load on I-Double Web Beam.....	87
Figure 5- 9: Convergence Study Analysis.....	88
Figure 5-10: Finite Element Mesh Density.	89
Figure 5-11: Numerical and Experimental load-deflection curves for CB. ..	91
Figure 5-12: Experimental and Numerical Failure Shape for CB.....	91
Figure 5-13: Numerical and Experimental Load-Deflection Curves for NMF.	92
Figure 5-14: Experimental and Numerical Failure Shape for NMF.	93
Figure 5- 15: Experimental and Numerical Failure Shape for NEF.	94
Figure 5- 16: Experimental and Numerical Failure Shape for NEF.	94
Figure 5-17:Numerical and Experimental Load-Deflection Curves for NFF.	95
Figure 5-18: Experimental and Numerical Failure Shape for NFF.....	96

Figure 5-19:Experimental and Numerical Failure Shape for RMF.....	97
Figure 5-20: Experimental and Numerical Failure Shape for RMF.....	97
Figure 5-21: Numerical and Experimental Load-Deflection Curves for REF.	98
Figure 5-22: Experimental and Numerical Failure Shape for REF.....	99
Figure 5-23: Numerical and Experimental Load-Deflection Curves for RFF.	100
Figure 5-24: Experimental and Numerical Failure Shape for (RFF).	100
Figure 5- 25: Stress Distribution for Control Specimen at Ultimate Stage.	102
Figure 5- 26: Stress Distribution for NMF Specimen at Ultimate Stage. ...	103
Figure 5- 27: Stress Distribution at Ultimate Load for NEF Specimen.	103
Figure 5-28: Stress Distribution at Ultimate Load for NEF Specimen.	104
Figure 5- 29: Stress Distribution for RMF Specimen at Ultimate Stage. ...	104
Figure 5- 30: Stress Distribution at Ultimate Load for REF Specimen.	105
Figure 5-31: Stress Distribution at Ultimate Load for RFF Specimen.	105
Figure 5- 32: Plastic Strain (PE22) at Side-Span Section of Control.....	107
Figure 5- 33: Plastic Strain (PE22) at Side-Span Section of NMF.	107
Figure 5- 34: Plastic Strain (PE22) at Mid-span Section of NEF.	108
Figure 5- 35: Plastic Strain (PE22) at Mid-Span Section of NFF.....	108
Figure 5- 36: Plastic Strain (PE22) at Side-Span Section of RMF.	109
Figure 5- 37: Plastic Strain(PE22) at Mid-Span Section of REF.....	109
Figure 5- 38:Plastic Strain (PE22) at Mid-Span Section of RFF.	110
Figure 5-39: Impact of The Compressive Strength on The Load-Deflection for NEF.....	111
Figure 5- 40: Deflection at Mid-Span with Different Yielding Strength of Steel.	112

List of Abbreviations

Term	Description
AASHTO	American Association of State Highway and Transportation Officials
ACI	American Concrete Institute
AISC	American Institute of Steel Construction
ASTM	American Society for Testing and Materials
BS	British Standard
CFST	Concrete Filled Steel Tube
Exp	Experimental
FEM	Finite Element Method
IQS	Iraqi Specification
LVDT	Linear Variation Displacement Transducers
Max.	Maximum
Min.	Minimum
MPa	Mega Pascal.
N/A	Not available
NA	Natural Aggregate.
NAC	Natural Aggregate Concrete
NACFST	Natural Aggregate Concrete-Filled Steel Tube
NC	Normal Concrete
RAC	Recycled Aggregate Concrete
RACFST	Recycled Aggregate Concrete-Filled Steel Tube
RCA	Recycled Coarse Aggregate.
S4R	Shell Element Four-Node Reduce Integration

List of Symbols

Term	Description
bf	Flange Width of Steel Double Web
C30	Compressive Strength of Recycled Concrete
C38	Compressive Strength of Normal Concrete
E_c	Modulus of Elasticity of Concrete
E_s	Modulus of Elasticity of Steel Profile
f_c	Compressive Stress in Concrete
F_u	Ultimate Strength of Steel
F_y	Yield Stress of Steel Profile
I	Moment of Inertia of Steel Profile
S	Section Modulus of Steel
tw	Web Thickness of Steel Double Web
X, Y, Z	Global Coordinates System
ε	Strain
ε_c	Confined Concrete Strain at Peak Stress
ε_{cc}	Confined Concrete Strain at Peak Stress
λ	Width -Thickness Ratio.
λ_p	Upper Limit for Compact Category
λ_r	Upper for Noncompact Category
ν	Poisson's Ratio of Concrete
ψ	Dialton Angle

Chapter One: INTRODUCTION

CHAPTER ONE INTRODUCTION

1.1. General

Every material is different from the others in terms of characteristics. So, no material provides all construction requirements. The tensile strength of steel plates and tubes is high. Nonetheless, they are prone to local compression buckling. However, when steel tubes are filled with concrete, the steel's buckling resistance increases, and heavy stiffeners are no longer required, making composite beams a cost-effective and feasible alternative to concrete bridges (**Johnson, 1994**). The reason for employing two or more materials and joining them together is to take full advantage of their qualities and to create a structural element that leverages the desirable properties of the materials. The favorable qualities of multiple materials are combined to generate a member with higher rigidity and a high carrying capacity. A structural member made of two or more materials is known as a composite member (**Adluri, 2013, Han et al., 2014**), as shown in Figure (1-1).

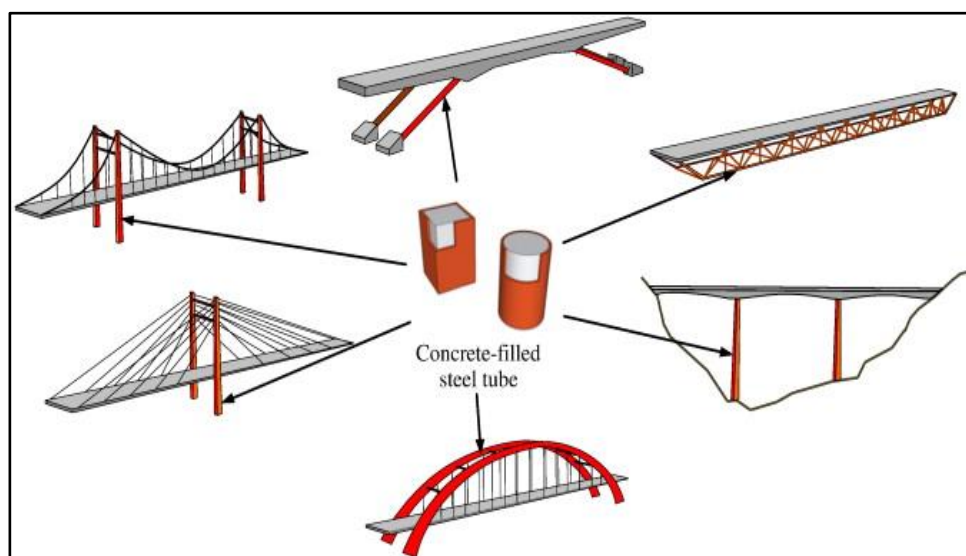


Figure 1-1: Typical Composite Steel Structure(**Han et al., 2014**).

1.2. Composite Action of Concrete-Filled Steel Tube (CFST)

Due to the transmission of shear stress between the concrete and the steel, composite work is developed between the steel tube and the infill concrete. The natural bond between the steel tube and the concrete or shear joints can be used to transfer stress (Abdalla, 2012). In general, the bond strength of CFSTs members is low. However, the circular cross sections provide higher bond strength and better confinement than the rectangular or square cross sections. Also, the local buckling will be prevented in the circular section and will be more likely to occur in rectangular or square shapes. Hence the circular cross-sections are preferable.

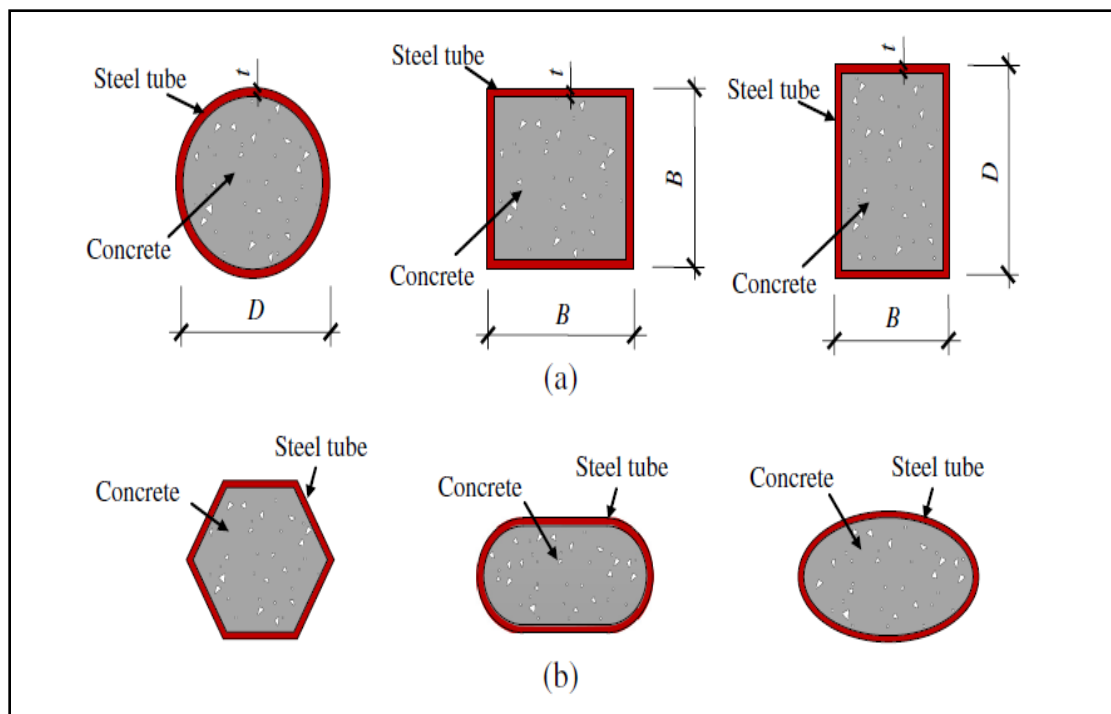


Figure 1-2: Typical Concrete-Filled Steel Tube Cross Sections (Abdalla, 2012).

1.3. Advantages and Disadvantages of Concrete-Filled Steel Tube Beams

The CFST has many advantages over the use of bar steel or reinforced concrete members; these advantages can be summarized as follows (**Chen et al., 2017, Al Zand et al., 2021, Abdalla, 2012, Matsumura et al., 2003**):

- 1) The construction of the CFST members is much easier as the steel tube will act as formwork for the casting of the concrete eliminating the need for shutters. This also means the construction time and cost will be reduced.
- 2) Concrete supports the local steel buckling. And the steel plate provides support from the outside.
- 3) High hardness and strength, excellent ductility.
- 4) Good acceptance to fire safety.
- 5) Energy absorption is high due to concrete infill and internal tube.

In addition to the advantages of CFST, they have some disadvantages (**Al-Zand et al., 2017, Abdalla, 2012**), such as:

- 1) Maintenance costs: Since the steel tube is confining the concrete, the steel will be exposed to air and humidity, which make the steel vulnerable to corrosion. Hence, the steel tube need to be painted and maintained continuously.
- 2) Fire resistance costs: Steel partitions have good load-carrying capacity at normal temperatures, but their strength decreases when exposed to high temperatures, which necessitates fire resistance.
- 3) Increase the weight of the beam: When adding concrete in a section of the entire sample, the subjective loads will increase; therefore, the loads applied to the sill will increase (**Al Zand et al., 2021**).
- 4) Another critical disadvantage of CFSTs members is the lack of sufficient knowledge regarding the bond strength between the infill concrete and the hollow steel section.

1.4. Failure Modes of CFST Beam under Bending

In general, CFSTs members subjected to flexural loads fail in a very ductile manner due to the increased stiffness of the member resulting from the confinement provided by the steel to concrete. When comparing the failure modes of CFSTs members under flexural loads to those of the reinforced concrete or hollow members, it was found that the behavior of CFSTs members is much better. The steel tube in the CFST member will only fail by outward local buckling of the compression flange, and the local buckling capacity will also be increased due to the support of the concrete core, while the hollow steel section will be subjected to a series of inward and outward local buckling. Regarding the infill concrete of the CFST member, cracks will be developed in the area under tension. However, the crack width and the distance between the cracks are smaller than those of reinforced concrete members. Figure (1-3) shows the differences in failure modes of CFSTs, reinforced concrete elements, and hollow steel members when subjected to bending.

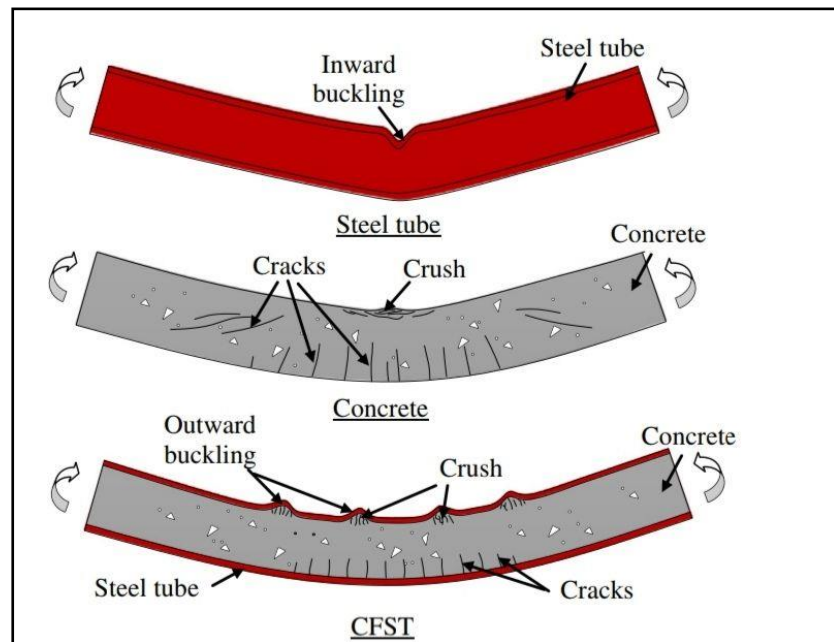


Figure 1-3: Failure Modes of CFST, Reinforced Concrete and Hollow Steel Members under Bending (Han et al., 2014).

1.5. Recycled Concrete Aggregate (RCA)

In the construction industry, the use of Recycled Concrete Aggregate (RCA) is a sustainable step. On the one hand, it reduces the continuous storage of waste disposal and prevents the consumption of existing natural resources. Natural aggregate (NA) can be replaced by RCA in concrete mixes. The concrete elements obtained from demolishing old concrete structures are crushed, washed, and graded to produce RCA (Rola et al., 2021), as shown in Figure (1-4). Due to the accumulated internal damage caused by the secondary crushing of RCA, the mechanical properties of recycled aggregate concrete (RAC) are weaker than those of natural aggregate concrete (NAC). Through many experimental studies, scholars confirmed that RAC has a lower strength, elastic modulus, and energy dissipation (Behera et al., 2014, El-Emam et al., 2016).

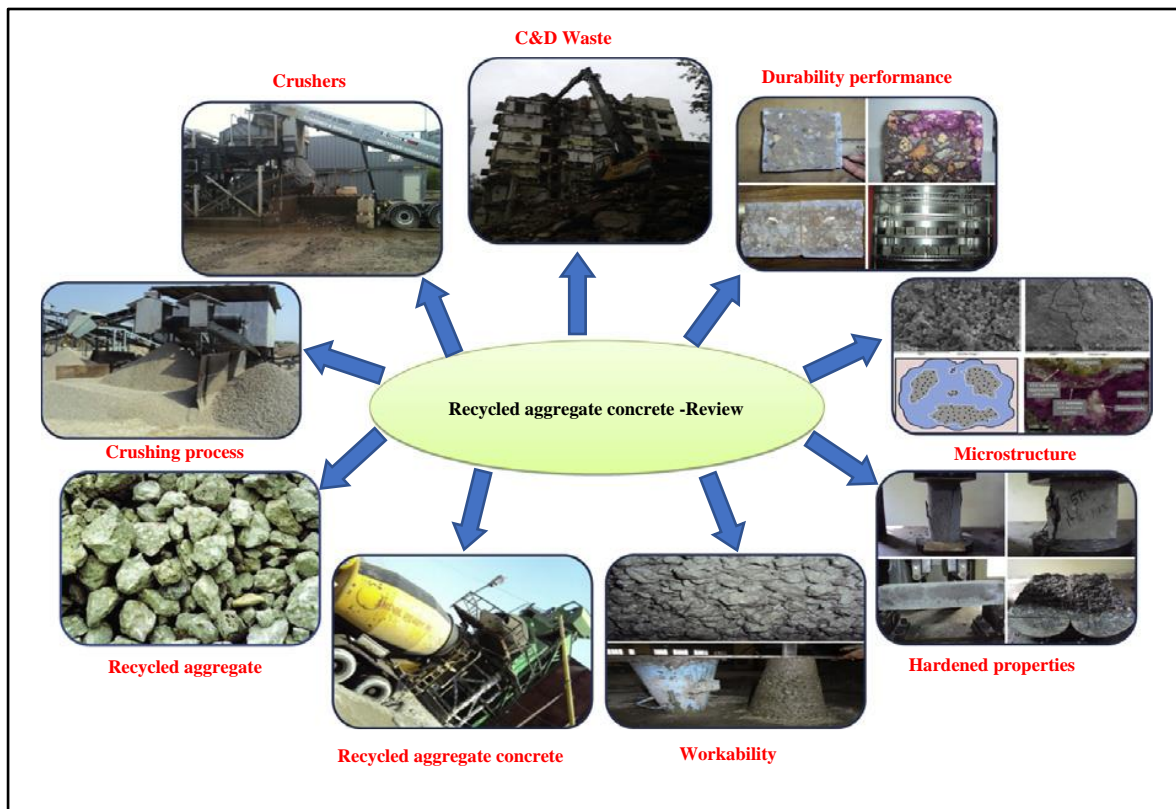


Figure 1-4: Recycling Process of RAC (Behera et al., 2014).

1.6. Classification and Calculation of Section Resistance by the AISC Manual

1.6.1. Classification of Shapes For Local Buckling

AISC Manual (AISC, 2016) Classified cross-sectional shapes as:

- ❖ Compact
- ❖ Noncompact, and
- ❖ Slender

Depending on the values of the width-thickness ratios of the individual elements that form the shape. The classification of shapes is found in section B4 of the specification “local Buckling.”

Table B(4-1).it can be summarized as follows:

λ = width - thickness ratio.

λ_p = upper limit for compact category.

λ_r = upper for the non-compact category.

If $\lambda \leq \lambda_p$ and the flange is continuously connected to the web, the shape is compact.

If $\lambda_r \leq \lambda \leq \lambda_p$, The shape is noncompact; and

If $\lambda > \lambda_r$, The shape is slender.

1.6.2. Bending Strength of Compact Shapes

When the beam is subjected to bending load, the bending stress in the extreme fiber is defined as:-

$$\text{Yield moment} \quad M_y = f_y * S \quad (1-1)$$

f_y =Yield stress S =Elastic section modulus.

$$\text{Plastic moment} \quad M_p = f_y * z \quad (1-2)$$

Z : Plastic section modulus

1.7. Research Objectives

The following points represent a summary of the objectives of this research:

- 1- A study of the effect of double web filling with concrete on beam behavior with changing filling site conditions.
- 2-Studying the effect of using different types of concrete (Normal Concrete, Recycled Aggregate Concrete) on the behavior of double web steel beams.
- 3-Explore the different parametric studies on the double web beam by using ABAQUS software with a three-dimensional nonlinear finite element method.

1.8. Search Limitation

The experimental study was limited to seven specimens of I-double web. The specimens are classified into two groups, in addition to one beam without concrete as a control beam. The first group included three double-web beams filled with normal concrete (the first one filled in middle region, the second beams filled with two side, the third beams filled full region), while the second group contained three double-web beams filled with recycled aggregate concrete (the first one filled in middle region, the second beams filled with two side, the third beams filled full region).

In ABAQUS (2021), Non-linear analysis was used to estimate the failure load and then record double web samples behaviour up to failure either by shear web buckling or top flange buckling and flexure failure.

1.9. Thesis Layout

This thesis consists of six chapters

Chapter 1 (Introduction): Includes a general introduction about composite beams, Composite action, failure modes, advantage and disadvantage of CFST beam, in addition to aims of study.

Chapter 2 (Literature Review): This shows a literature review of this research work, including the use of various types of concrete in the production of composite beams and different sections.

Chapter 3 (Experimental Program): Devotes to the experimental program, detail specimens, material properties, and test procedure.

Chapter 4 (Results and Discussion): Clarifies the experimental results and the discussions involving them.

Chapter 5 (Numerical Simulation): Illustrates the numerical analysis of the studied models by finite element (ABAQUS) to build a verified model that reasonably predicts the new proposed case studies.

Chapter 6 (Conclusions and Recommendations): Represents the conclusions of the research and recommendations for future work.

Appendix A: Design of I-double web steel beam.

Appendix B: Materials properties used In the Abaqus Software.

Chapter Two. LITERATURE REVIEW

CHAPTER TWO

LITERATURE REVIEW

2.1. Introduction

This chapter focus on the general overview of concrete-filled steel tubes (CFST) and the effect of confinement on composite beams, as well as previous studies of experimental and theoretical work on steel beams filled with different types of concrete. In additional studied variables such as section type, load type,specimen details, conclusions, and previously obtained results.

2.2. Overview of Concrete-Filled Steel Tubes (CFSTs)

CFST is a composite structural element developed by combining a hollow steel section (HSS) and infill concrete. The steel tube, which can be in any shape (circular, rectangular, square, etc.), provides confinement to the concrete resulting in an increase in the compressive strength of concrete and enhances its inelastic behavior, whereas the infill concrete improves the global and the local buckling capacity of the steel tube (**Roeder et al., 2010, Lin, 2004**).

When the concrete-filled steel tube is exposed to compression, a gap occurs between the steel tube and the concrete core in the elastic range because Poisson's ratio of the concrete is smaller than that of the steel tube. Beyond the elastic range, the inner concrete dilates (strains transversely) at a higher/faster rate than the steel tube, hence making contact between the steel tube and the concrete to develop again. As the axial compressive stress increases further, continued dilation of the concrete core is restricted by the steel tube, generating a variable confining pressure in the concrete in the transverse direction. This confining pressure effectively increases the compressive strength of the concrete core. In a CFST, the concrete is confined

by a steel tube section, which results in increased ductility and strength of the concrete core compared to unconfined concrete (Shanmugam and Lakshmi, 2001, Susantha et al., 2001, Kovac, 2010), as shown in Figure (2-1)

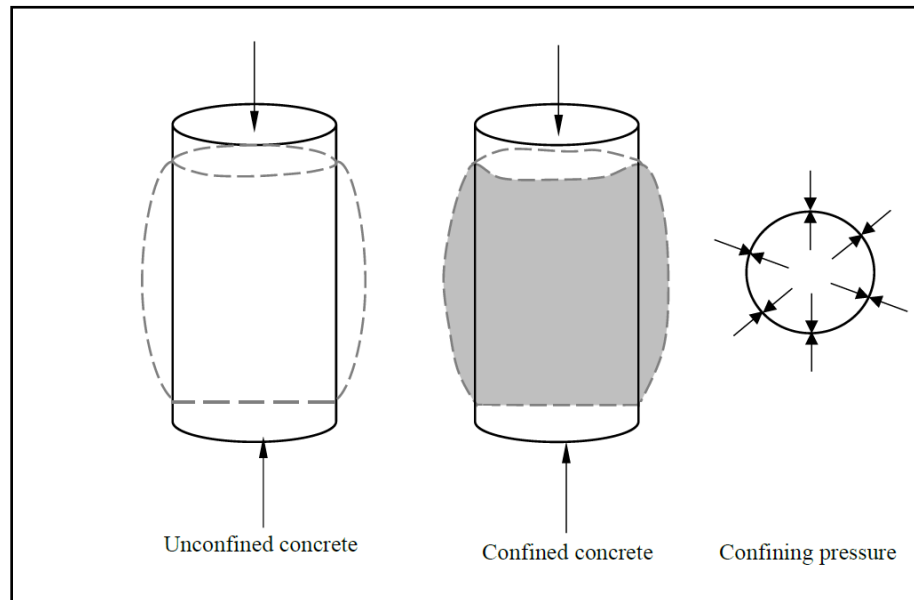


Figure 2-1: Confining pressure engaged by the dilation of concrete (Harries and Kharel, 2003)

The ultimate load of a CFST is larger than the sum of loads that can be achieved by the independent loading of concrete and steel (Susantha et al., 2001). In economic terms, a steel tube is used as formwork, reducing manpower, time, and construction costs. Generally, because of the high confinement offered by the circular tube, the post-yield and stiffness for the circular sections are greater than that square and rectangular tubes. The confinement in the rectangular and square sections is limited, being located around the corners and center, as the straight parts of these sections are too weak to resist the internal pressures because of the dilation of the concrete core (Hu et al., 2003, Kovac, 2010). Figure (2-2) demonstrates the difference between circular and square sections in the confining effect. Local buckling

is less likely to occur due to a strong confinement effect in the circular section (Hu et al., 2005).

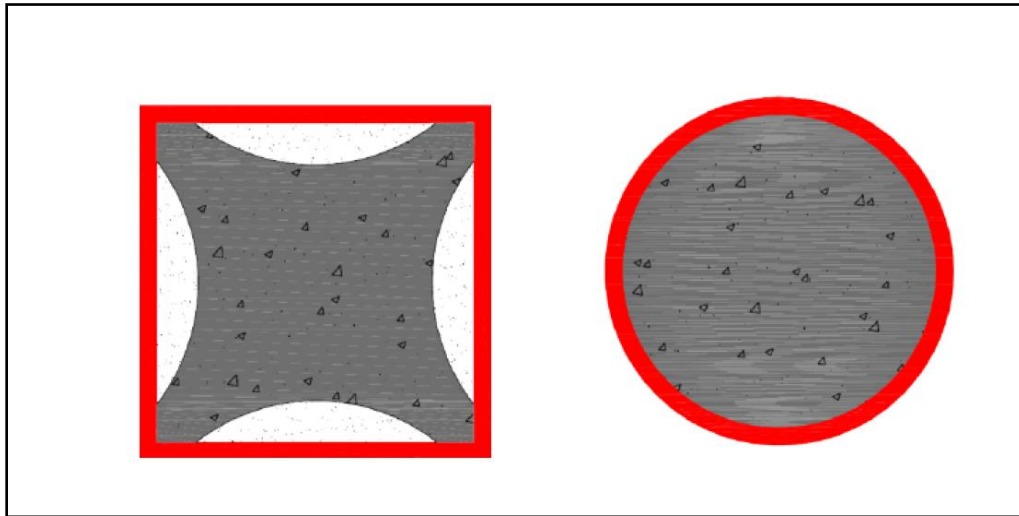


Figure 2-2: The Confinement Effect in Circular and Square Sections (De Oliveira et al., 2009).

To simulate the behavior of the confined concrete core, (Mander et al., 1988) developed a theoretical stress-strain model for confined concrete and implemented it using concrete damage plasticity. To simulate steel behavior, an elastic-plastic response was assumed. Tests revealed that strength development from confinement and the slope of the descending branch of the concrete stress-strain curve has a significant effect on the flexural strength.

The theoretical stress-strain model, as shown in Figure (2-3), was adopted by (Mander et al., 1988). Other researchers, such as Ellobody and Dai and Lam (2010) studied the behavior of circular, square, and elliptical concrete-filled steel tubes. Generally, the numerical models have been successful in predicting the compressive behavior of concrete-filled steel tubes with various cross-sectional forms.

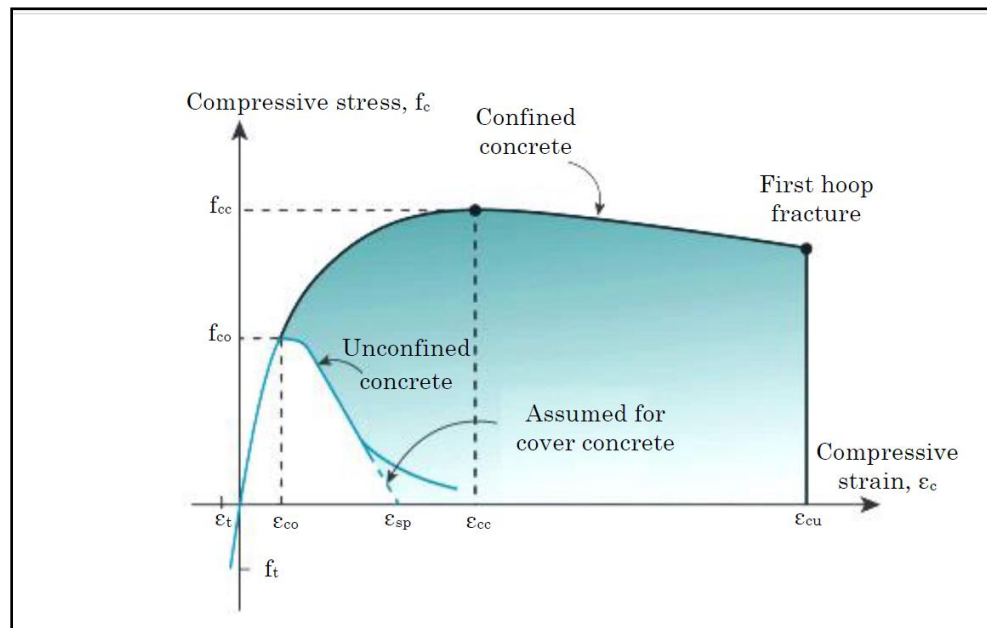


Figure 2-3: Mander's Model for Confined Concrete (Mander et al., 1988).

2.3. Previous Studies on Mechanical Properties of (RAC)

Due to the building industry's contribution to the depletion of natural resources, and because the concrete industry is a major user of natural resources, the sustainability of structures has become a significant requirement in recent years. This is due to population growth and the construction of high-rise buildings. Due to the availability of waste concrete from the demolition of old structures and natural catastrophes, as well as the decreased cost of procuring natural aggregate, the concrete industry has begun to employ recycled coarse aggregate (RCA) in place of natural aggregate.

Recycled aggregates are generated by crushing and treating destroyed structural parts' waste concrete. After processing, the primary distinction between recycled coarse aggregate and natural coarse aggregate is the cement that is bonded to the recycled coarse aggregate's core, which makes the mechanical characteristics of RAC highly complex (Hansen, 1992, El-Emam et al., 2016, Abed et al., 2017, Attom et al., 2016, Abed et al., 2018).

The mechanical properties of RAC can be summarized:

- 1- Compressive Strength: the compressive strength of RAC depends on many factors, such as the properties of recycled aggregate, w/c ratio, and the mixing procedure. In general, at the same w/c ratio, the increase of the recycled aggregate amount will lead to a decrease in the concrete compressive strength, up to 10 % compared with NAC (**Bairagi et al., 1993**).
- 2- Flexural Strength: similar to the behavior of compressive strength, the flexural strength of RAC will decrease with increasing the recycled aggregate replacement ratio. For example, a study made by (**Bairagi et al., 1993**) observed that the flexural strength of RAC with a 25 % and 50 % replacement ratio is lower by 6% to 13 %, respectively, than the flexural strength of Natural Aggregate Concrete (NAC).
- 3- Modulus of Elasticity: the effect of recycled aggregate on the modulus of elasticity is more obvious than the compressive and flexural strength for high replacement ratios. (**Kou and Poon, 2013**) reported that the modulus of elasticity declined by 12.6 % and 25.2 % for 50 % and 100 % replacement ratios, respectively, while (**Pereira et al., 2012**) stated that the modulus of elasticity almost remained the same for replacement ratios less than 30 %.

2.4. Related Theoretical and Experimental Investigations of Steel Beams Filled with Concrete.

(Ghannam, 2016) studied the ultimate load capacity of composite concrete-filled steel tubes (CFST) filled with different types of concrete (normal concrete and concrete with partial substitution of coarse aggregate by granite) under bending only. The samples were classified into two groups, the first group (88.9 * 88.9) and the thickness was 3.2 mm, and the second group (114.3 * 114.3) and the thickness was 4.8 mm. The square tube depth to the thickness ratios (d/t) are 27.8 and 23.8, as shown in Figure (2-4). The author said that the final strength of composite beams where granite is used to replace some of the coarse aggregate is the same as that of normal concrete. It can be said that replacing some of the coarse aggregate in normal, conventional concrete with fine aggregates will not only lower the cost of concrete but also save a lot of coarse and fine aggregates. Also, it has been seen that when thicker square steel tube beams with a smaller diameter-to-thickness ratio (d/t) are used, the beam's load capacity goes up a lot.

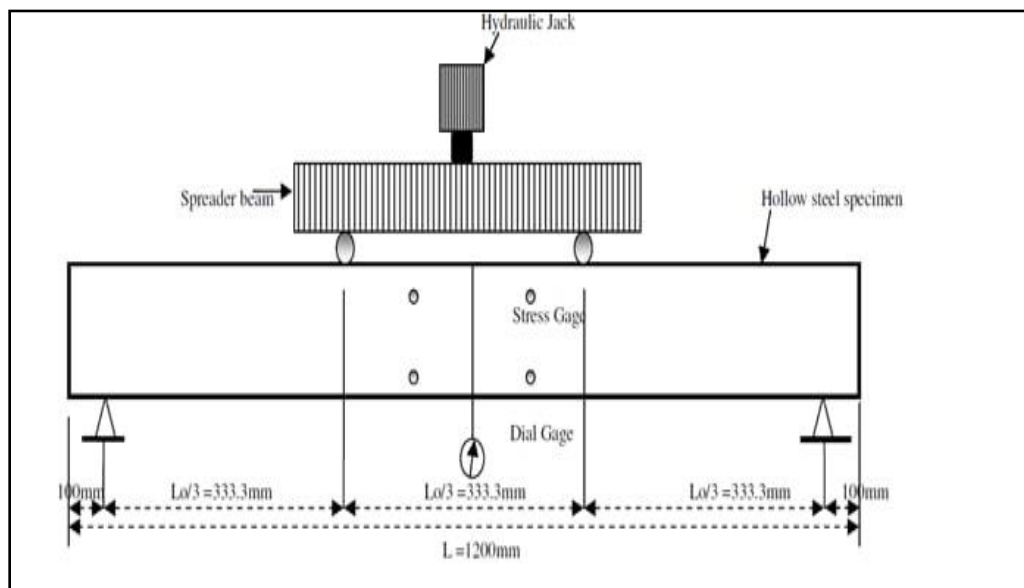


Figure 2-4: Test Machine (Ghannam, 2016).

(Al-Zand et al., 2017) studied the influence of using the concrete-filled steel tube (CFST) rectangular composite beams in the modern structural projects, the flexural and energy absorption capacities of simply supported rectangular hollow steel tube (HST) beams filled with normal concrete was investigated in this study. Eight downscale specimens (HST and CFST beams) were tested experimentally under static four-point bending, where these beams have varied tube section classifications thickness (3 mm and 1.5 mm) and lengths. Generally, the results confirmed that both of the moment and the energy absorption capacities of hollow steel tube beams were significantly improved when filled with concrete, specifically for those with section (1.5 mm). However, this improvement ratio, reduced gradually with increasing of tube's thickness (3mm) and/or beam's length.

(T SIVA NAGA and MADHURI, 2017) studied steel tubes filled with concrete, and they employed specimens with the following measurements: The span length is 1.0 m, the thickness is 3.2 mm, the breadth is 3.2 mm, and the height is 120 mm. Concrete with a compressive strength of 25 MPa was used to fill all specimens. The bonding process between the inner surface of the steel tube and the concrete was the subject of the parametric analysis conducted as part of the investigation. To evaluate the bonding effect, steel connectors and sand-coated sand were put on the internal surface of the steel tube. The findings demonstrated that the section's flexural properties were enhanced by employing steel tubes filled with concrete. Although the bonding techniques varied, the beams' flexural performance remained constant.

(Javed et al., 2017) studied Finite element analysis, modelling of the flexural behavior of square and rectangular steel tubes filled with normal and high-strength concrete, as shown in Figure (2-5). More than 50 experimental results were used to verify the FE model, and it was found that the FE model

accurately predicts the load-deflection curve and the ultimate moment capacity of the concrete-filled steel tube (CFST) beams. Thereafter, a parametric study was carried out to evaluate the effect of depth-to-thickness ratio (20–200), compressive strength of infilled concrete (20–100 MPa), shear span-to-depth ratio (1–8), depth-to-width ratio (0.6–2), and yield strength of steel tube (380–490 MPa) on the flexural behavior of square and rectangular CFST members. It was found that the depth-to-thickness ratio, the yield strength of steel, and the height-to-width ratio have a significant effect on the ultimate capacity of CFST beams.

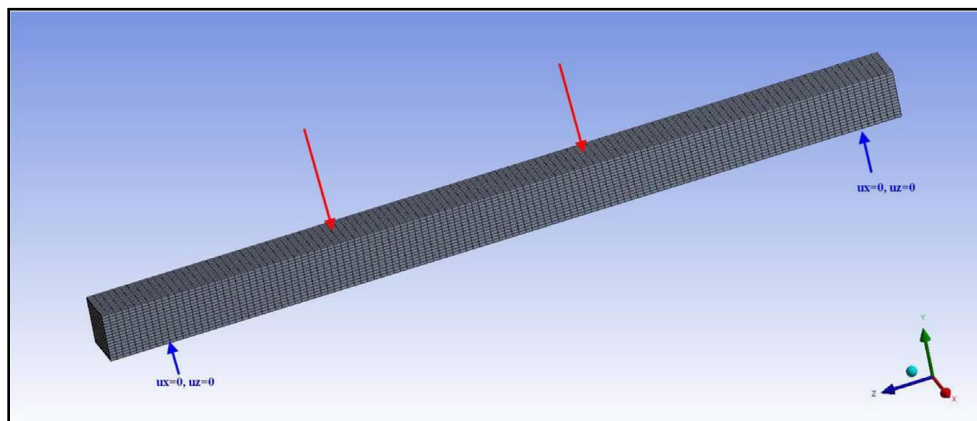


Figure 2-5: Boundary Conditions and Mesh Used for Square and Rectangular (Javed et al., 2017).

(Shallal, 2018) studied composite section (circle and rectangle) concrete-filled steel tubes (CFST) under flexural load to investigate the failure modes, ultimate load capacity, and load-deflection relationship of such composite beams, as illustrated in Figure (2-6). The variables studied are the ratio of thickness to the depth of the section, which was 33.34 and 37.5, respectively, and concrete, where compressive strength differences were used to fill the steel sections (22.9 and 31.9 MPa). It was found that the square-section beams have higher load capacities than the circular-section beams,

which were compared with beams that have identical D/t and concrete strength; the load-deflection behaviors of the CFST composite beams were similar for all groups. All CFST specimens have a greater ultimate loading capacity than their hollow beams. Increase in load capacity from 47.15 % to 105.41 %.



Figure 2-6: Samples Composite During Test Process (Shallal, 2018).

(Al-Obaidi et al., 2018) tested eight specimens of rectangular concrete-filled steel tube (CFST) beams. Two groups of specimens have been investigated. The first group (A) has dimensions (height*width*thickness) of 100*50*2 mm, and the second group (B) has dimensions of 100*50*3 mm and 900mm in length, as illustrated in Figure (2-7). The main objective of this research project is to investigate the flexural behavior of composite beams consist of a rectangular hollow steel tube filled with different types of concrete, such as normal mixed concrete, high strength concrete, and concrete with waste concrete aggregates, and also the effect of the thickness of the steel

tubes. The results indicate that the composite beams performed better than the hollow steel tube beam in terms of ductility and overall flexural capacity.

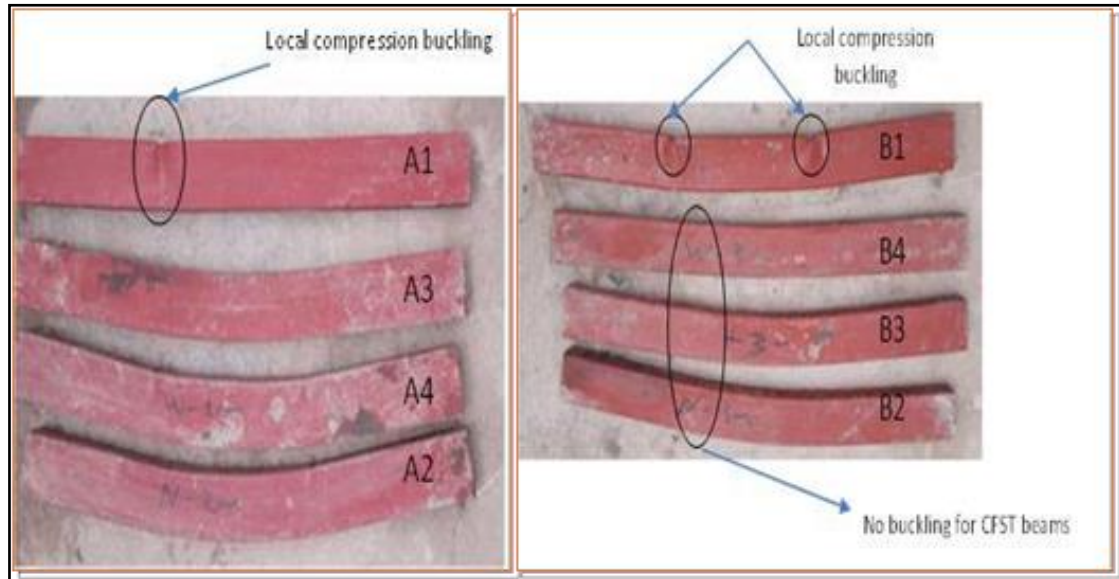


Figure 2-7: Failure Pattern of Composite Specimens (Al-Obaidi et al., 2018).

(Wang et al., 2020) studied experimentally and numerically the performance of steel-reinforced concrete-filled steel tubular (SRCFST), as the experiential program included six square samples and four rectangular samples, and their failure conditions were studied, Data deformation, instantaneous capacity under four-point bending, and the variables that studied the shear extension ratios (a/D) and depth to width ratios (D/B) on the bending performance. Then the validity of the data is evaluated by the finite elements. There is a good convergence regarding the final capacity and failure modes. Then the results are compared with the determinants of the current design method for the members of the vehicle stipulated in Eurocode 4 (EC4) (2004), while the results show high accuracy can be obtained to predict the bending capacity.

(Abed et al., 2021) studied concrete-filled steel tubes (CFSTs). The main goal of this research is to investigate the flexural response of recycled aggregate concrete-filled steel tube (RACFST) experimentally and theoretically considering circular and rectangular cross-sections. For this purpose, a total of 12 circular and 8 rectangular CFST beams with different diameter-to-thickness (D/t) and depth-to-thickness (h/t) ratios were tested under four-point bending. Concrete compressive strengths of 30 and 50 MPa and recycled coarse aggregate replacement percentages of 50 and 100 % were used in the experimental investigation. The test results revealed promising outcomes on the feasibility of using RAC in CFST systems under flexure. The flexural behavior of RACFST was found to be very similar to natural aggregate concrete-filled steel tube (NACFST), and the change in the concrete compressive strength and the recycled coarse aggregate replacement percentage slightly affected the flexural behavior of RACFST. In addition, the experimental flexural capacity of RACFST beams were compared to the theoretical nominal moments predicted by well-known design codes and methods, including the AISC-LRFD, the Architectural Institute of Japan (AIJ), EuroCode4, the British Standard (BS), and Han's method. The AIJ design code was the most accurate to predict the flexural capacity of RACFST, followed by the EuroCode4, as they underestimated the flexural capacity of RACFST beams by an average of 5 % and 12 %, while the British Standard significantly underestimated the flexural capacity of the tested RACFST beams by an average of 34 %.

(Al Zand et al., 2021) conducted study to investigate the flexural behavior of a slender steel tube beam that was produced by welding two pieces of C-sections (double-C sections) and was filled with recycled-aggregate concrete materials) in different proportions (0 %, 30 %, 50 %, and 70 %), as

illustrated in Figure (2-8). The practical program included five specimens. One was a specimen that was tested without concrete material (hollow specimen), while the other specimens were filled with concrete and examined under the static load. All composite specimens have different compressive strengths. The researcher found that the composite beams bending ability, stiffness, and the energy absorption index were improved. Compared to a hollow specimen, the ability to bend was increased by about 3.7 times, even when 70 % of the space was filled with recycled concrete.

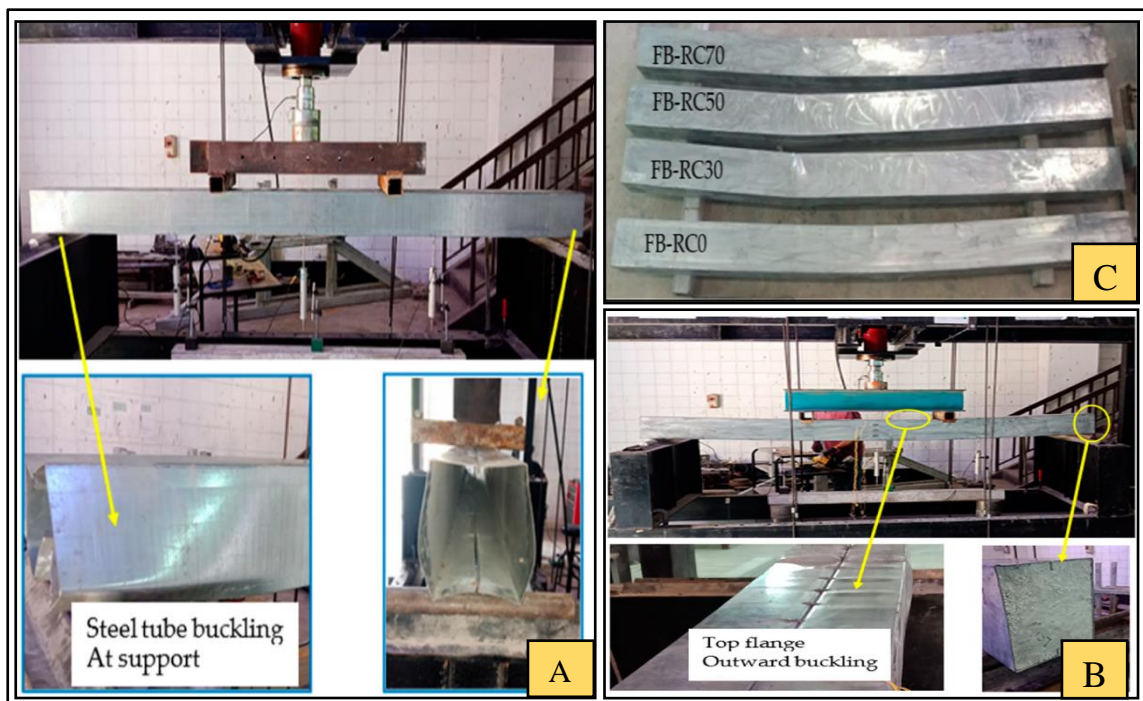


Figure 2-8: Typical Failure Modes:(a) unfilled specimen (HB); (b) filled specimen (FB-RC30); (c) all filled specimens after testing (Al Zand et al., 2021).

(Rola et al., 2021) Studied the experimental and analytical behaviour of light-gauge steel box sections filled with concrete made with a combination of natural aggregate (NA), recycled concrete aggregate (RCA), and recycled asphalt pavement (RAP). Incorporating experimental work, 30 composite beams, 15 plain concrete beams, and 2 hollow steel beams were tested. The specimens have the same cross-sectional dimensions (100*100 mm) and two

thicknesses (2 mm and 2.4 mm), and the span of all the beams was 1200 mm. Used coarse aggregate type and replacement ratios RCA and RAP replaced NA with replacement levels of 20 %, 40 %, 60 %, 80 %, and 100 % of the total weight of NA. In addition, RCA and RAP were incorporated into the same mixes with four replacement levels of (20 % RCA and 80 % RAP); (40 % RCA and 60 % RAP); (60 % RCA and 40 % RAP); and finally, with (80 % RCA and 20 % RAP). The specimens were tested under a static two-point load, as shown in the Figure (2-9). The experimental results showed that the ultimate capacity of composite beams decreased with the increase of RCA and RAP percentages. However, both RCA and RAP enhanced the capacity of composite beams.

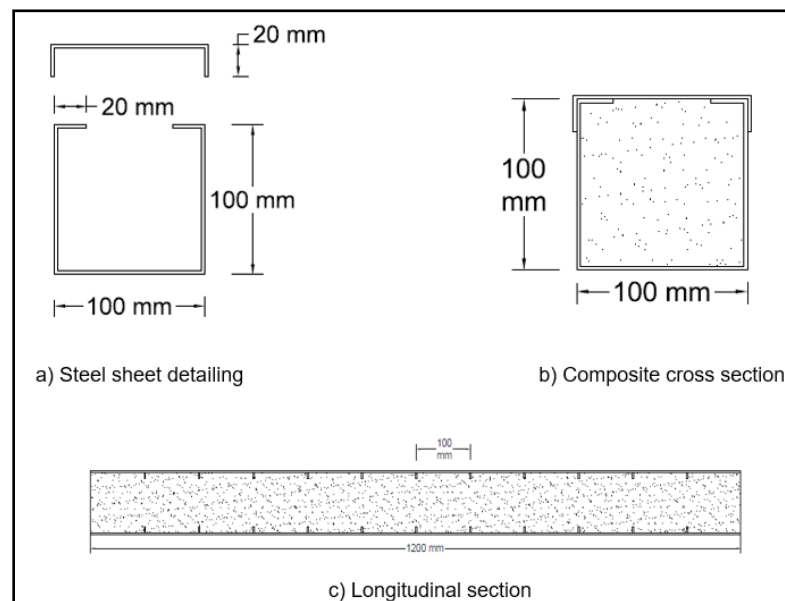


Figure 2-9: Composite Beams Sections: (a) steel sheet detailing. (b) composite cross-section. (c) Longitudinal section (Al Zand et al., 2021).

(Han,2021) studied the flexural behavior of CFSTs using self-consolidating concrete (SCC) instead of normal concrete. They tested a total of 36 beams with circular and square sections, and the parameters they considered are the steel yielding stress (from 235 to 282 MPa), the tube

diameter to thickness (d/t), and the shear span to depth ratio a/d (from 1.25 to 6). They stated that in general, the flexural behavior of self-consolidating CFSTs is very similar to those of normal CFSTs. Considering the effect of their parameters on the behavior of beams; they reported that the shear span to depth ratio has no obvious effect on the flexural behavior of CFSTs. They also compared their results with several design codes (AISC, BS5400, AIJ, and Eurocode4) and they found that the moment capacity and the flexural stiffness of self-consolidating CFSTs can be conservatively predicted by these codes.

(**J.Chen 2021**) investigated the behavior of RACFSTs under combined loading. They conducted an experimental program using 48 circular columns and 3 beams divided into 17 groups where each group has 3 identical specimens to check the scatter of the test results. Their study also included the effect of the replacement ratio and the steel to concrete area ratio. They concluded that for all identical specimens the results were consistent with differences less than 3% for each group. They attributed these results to the confinement effect by the steel tube. They also added that there is a small reduction of 4.5% to 11.2% in the maximum compressive load of RACFSTs when the replacement ratio is 100% compared to normal CFSTs. They also noted that the higher the steel to concrete area ratio the better the ductility of the specimen, while the replacement ratio has no significant effect on the ductility of the specimen. In addition to all of that, they compared their results with current CFSTs design provisions to check the applicability of these methods on RACFSTs. They recommended to use the method proposed by EuroCode4 as it gave close prediction to the test results.

2.5 Summery and Conclusion

From previous researches, despite the research on the flexural behavior of steel filled with different types of concrete has increased in recent years, there are still very limited studies on the behavior of composite beams filled concrete under bending. The parameters considered in this research are the type of concrete, and the fill area of the double web steel section. However, it deduces some important points from previous studies.

1-The concrete filling materials improved the flexural behavior of CFST beam significantly.

2-Used concrete as fill materials for composite beams could increase the maximum load capacity and deflection of the beam if compared to the hollow beam.

3- There is a lack of information and tests on the flexural behavior of concrete-filled tubes.

4- The flexural capacity of composite beams decreased with the decrease of the concrete compressive strength because of the use of recycled aggregates.

After reviewing the previous mention studies and reviewing theses and papers observed there are not previous studies within the specialization for the same adoption in this topic double web steel (built-up) section filled with difference types of concrete.

Chapter Three. Experimental work

CHAPTER THREE

EXPERIMENTAL WORK

3.1. Introduction

Experimental work was conducted in the materials lab at Kerbala University. The main objective of the experimental work of this research is to study the behavior of I-double web steel beams and the effect of the type and location of packed concrete. This chapter also included a description of the samples, the properties of the materials used, and the testing process.

3.2. Specimens Description

The experimental work involved the manufacturing and testing of seven simply supported double web steel beams. All beams have the same span length and cross-section (I-section) and were tested under the same load type and boundary conditions. The steel beams were built up from steel plates, of which the width and thickness of the flange plates were 120 mm and 6 mm, respectively, while the height of the web plates was 188 mm with a 3 mm thickness. The span of all beam specimens was calculated at 1100 mm between two supports. One of these specimens, which was without concrete, was marked as a reference beam, while the other six specimens were divided into two groups. Group One consists of three I-double web steel beams filled with normal concrete (the first one filled in middle region, the second beams filled with two side, the third beams filled full region), and group two consists of three double web beams filled with recycled concrete (the first one filled in middle region, the second beams filled with two side, the third beams filled full region). Figure (3-1) shows the details and characteristics of the cross-section of the double web beam, Figure (3-2) shows the diagram of the simply

supported beams, Table (3-1) shows the samples details and the concrete location.

Table 3-1: Details of The Tested Samples.

Group	Reference beam	Group one			Group two		
Name of sample	CB	NMF	NEF	NFF	RMF	REF	RFF
Location of concrete	----	Middle of the Beam	Both Sides of The Beam (Partial)	Full	Middle of the Beam	Both Sides of The Beam (Partial)	Full

Where:

NMF: Normal Concrete Beam Middle-Filled, **NEF:** Normal Concrete Beam Edges-Filled, **NFF:** Normal Concrete Beam Full Filled, **RMF:** Recycled Concrete Beam Middle-Filled, **REF:** Recycled Concrete Beam Edges-Filled, **RFF:** Recycled Concrete Beam Full Filled.

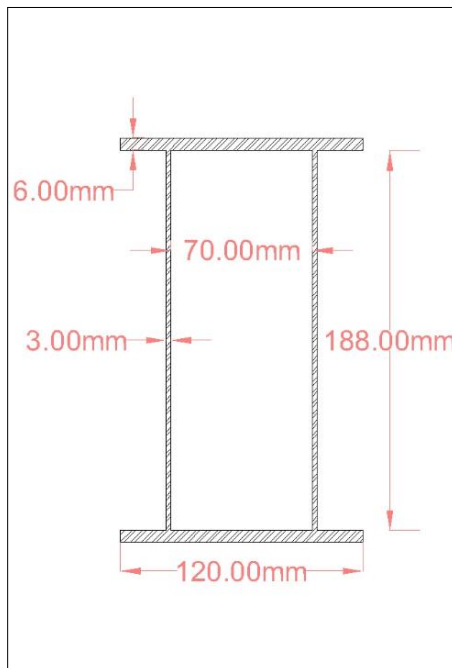


Figure 3-1: I-Double Web Steel Section Details.

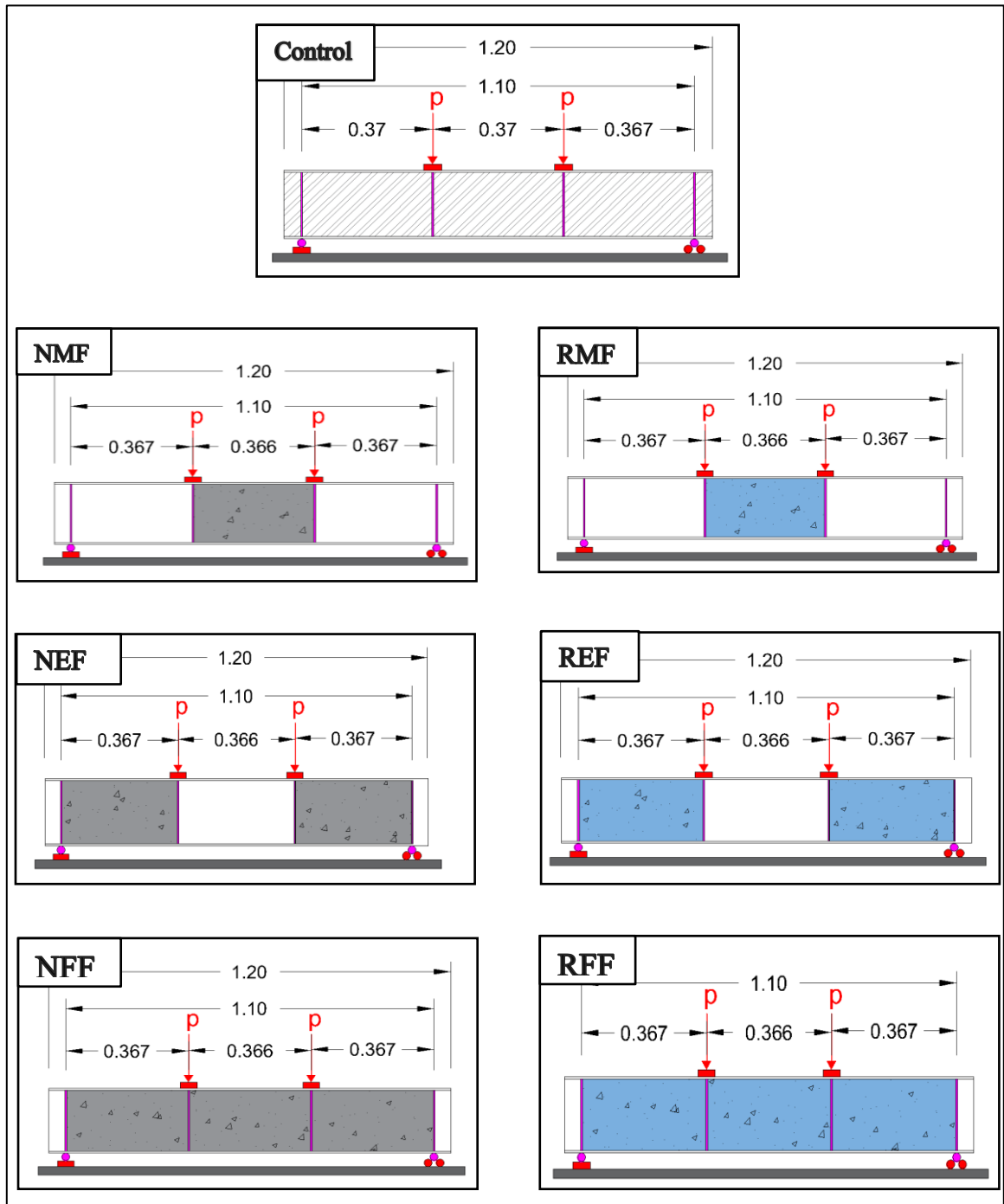


Figure 3-2: Schematic of The Simply Supported Beams (All Units in m).

3.2.1. Stiffeners

Vertical stiffeners of 6 mm were fixed, where each of the I-double web steel beam was equipped with four stiffeners. Two of them were immediately welded to the supports, while the other two were welded under applied load. These stiffeners were used to prevent local buckling and permit load-induced deformation, as illustrated in Figure (3-3).



Figure 3-3: Shows The Locations of The Stiffeners.

3.2.2. Support Used

All tested samples were simply supported; the system of support was a roller at one ends and pin at the other end. The roller support is made of one steel shaft diameter of 25 mm free. Figure (3-4) shows the details of support conditions.

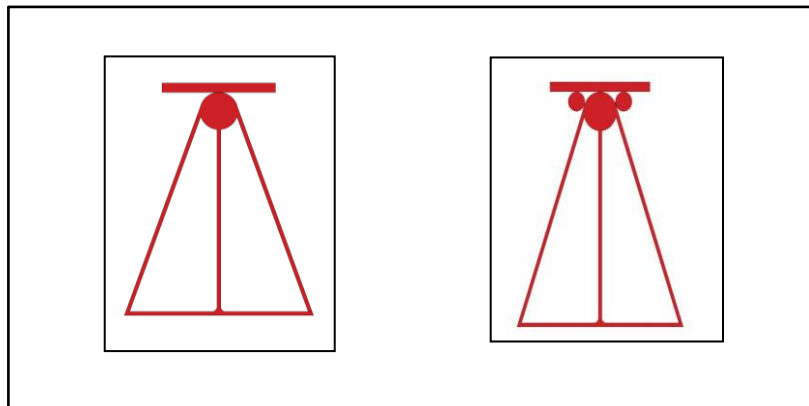


Figure 3-4: Supports Details.

3.3. Double Web Steel Beam Manufacturing Process

3.3.1. Preparing of Flanges and Webs

The flanges and webs of all double web beams were cut from 6 mm and 3 mm thick plates, respectively. The beams' webs were cut from the plates in the shape of a rectangle, and the flanges were then welded to the web. All steel beam components (webs, flanges, and stiffeners) were cut on a cutting machine, as illustrated in Figure (3-5). Computer Numerical Control (CNC) was used to make sure that the required dimensions were cut with great precision.



Figure 3-5: Cutting Parts for Flange and Web Plates by CNC machain

3.3.2. The Welding Method

Manual fillet welds were utilized to combine different elements of the built-up steel double beams to provide full strain compatibility between the parts of the steel beam. The process for welding was as follows:

1. The lower flange of the double web beam is welded with stiffeners.

2. One of the side webs of the beam was welded from the bottom with the beam's bottom flange and from the side with stiffeners. The process was repeated for the other side of the double web beam.
3. Normal or recycled concrete is placed in the web area according to the part designated for it in the sample .
4. Finally, the upper flange is welded into a web to become a complete double web sample , As illustrated in Figure (3-6).



Figure 3-6: Steps Welding Process of Double Web Beams.

3.4. Material Properties

3.4.1. Cement

In all experiments work, sulfate-resistant cement (R32.5) manufactured in Iraq by the "Lafarge Al-Jisr" company was used. And the requirements of Iraqi specifications (**IQS, No.5/2019**) have been met for this type of cement. Tables (3-2) and (3-3) show the chemical and physical properties of the cement used in the mix.

*Table 3- 2: The Main Components and Chemical Composition of The Cement **

Composition of oxides	% By weight	Limit of (IQS. No. 5/2019)
Sulfate (SO ₃)	2.2	≤ 2.8%
Magnesia (MgO)	3.6	≤ 5%
Loss of Ignition (L.O.I)	3.2	≤ 4%
Lime saturation (L.S.F) factor	0.86	0.66-1.02
Insoluble residue (I.R)	0.68	≤ 1.5
Main compounds (Bouge's eq.)	% By weight	Limit of (IQS. No. 5/2019)
Tricalcium silicate (C ₃ S)	48.04	-
Dicalciumsiliccat (C ₂ S)	22.5	-
Tricalcium aluminate (C ₃ A)	1.55	≤ 3.5%
* The Chemical analysis was carried out at Engineering Consulting Bureau / University Kerbala		

*Table 3-3: The Physical Properties of the Cement **

Physical properties	Test result	Limit of (IQS. No. 5/2019)
Setting time (vicats method)		
Initial setting (min)	120	≥ 45
Final setting (hr)	3.38	≤ 10
Compressive strength (MPa)		
Two days	13.5	≥ 10
Twenty-eight days	33	≥ 32.5
* The Physical analysis was carried out at Engineering Consulting Bureau / University Kerbala		

3.4.2. Fine Aggregate(F.A)

In the experimental work, natural sand from AL-UKHADER region with a maximum particle size of 4.75 mm was used. Table (3-4) and Figure (3-7) show the sieve analysis of fine aggregate and the grading curve according to Iraqi Standards (IQS, No. 45/1984). In Table (3-6), the physical and chemical properties are detailed according to the same specification.

Table 3-4: Grading of The Fine Aggregate.

Sieve size (mm)	Percentage passing of fine aggregate (F.A)	Limits of (IQS. No. 45/1984) (zone 2)	
		Max. Limit	Min. Limit
9.5	100	100	100
4.75	99	100	90
2.36	83	100	75
1.18	70	90	55
0.6	58	59	35
0.3	26	30	8
0.15	5	10	0

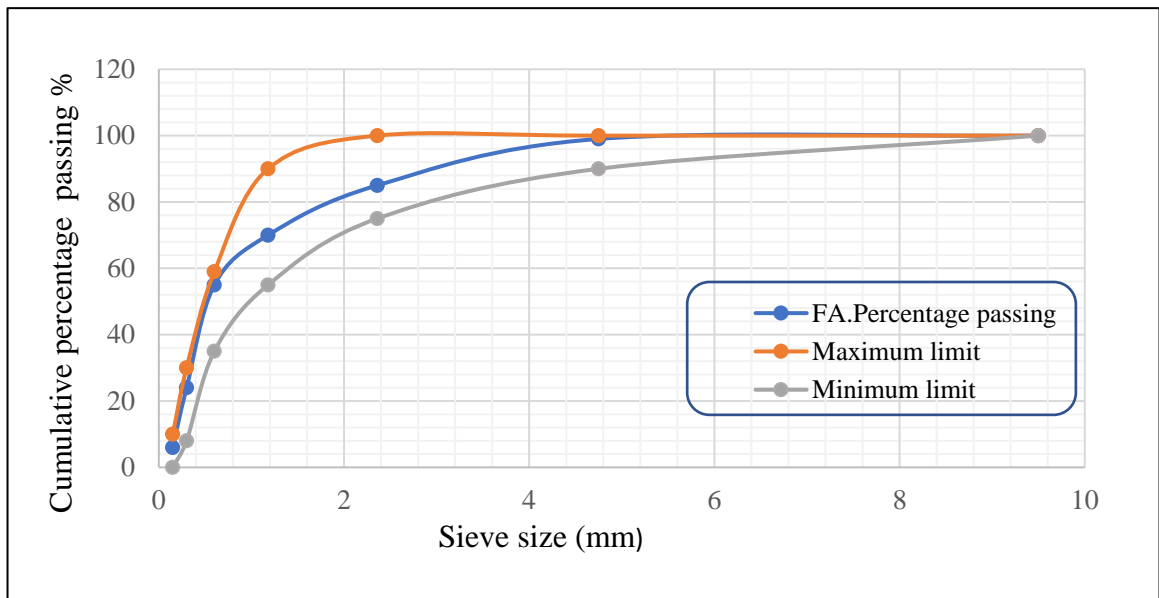


Figure 3-7: Fine Aggregate Grading Curve According to Iraqi Specification.

Table 3-5: The Fine Aggregate Physical and Chemical Characteristics *

Characteristics	Test results	Limits of (IQS. No. 45/1984)
Sulfate content (SO ₃) %	0.1	0.5% (max.)
Material finer than 75µm	2.1	5% (max.)
* The Physical and chemical analysis was carried out at Engineering Consulting Bureau / University Kerbala		

3.4.3. Coarse Aggregate

Pre-graded gravel from the (AL-UKHIDIR) region was used in the experiments, with a maximum particle size of 10 mm. The gravel was washed to remove any dust before being dried in the air to achieve a saturated surface for each batch. Table (3-6) and Figure (3-5) show the gravel sieve analysis and grading curve according to American standards (ASTM, C33-03). The physical and chemical characteristics were compared to the Iraqi standard (IQS, No. 45/1984) in Table (3-7).

Table 3-6: Grading of The Coarse Aggregate.

Sieve size (mm)	Percentage passing of coarse aggregate (C.A)	Limits	
		ASTM C33/2003	(IQS. No. 45/1984)
12.5	100	100	100
9.5	100	100-85	100-85
4.75	14	30-10	30-10
2.36	3	10-0	10-0
1.8	0	5-0	5-0

Table 3-7: The Coarse Aggregate Physical and Chemical Characteristics *

Characteristics	Test results	Limits of (IQS. No. 45/1984)
Sulfate content (SO ₃) %	0.062	0.1% (max.)
Material finer than 75 µm	0.3	3% (max.)
* The Physical and chemical analysis was carried out at the University of Kerbala consulting office central laboratory.		

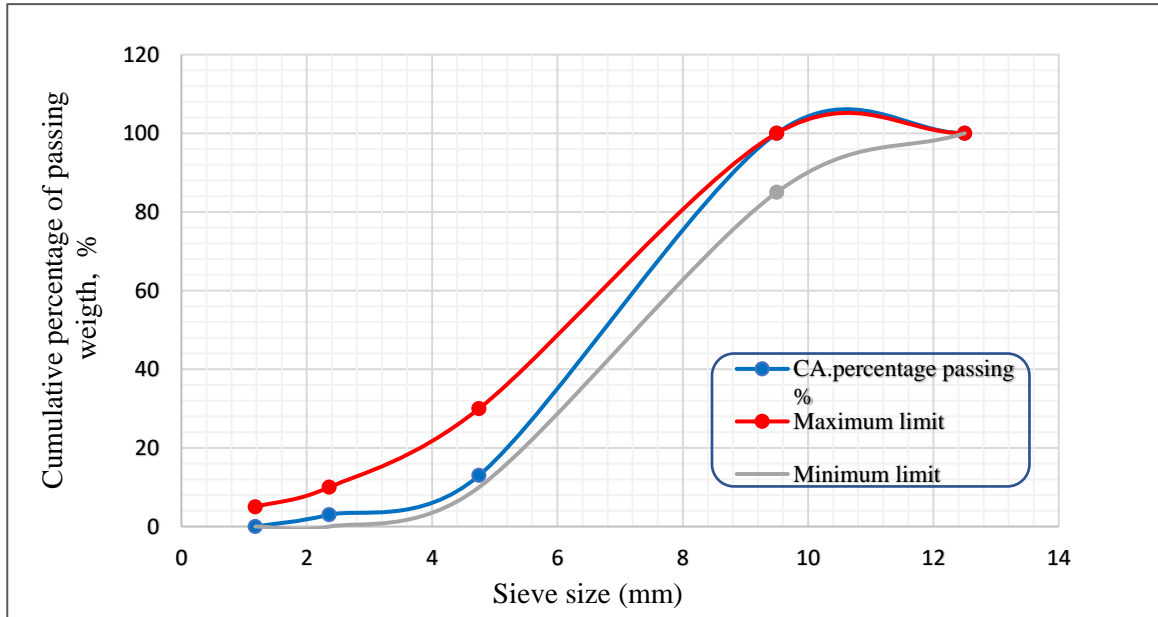


Figure 3-8: Grading curves for coarse aggregate according to (ASTM C33/2003).

3.4.4. Recycled Coarse Aggregate

In the experimental work, recycled gravel was used, which was get from concrete cubes (waste material), where the cubes that were broken after the age of 28 days are selected to ensure the end of the cement reactions and are crushed by an steel hammer with different gradations, and then a gradient is made for them so that it is almost similar to the gradient of natural aggregates. The recycled gravel was washed to remove dust and then dried in the air to achieve a saturated surface. The gravel sieve analysis and grading curve are shown in Table (3-8) and Figure (3-10), respectively, and are by American standards (ASTM C33/2003).



Figure 3-9: The Assembly and Crushing Of R.C.A.

Table 3- 8: Grading of the Recycled Coarse Aggregate.

Sieve size (mm)	Percentage passing of Recycled coarse aggregate (R.C.A)	Limits ASTM C33/2003	
		Max. Limit	Min. Limit
12.5	100	100	100
9.5	100	100	85
4.75	13	30	10
2.36	2	10	0
1.8	0	5	0

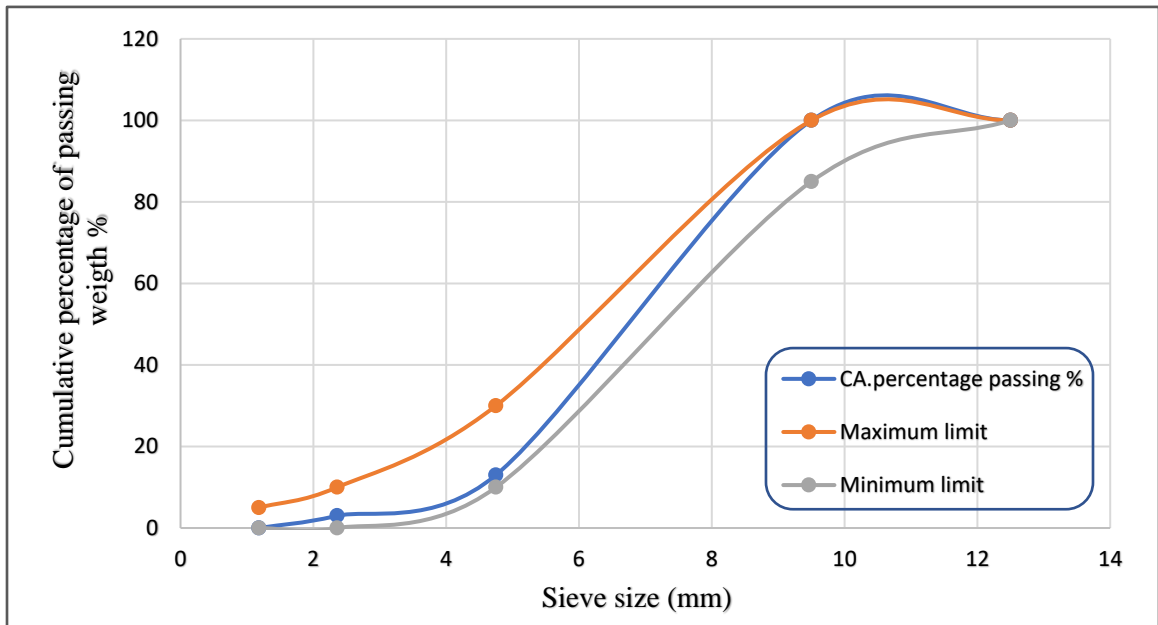


Figure 3-10: Grading Curves for Recycled Coarse Aggregate According to (ASTM C33/2003).

3.4.5. Water

Water was used in the Experimental program, clean water that complies with the conditions and requirements of the Iraqi specification (IQS, No.1703/1992).

3.4.6. Steel Plates Properties

All samples were examined at National Center for Laboratories and Structural Research to know the properties of the steel plates used in the manufacture of the double web beams. Four tensile coupons were cut from the 6 mm and 3 mm thickness flange and web plates, respectively. The coupon measurements corresponded to the (ASTM, A370) for the tensile testing of steel products, based on a length of 450 mm. Figure (3-12) shows the dimension of the specimen used in the tensile testing and Figure (3-11) typical tensile test of coupon. Table (3-9) shows the values for the yield stress, the ultimate stress, and the modulus of elasticity.

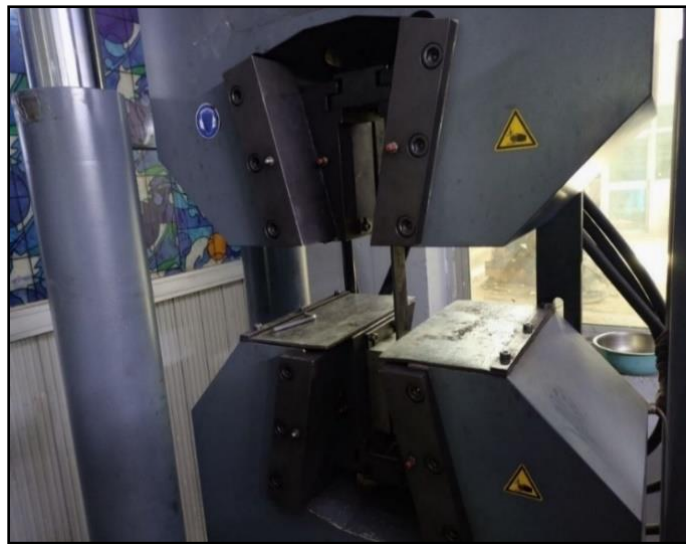


Figure 3-11: Typical Tensile Test of Coupon.

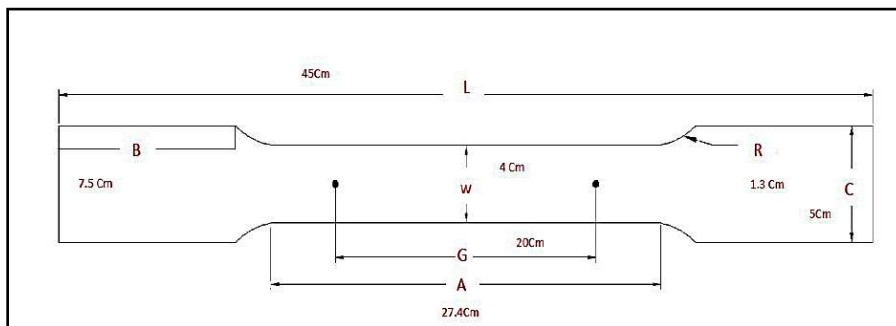


Figure 3-12: Descriptions of Dimension Coupon According to (ASTM-A370).

Table 3- 9: Properties of The Steel Coupon.

No. of coupon	Part	Yield Stress (N/mm ²)	Ultimate Stress (N/mm ²)	Modulus of Elasticity (Gpa)
1	Flange (6mm)	267	392	190
2		287	408	190
3		289	404	190
4		273	404	190
Mean		279	402	190
5	Web (3mm)	-	352	190
6		286	350	190
7		287	358	190
8		308	358	190
Mean		293.66	354.5	190

3.5. Concrete Mixes

3.5.1. Normal Concrete (NC)

Several trial concrete mixes were cast in order to determine a concrete mix that meets the requirements of this research. The reference concrete mix has been designed to achieve the normal strength of concrete (about 38 MPa) at (28) days. The mixing ratios were selected using the (ACI, 211.1-91) method for concrete mix design, depending on the material properties and the required strength. A mixer of 0.018 m³ was mixed and tested, as shown in Figure (3-13). The workability (slump test) was checked as the control test for the fresh concrete properties, and if the mix passed the test, It was approved for the rest of the work. The final mixing ratios are mentioned in Table (3–10).



Figure 3-13: Rotating Machine Used for The Production of (NC).

Table 3-10: Quantities of Materials in (Kg/m^3) of (NC) Mix.

Cement	Fine Aggregate	Course Aggregate	Water
400	720	1073	160

3.5.2. Recycled Aggregate Concrete (RAC)

This mixture consists of the same components as a normal mixture, except for replacing natural coarse aggregate with recycled coarse aggregate from concrete cubes (waste materials), whose age has exceeded 28 days to ensure no cement reactions. Table (3-11) below shows the proportions of the quantities of mixing ratios per cubic meter.

Table 3-11: Quantities of Materials in (Kg/m^3) of (RAC) Mix.

Cement	Fine Aggregate	Recycled Aggregate	Water
400	720	1073	160

3.6. Procedure for Mixing, Preparing, and Casting Double Web Beams

(1) All parts of the concrete mix were weighed and placed in clean bags. After that, the concrete was mixed and homogenized well mixed, as shown in Figure (3-14 A,B).

(2) The mixer was slowly filled with water and was left running for 1 minute and 30 seconds, as shown in Figure (3-14 C).

(3) Fresh concrete was carefully poured into a steel mould and poured vertically. Then the trapped air was ejected with the help of a vibrator by placing it on the sides of the steel mold. Then, the upper surface of the mould was levelled to obtain a smooth surface, as shown in Figure (3-14 D).

(4) After 48 hours, all double webs filled with normal or recycled concrete were stacked together. And covered with burlap and nylon plate, in addition curing with water daily for 28 days. The top edge of the specimens was then welded, and the composite specimens were colored, planned, and prepared for laboratory testing, as shown in Figure (3-14 E,F,H,I).

(5) The samples for hardening tests of normal and recycled concrete are (12) cylinders with a diameter of 10 cm and a length of 20 cm, (3) prisms of 10 x 10 x 40 cm dimensions were cast throughout each mixture type casting. The concrete was formed in standard test molds in conditions comparable to those seen in the casting of Specimens. Samples were placed in water tanks for the curing process for a test life of 28 days. After the curing time, the samples were taken out of the water and set up for testing based on the test standards. As shown in Figure (3-14 G).





Figure 3-14: Stages In The Production of Test Specimens (A, B) Preparation And Mixing Of Materials; (C, D)- Casting And Vibration Of Concrete;(E) Curing Of Concrete;(F-I) Painting And Layout Of Samples.

3.7. Hardened Concrete Testes

3.7.1. Compressive strength test

The compressive strength of cylinder concrete (f_c') tested according to (ASTM, C39-05). Three cylinders (100×200 mm) from each NC and RAC

mix were tested at age 28 days by using a digital compression testing machine of 2000 kN capacity shown in Figure (3-15) and Table (3-12).



Figure 3-15: Compression Strength Machine.

Table 3-12: Results Compressive Strength of Concrete Mixes.

No. of Cylinder	Normal concrete(NC)	Recycled Aggregate Concrete (RAC)
	Compression Strength	
C1	37.2	30.7
C2	38.5	28.1
C3	38.5	31.4
Average	38	30

3.7.2. Splitting Tensile Strength Test

At 28 days, this test was conducted using a cylinder (200 x100) mm in compliance with (ASTM, C496-11). The cylinder was positioned horizontally between two plates of steel, as illustrated in Figure(3-16), to evenly distribute the compressive machine's loads on the upper and bottom sides of the cylinder. A diametrical compressive force of 2000 kN was applied throughout the length of the specimen until the cylinder failed when a longitudinal crack split it in half. The splitting tensile resistance was estimated using the equation below (ASTM C496) based on the average of three-cylinder samples ,As illustrated in Table (3-13):

$$f_{sp} = \frac{2P}{\pi LD} \quad (3-1)$$

f_{sp} = Splitting tensile strength (MPa). L= Height of the sample (mm).

P = Total load of failure (N). D = Diameter of the sample (mm).



Figure 3-16: Tensile Splitting Machine.

Table 3-13: Results Splitting Test of Concrete Mixes.

No. of Cylinder	Normal concrete(NC)	Recycled Aggregate Concrete (RAC)
	Splitting Strength	
C1	3.7	3.7
C2	4.4	3.7
C3	4.6	3.4
Average	4.2	3.6

3.7.3. Modulus of Rupture

The flexural stress test was performed using a (100 x 100 x 400) mm prism, as illustrated in Figure (3-17), according to the (ASTM, C78-02) standard at 28 days. The test was carried out utilizing a flexural machine with a capacity of 150 kN to apply two-point loads. The modulus of rupture was calculated using the average value of the three samples, as illustrated in Table (3-14) using the following equation (ASTM C78):

$$f_r = PL / bd^2 \quad (3.2)$$

f_r = Flexural stress (MPa).

P = Total load of failure (N).

L = supports distance (mm).

b = section width of prism (mm).

d = section depth of prism (mm).



Figure 3-17: Modulus of Rapture (Test Sample and Machine).

Table 3-14: Results Modulus of Rapture Test of Concrete Mixes.

No. of Cylinder	Normal concrete(NC)	Recycled Aggregate Concrete (RAC)
	Modulus of Rapture	
C1	6.3	5.3
C2	6.1	6.2
C3	6.2	5.5
Average	6.2	5.6

3.8. Instrumentation and Test Procedure

After coating and planning the specimens on mesh shape, the specimens can be examined. Tests were carried out using the hydraulic testing machine. Manufactured for the Civil Engineering Department Engineering College, Kerbala University. Specimens were detected at every loading stage during testing, as displayed in Figure (3-18).

Each double web beams have the same 1.2 m overall length with a 1.10 m clear span. Under a system in which a two-point load was applied, the specimens were tested up to failure. A steel plate was utilized to avoid any local failure in the flange to focus the weight. The support system was a beam that was simply supported (roller and pin). The hydraulic universal testing machine depicted in Figure (3-18) was used in the test. The units contain a hydraulic actuator, load cell, extension supports, applicable load cell, and the computer programmer (laboratory display). The device's maximum capacity was roughly 2000 KN.

The utilized instruments comprise one linear variable displacement transducer (LVDT) positioned below the midspan beam with a 100 mm vertical measuring capacity, as the LVDT has been calibrated to ensure the safety of its work. Utilizing a hydraulic jack that was manually operated with the aid of a hydraulic pump. A load cell was installed between the hydraulic jack and a highly rigid steel beam sitting on load plates at the top of the compression flange to manage the load. Then, the load and displacement values were stored in a computer programmer, as displayed in Figure (3-19).

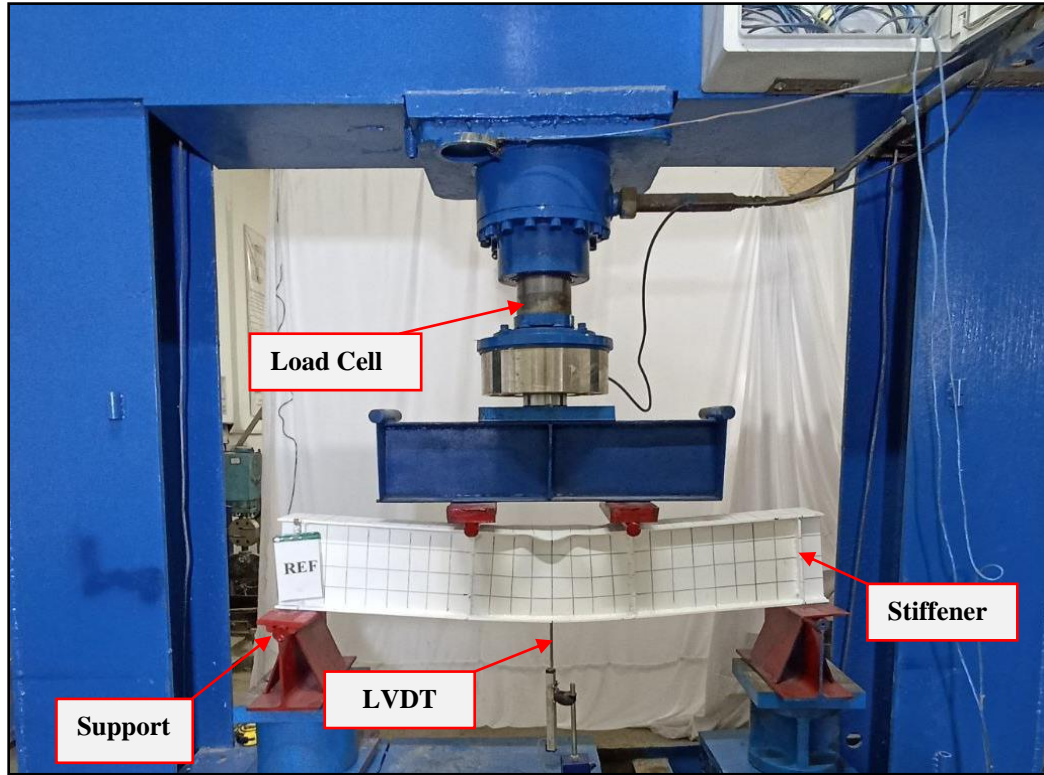


Figure 3-18: Hydraulic Testing Machine and Typical Details of the Test Setup.

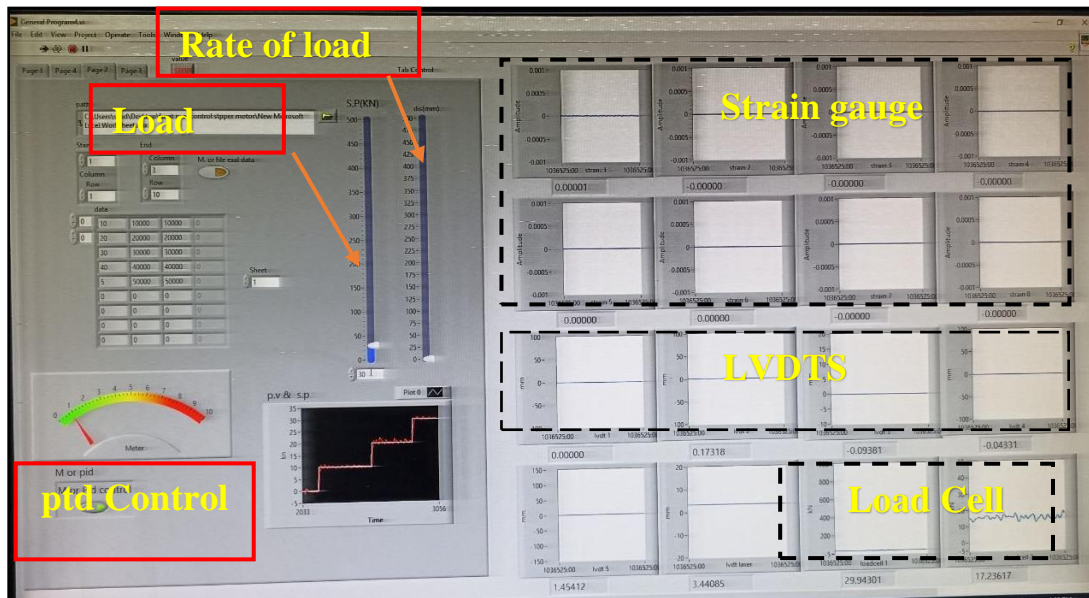


Figure 3-19: View of The Controlling Program.

Chapter Four. RESULTS AND DISCUSSION

Chapter Four

RESULTS AND DISCUSSION

4.1. Introduction

This chapter contains the results and discussions of the experimental work described in chapter three of this study.

First, it explains and discusses the results of the mechanical properties of concrete obtained from studies of normal concrete and recycled aggregate concrete, such as compressive strength, splitting tensile strength, and flexural tests.

Second, all the experimental results of the ultimate load and failure mode will be reviewed, as well as a comparison between the study cases and the specimen with a double web hollow (steel only). Seven specimens were examined and divided into groups according to the type and location of the concrete used for the specimen. The load was applied gradually within the specified increment step for all of the tested beams. In addition, load versus deflection in the mid-span of each beam was measured experimentally for loading steps. Each beam's failure mode (local or global buckling) events were also recorded and discussed. In addition to stiffness, and ductility index.

4.2. Properties of Hardened Concrete

4.2.1. Cylinder Compressive Strength

Compressive strength is one of the most important parameters of hardened concrete. To describe the effect of this property on the behavior of composite beams, two types of concrete have been adopted in this research work; NC and RAC. Found that cylinders filled with NC gave higher results than cylinders filled with RAC, with an increase of approximately 26.6 % at the age of 28 day. The coarse aggregate in the NC mixture is stronger and better than that in the RAC mixture. The compressive test results of the two mixtures are shown in Figure (4-1). The average value of three samples has been taken from the results of the mixtures cylinder represents compressive strength. Figure (4-2) shows failure modes of Mixtures in Compression.

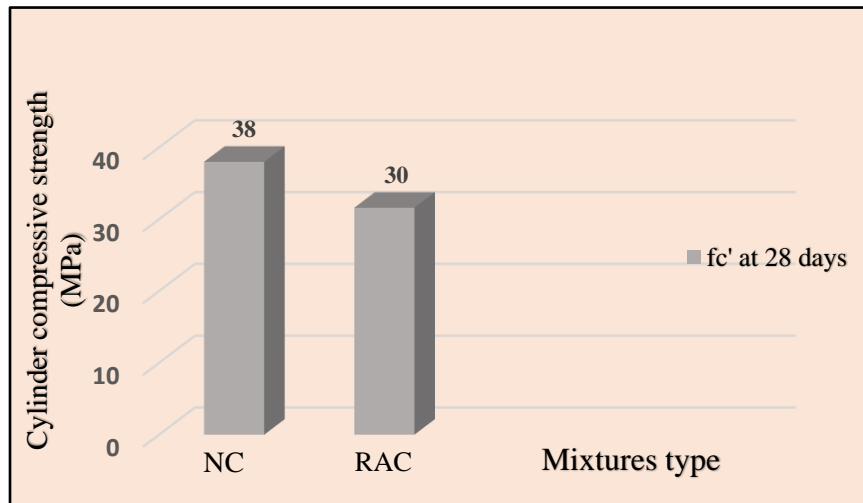


Figure 4-1: Results of The Mixtures Cylinder Compressive Strength.

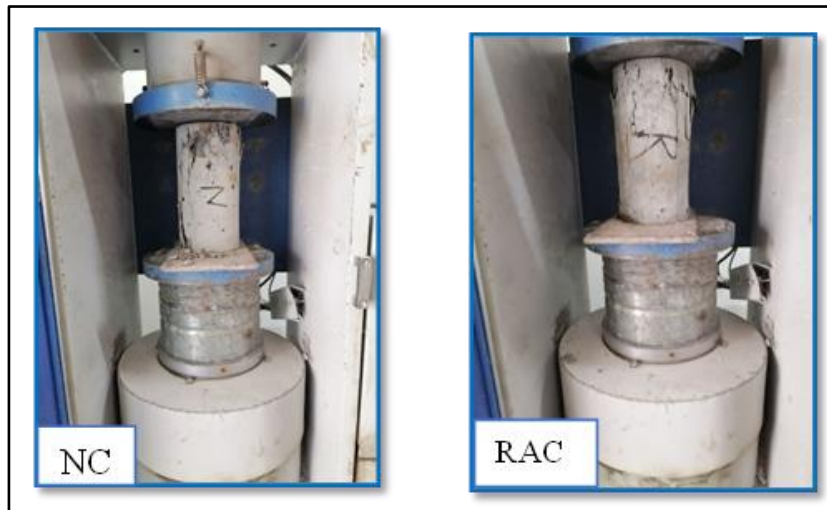


Figure 4-2: Failure Modes of Different Mixtures in Compression.

4.2.2. Tensile Strength of Splitting

The indirect test method is represented by splitting tensile strength. The tensile strength of concrete was measured by the average of three-cylinder samples for each mixture. It was noticed that cylinders loaded with NC produced approximately 16.6 % increase than cylinders filled with RAC because the coarse aggregate in the NC mixture is stronger and better than in the RAC mixture. Figure (4-3) shows tensile strength values of mixtures for NC and RAC. Figure (4-4) shows failure modes of mixtures in splitting.

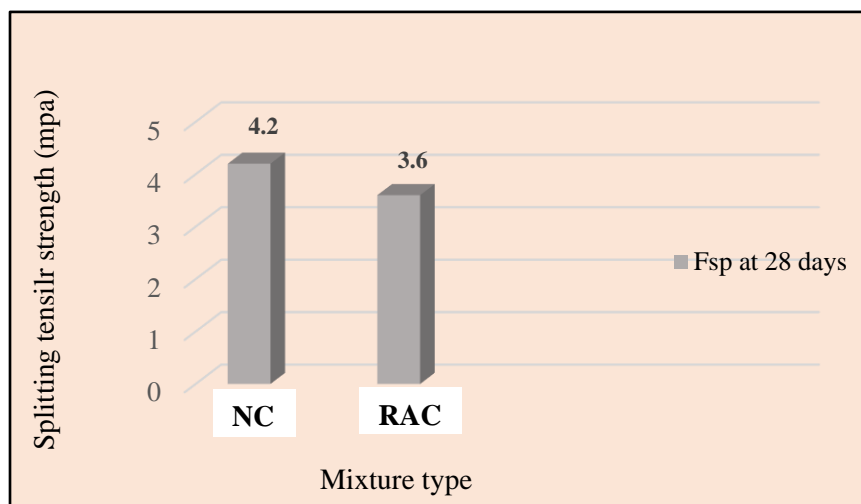


Figure 4-3: Results of Splitting Tensile Strength.

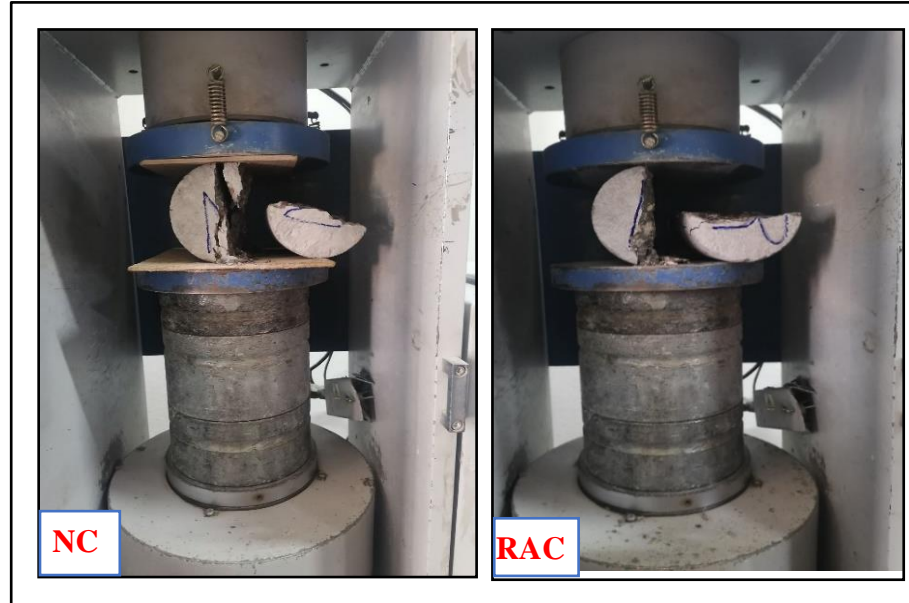


Figure 4-4: Failure Modes of Mixtures in Splitting.

4.2.3. Results of Modulus of Rupture

Figure (4-5) shows that the bending results of the normal mixture are greater than those of the recycled mixture by about 10.7 % because the coarse aggregate in the NC mixture is stronger and better than in the RAC mixture. Figure (4-6) shows failure modes of mixtures in flexure.

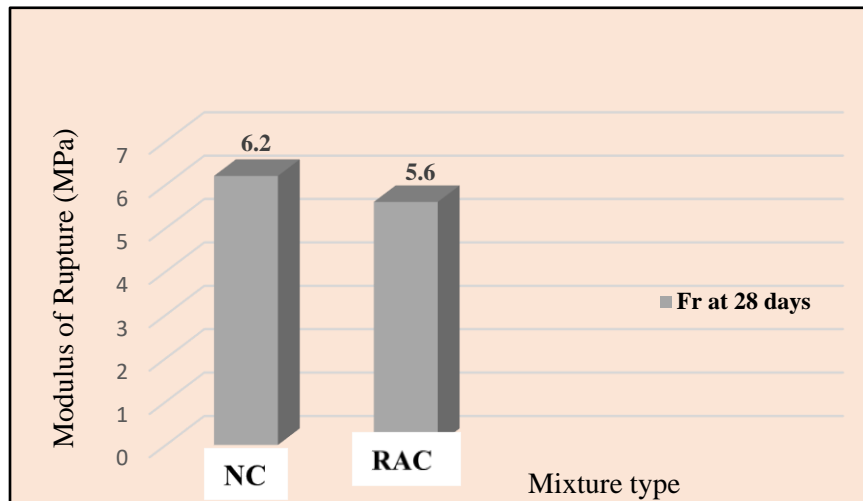


Figure 4-5: Modulus of Rupture Results for Concrete mixs

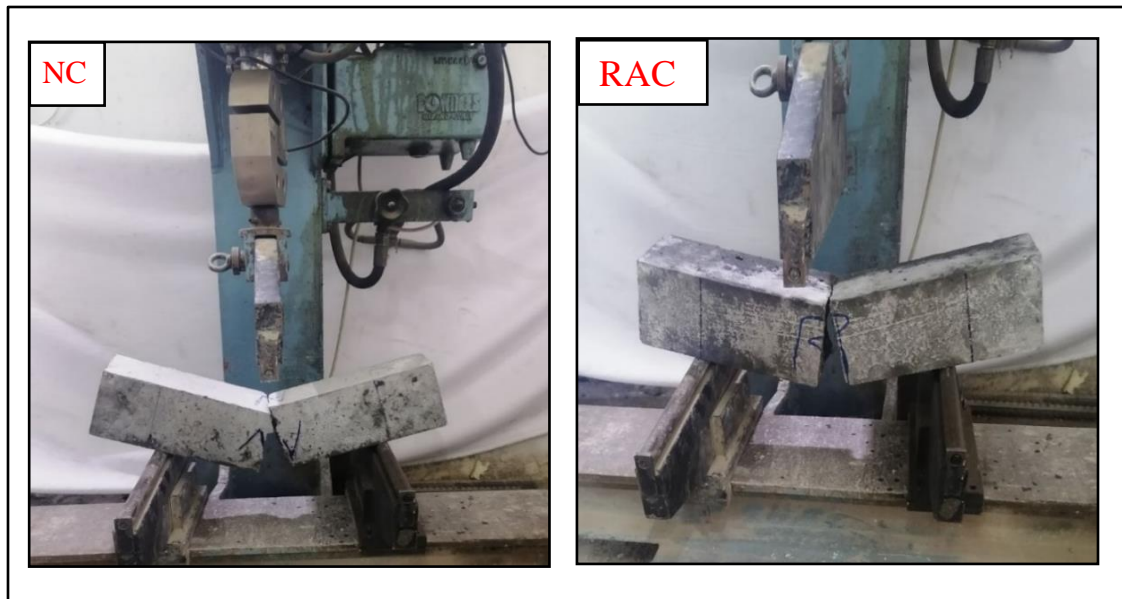


Figure 4- 6: Failure Modes of Mixtures in Flexure.

4.3. Experimental Results for Tested Double Web Beams

This part deals with the structural behavior of the double web beam hollow and filled with normal concrete or recycled aggregate concrete.

4.3.1. Control Beam (CB)

After installing the I-double web hollow specimen on the testing machine and setting up the LVDT in their positions below the specimen middle, the load was applied gradually to the control beam. Increasing the applied load led to the shear failure at ultimate load of 320.59 kN due to web shear buckling. The value of the vertical load-deflection curve noted that the ductility index and stiffness were 2.10 and 56 kN/mm, respectively. As shown in Figure (4-7), the load midspan displacement curve of the control beam is shown, while Figure (4-8) illustrates the failure mode of the beam CB During the lab testing and Figure (4-9) illustrates the failure mode of the beam CB after end loading stage.

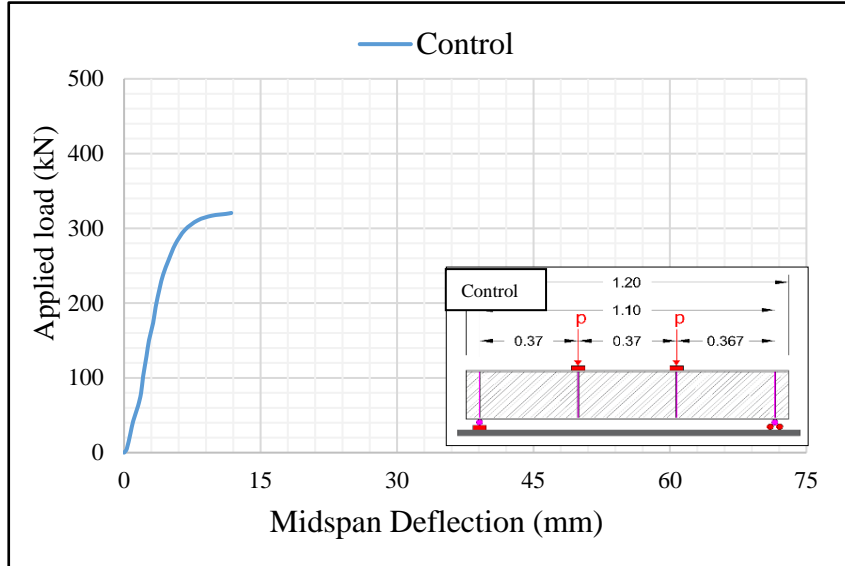


Figure 4-7: Load-Deflection Curve for CB.



Figure 4-8: CB During the Lab Testing.

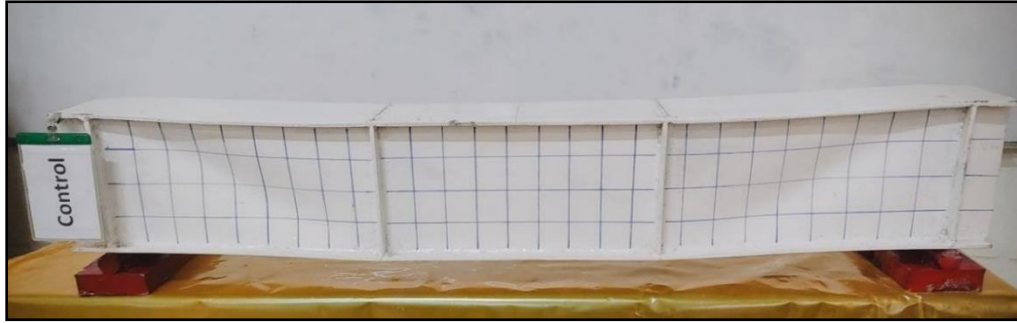


Figure 4-9: Failure Mode for CB.

4.3.2. Doble Web Beams Filled with Normal Concrete (N.C) (Group 1)

The first group contains three specimens with the same properties as steel. These specimens were divided according to the part filled with normal concrete (middle , two sides , fully beam), as we will explain below.

4.3.2.1. Normal Concrete Beam, Middle-Filled (NMF)

This specimen was enhanced by the middle web zone filling technique at one-third of the NMF specimen length. Two loads were gradually applied to the specimen, and the deflection was measured for each load step value, as shown in Figure (4-10) load-deflection for both NMF and CB. This specimen failed at a load of 353.2 kN due to global web shear buckling, as shown in Figure (4-11) NMF during the laboratory examination. When compared to the control beam, the ultimate load and deflection can go up by up to 10.19 % and 3.05 %, respectively. Furthermore, the failure mode was not changed, as shown in Figure (4-12); however, concrete increases the flexural resistance, ductility factor, stiffness, and the curve of composite beam. Because the middle section was made stronger by filling it with normal concrete, the web area was made stronger.

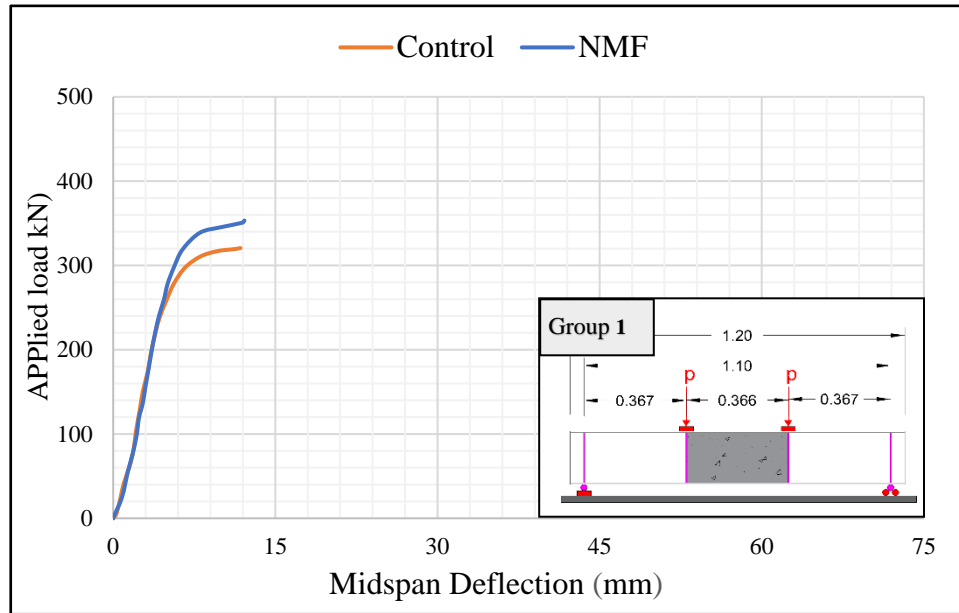


Figure 4-10: Load-Deflection Curve for NMF.

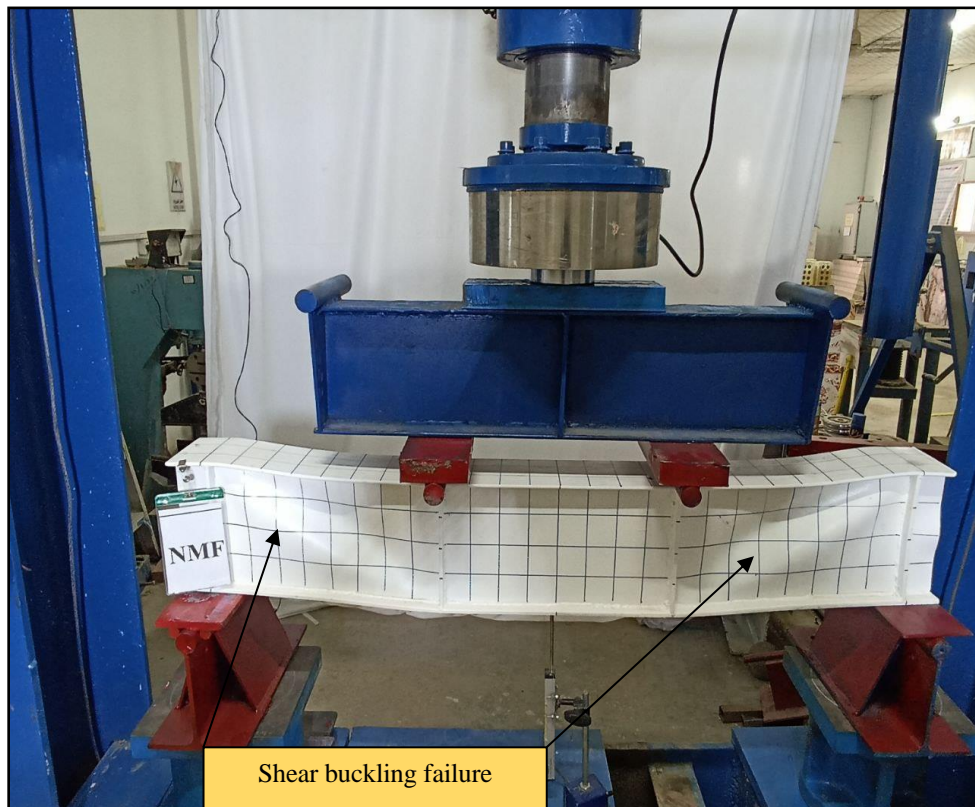


Figure 4-11: NMF During the Laboratory Examination.

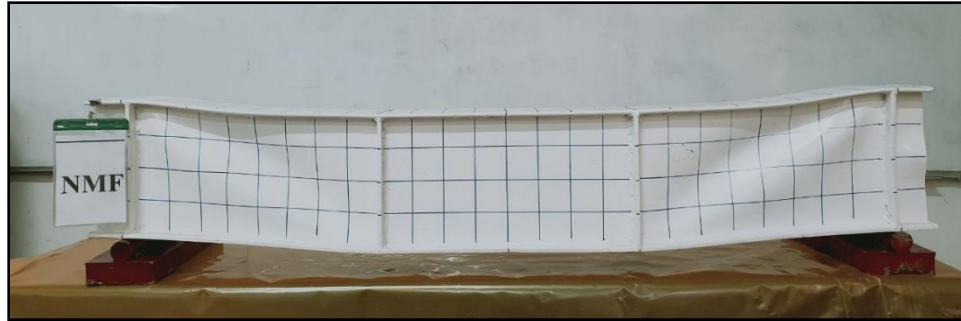


Figure 4- 12: Failure Mode for NMF.

4.3.2.2. Normal Concrete Beam, Two Sides-Filled (NEF)

This beam has normal concrete on the sides. Figure (4-14) illustrates the beam NEF during the loading procedure. The load-deflection curve shows that this beam ultimate load is 399.70 kN, which is larger than that of a control beam of around 24.6 %. The deflection at maximum load was 32.06 mm, which is larger than the control beam, as shown in Figure (4-13). However, the failure mode was also changed from shear buckling to flexural, as shown in Figure (4-15), because the side parts were made stronger by filling them with normal concrete, so the web area was also made stronger. This will increase the flexural resistance, ductility index, stiffness, and toughness of the composite double web beam, where the ductility index and stiffness are 5.24 and 60.8 kN/mm, respectively.

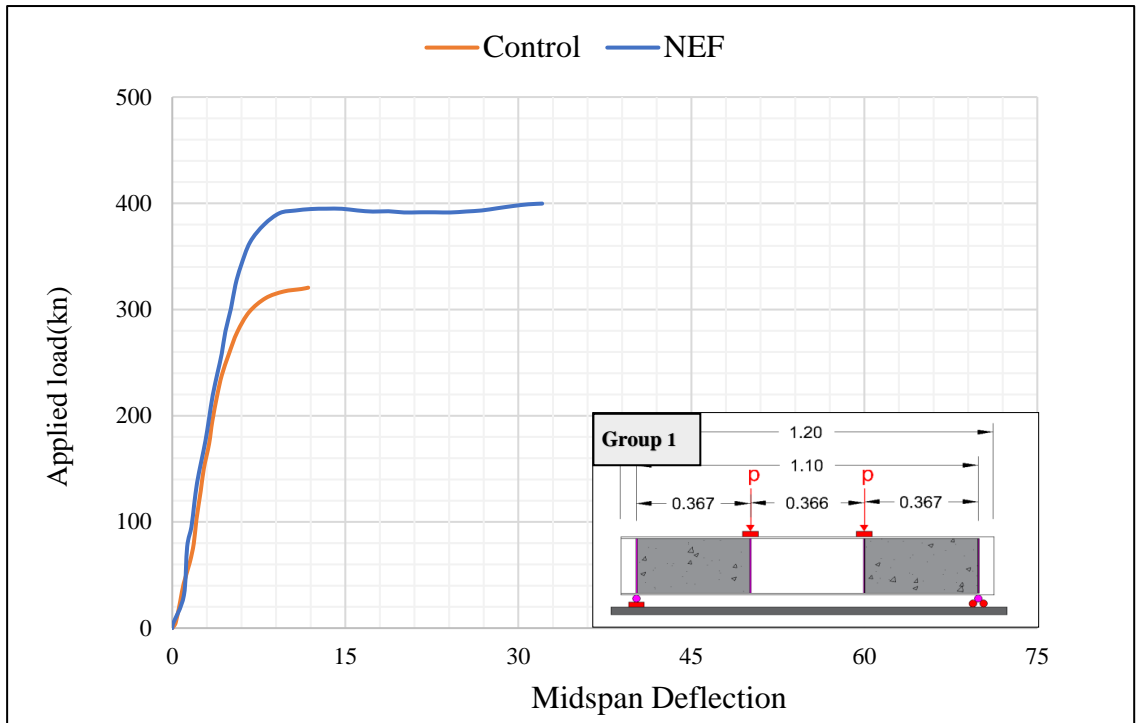


Figure 4-13: Load-Deflection Curve For NEF.

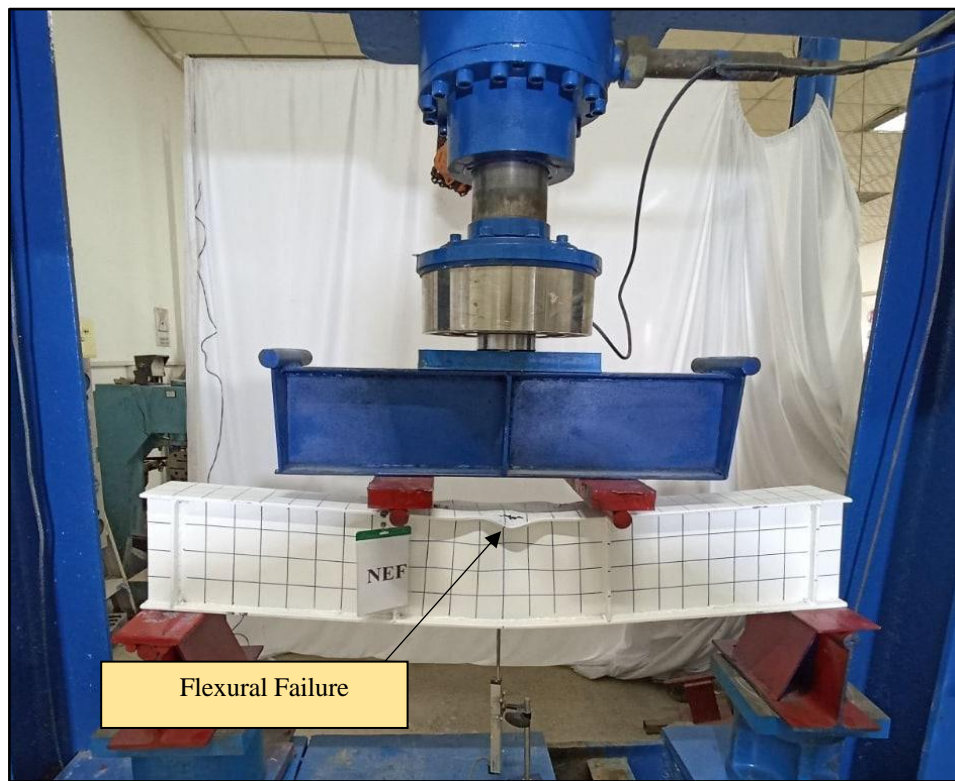


Figure 4-14: NEF During the Laboratory Examination.

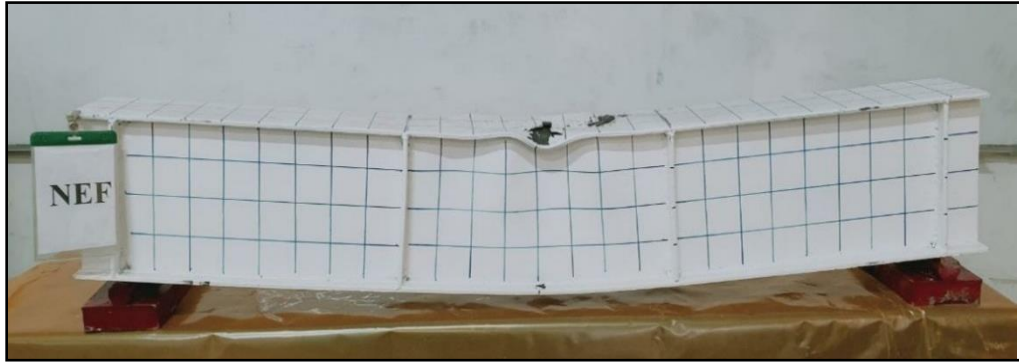


Figure 4-15: Failure Mode for NEF.

4.3.2.3. Normal Concrete Beam, Full-Filled (NFF)

This specimen was enhanced by the middle and edges web zones filling technique. The load was applied gradually to the specimen. However, in the progress of the loading process, the beam NFF failed at a load applied of 497.88 kN due to flexural, as shown in Figure (4-17). It is worth mentioning that the load capacity of this specimen increased effectively, which might result from the significant effect of the containment of concrete in the web area of the NFF specimen, which leads to an increase in the ultimate capacity. Therefore, the structural behavior for this specimen has been improved due to the increment that happened in the ultimate load compared to CB, as shown in Figure (4-16). Based on data from the load-deflection curve, it has also been noted that the structural behavior of this specimen improved due to the increase in the ductility index and stiffness, which were 14.03 and 78.2 kN/mm, respectively.

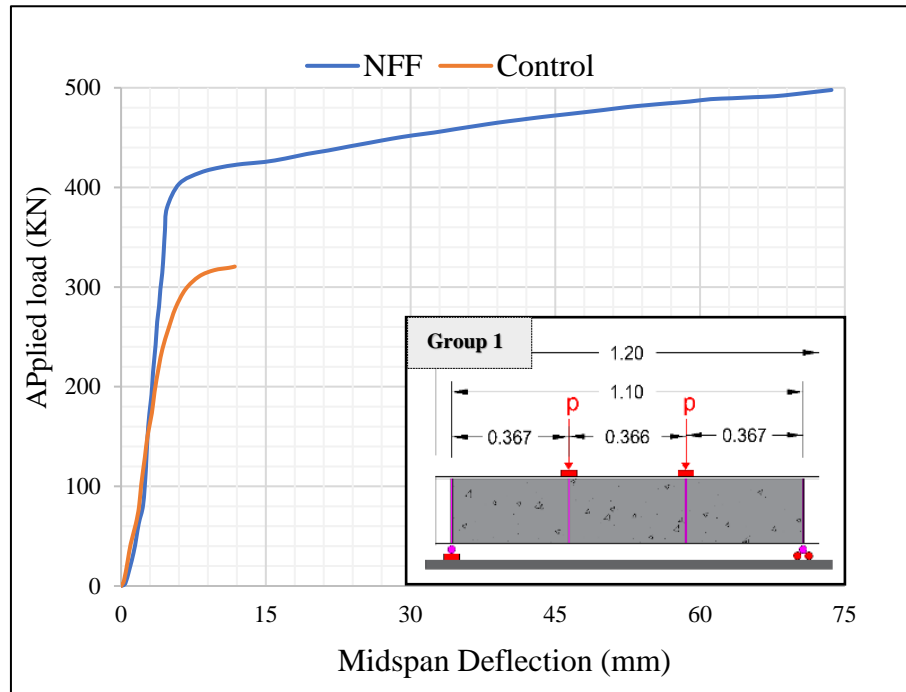


Figure 4-16: Load-Deflection Curve For NEF.

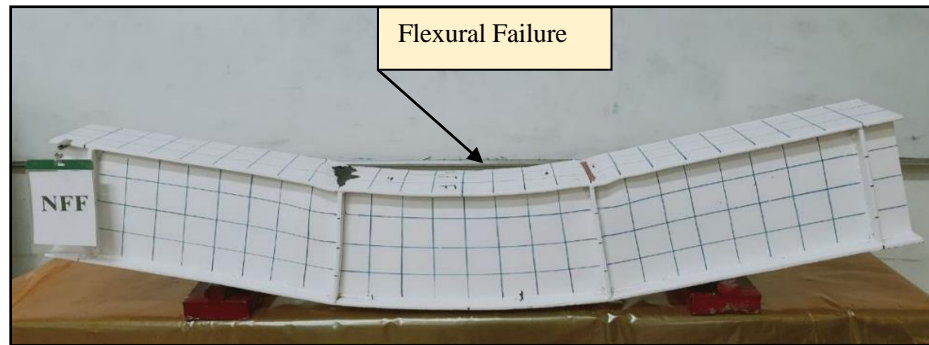


Figure 4-17: Failure Mode for NFF.

4.3.3. Doble Web Beams Filled with Recycled Aggregate Concrete (RAC) (Group 2)

The second group contains three specimens with the same properties as steel. These specimens were divided according to the part filled with recycled

aggregate concrete (RAC). (middle ,two sides , fully beam), as we will explain below.

4.3.3.1. Recycled Aggregate Concrete Beam, Middle-Filled (RMF)

This specimen was enhanced by the middle web zone filling technique at one-third of the RMF length. Two loads were gradually applied to the specimen, and the deflection was measured for each load step value, as shown in Figure (4-19) specimen RMF during the laboratory examination. This specimen failed at a load of 351.12 kN due to global web shear buckling, as shown in Figures (4-20) failure mode for RMF specimen. When compared to the control beam, the ultimate load and deflection can go up by up to 9.52 % and 6.5 %, as shown in Figures (4-18) respectively. Furthermore, the failure mode was not changed, it increases the flexural resistance, stiffness, and area under the curve of composite double web. Because the middle section was made stronger by filling it with recycled aggregate concrete, the web area was made stronger.

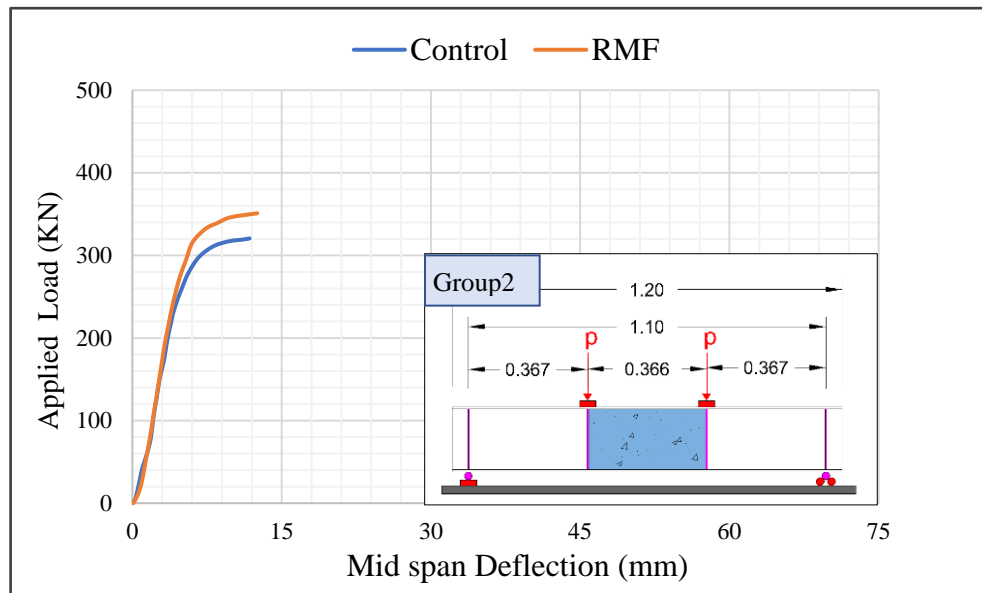


Figure 4-18: Load-Deflection Curve For RMF.



Figure 4-19: Specimen RMF During the Laboratory Examination.

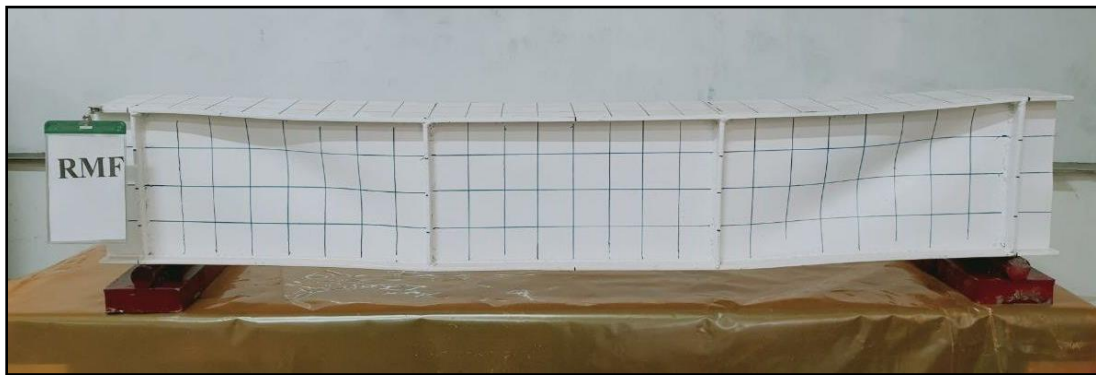


Figure 4-20: Failure Mode for RMF.

4.3.3.2. Recycled Aggregate Concrete Beam, Two Sides-Filled (REF)

This beam has recycled aggregate concrete in the two sides. Figure (4-22) illustrates the beam REF during the loading procedure. has been from the load-deflection curve in Figure (4-21) that the ultimate load of this beam is 386.05 kN, which is larger than that for a control beam of around 20.4 %. The deflection at maximum load was 33.42 mm, which is larger than the control beam. However, the failure mode was also changed from shear buckling to flexural, as shown in Figure (4-23), because the side parts were made stronger by filling them with recycled aggregate concrete, and the web area was also made stronger. This will increase the flexural resistance, ductility index, stiffness, and toughness of the composite double web beam, where the ductility index and stiffness are 5.34 and 61.47 kN/mm, respectively.

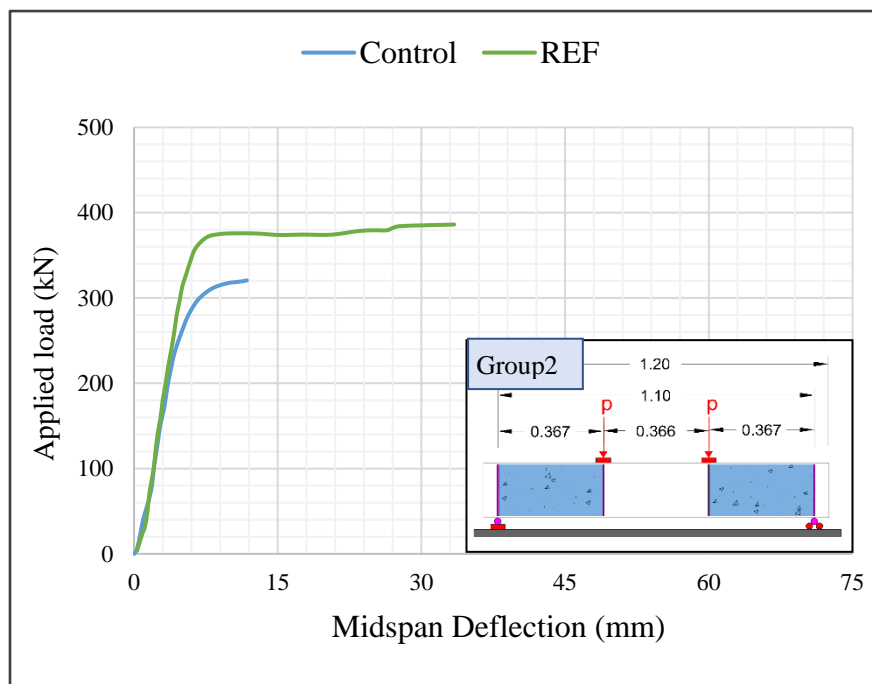


Figure 4-21: Load-Deflection Curve For REF.

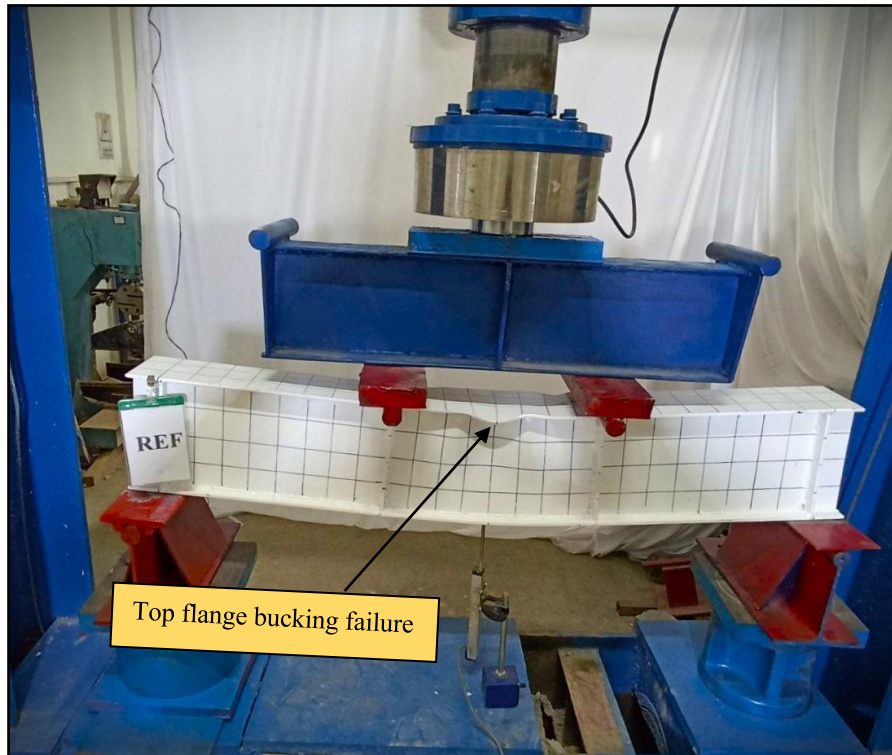


Figure 4-22: Specimen REF During the Laboratory Examination.

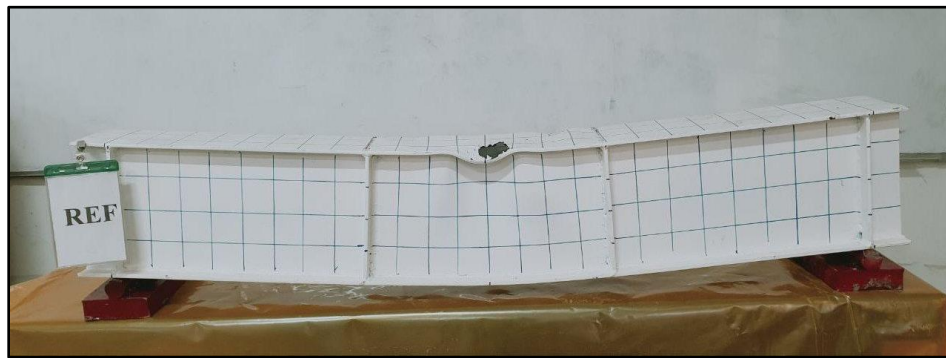


Figure 4-23: Failure Mode for REF Specimen.

4.3.3.3. Recycled Aggregate Concrete Beam, Full-Filled (RFF)

This specimen was enhanced by the middle and edges web zones filling technique. The load was applied gradually to the specimen; however, during the progress of the loading process, as shown in Figure (4-25), the beam RFF failed at a load applied of 455.34 kN due to flexural, as shown in Figure (4-26). It is worth mentioning that the load capacity of this specimen increased effectively, which might result from the significant effect of the containment of concrete in the web area of the RFF specimen, which leads to an increase in the ultimate capacity. Therefore, the structural behavior for this specimen has been improved due to the increment that happened in the ultimate load compared to CB, as shown in Figure (4-26). Based on data of the load-deflections curve, it has also been noted that the structural behavior of this specimen improved due to the increase in the ductility index and stiffness, which were 10.08 and 60.5 kN/mm, respectively.

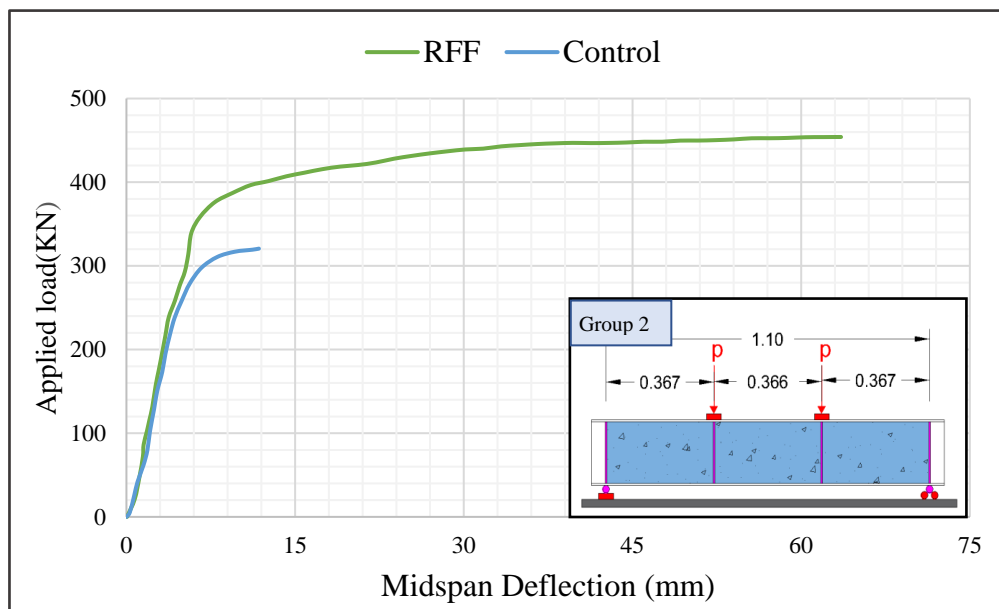


Figure 4-24: Load-Deflection Curve For RFF.

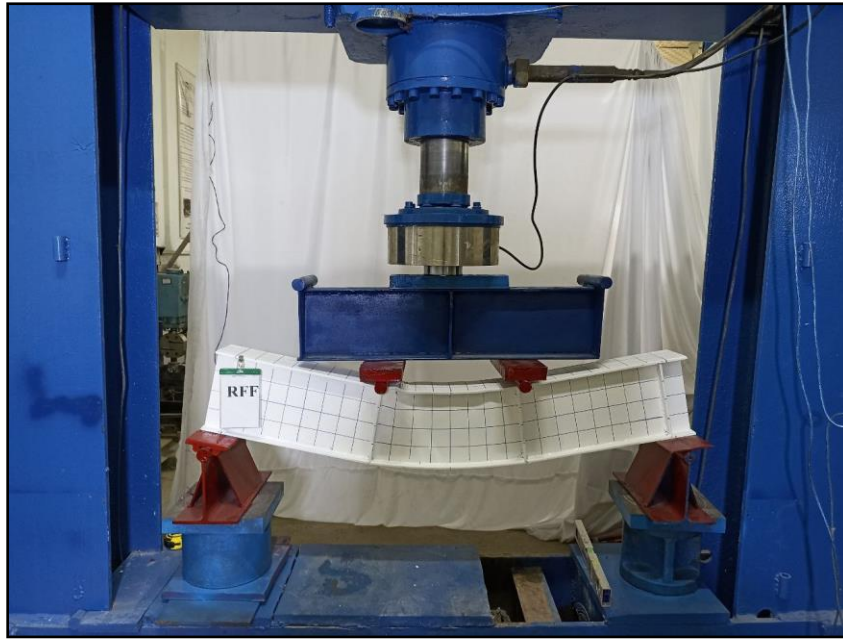


Figure 4-25: Specimen RFF During the Laboratory Examination.

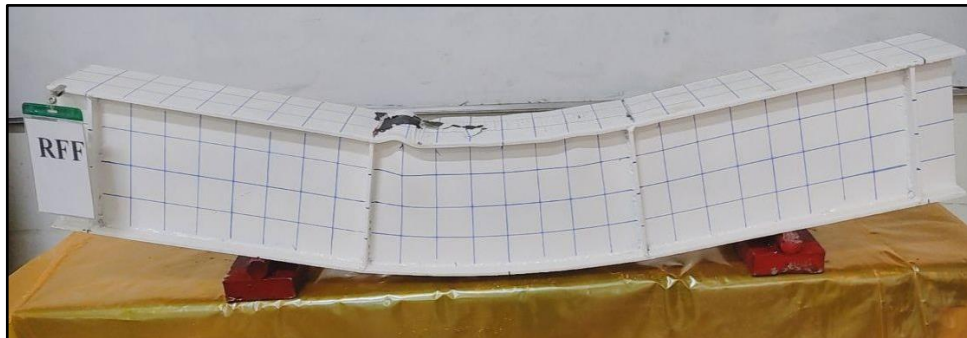


Figure 4-26: Failure Mode for RFF Specimen.

4.4. Discussion of Results

This part shows a discussion and comparison of I-double web specimens filled with normal concrete (first group) and recycled concrete (second group) with the hollow specimen in terms of percentages of increase in load and displacement for each group and failure and conversion modes. As well as discussing the increase in the index of ductility and stiffness. Where is ductility index, the ability to resist inelastic deformation without a reduction in ultimate load until failure, It is calculated from the equation:

$$DI = \frac{\Delta u}{\Delta y} \quad (4-1)$$

Where:

Δy : deflection at service load.

Δu : ultimate deflection at ultimate load.

In addition, the stiffness (K) of a body is a measure of the resistance offered by an elastic body to deformation. It is calculated from the equation:

$$k = \frac{Ps}{\Delta s} \quad (4-2)$$

Ps = service load value .

Δs = deflection at service load.

4.4.1. Beams Filled with Normal Concrete (N.C)

This set contains three double web specimens filled with normal concrete in the web area in the middle, edges, or the whole specimen. The location of normal concrete in the web area has a significant impact on the structural performance of composite double web samples, causing an increase in the final load. The NMF, NEF, and NFF specimens exhibit an increase in the load, the final percentages are 10.19 %, 24.6 %, and 55.30 %, respectively, when compared with the reference sample. The normal concrete infill had a positive impact on the ultimate shear capacity as it stiffened the web and delayed the shear buckling, thereby increasing the ultimate shear capacity. The failure mode in the middle-filled specimen was shear buckling in the web, while the side-filled specimen was top flange buckling, and the fully-filled specimen failed to flexure, as shown in Table (4-1) and Figure (4-27).

Compared to the double web without concrete (control beam), the ductility index of the specimen filled with sides and the specimen filled in its full increased by up to 149 % and 568 %, respectively, as shown in Table (4-2) and Figure (4-28). And it was observed that the stiffness of the composite double web beams increased by (2.67 % to 39.6 %) as shown in Table (4-3) and Figure (4-29), where the normal concrete filling prevents double web steel local buckling and contributes to the section's inertia and internal forces, which increase the flexural strength and stiffness of the member.

4.4.2. Beams Filled with Recycled Aggregate Concrete.

This package includes three double web specimens filled with recycled aggregate concrete in the centre, on the sides, or across the whole sample. In cases where the position of recycled aggregate concrete in the web region has a significant effect on the structural performance of composite double web specimens, resulting in an increase in the ultimate load, the ultimate proportions for the RMF, REF, and RFF specimens are 9.52 %, 20.60 %, and 42.03%, respectively, when compared to the reference sample. By strengthening the web and delaying shear buckling, conventional concrete infill improved the final shear capacity. As shown in Table (4-1) and Figure (4-27), the failure mode of the middle-filled sample was shear buckling in the web, while the failure mode of the side-filled sample was top flange buckling and the failure mode of the fully-filled sample was flexure.

The ductility indicators of the specimen filled with sides and the specimen filled full increased by up to 154 % and 380 %, respectively, as compared to the double web without concrete (control beam), as shown in Table (4-2) and Figure (4-30). and the stiffness index of the composite double web beams increase from (2.67 % to 39.6 %), as shown in Table (4-3) and Figure (4-29). Recycled aggregate concrete infill prevents the steel shell from local buckling and adds to the section inertia and internal forces, which raise the flexural strength and stiffness of the member

Table 4-1: The Load Capacity for The Tested Beams

Group number	Specimen	Ultimate strength (fu) kN	Ultimate load ratio %	Failure mode
Control	CB	320.59	-----	Shear buckling in web
Group 1	NMF	353.1	10.19	Shear buckling in web
	NEF	399.7	24.6	Top flange bucking failure
	NFF	497.88	55.30	Flexural failure
Group 2	RMF	351.12	9.52	Shear buckling in web
	REF	386.05	20.4	Top flange bucking failure
	RFF	455.34	42.03	Flexural failure

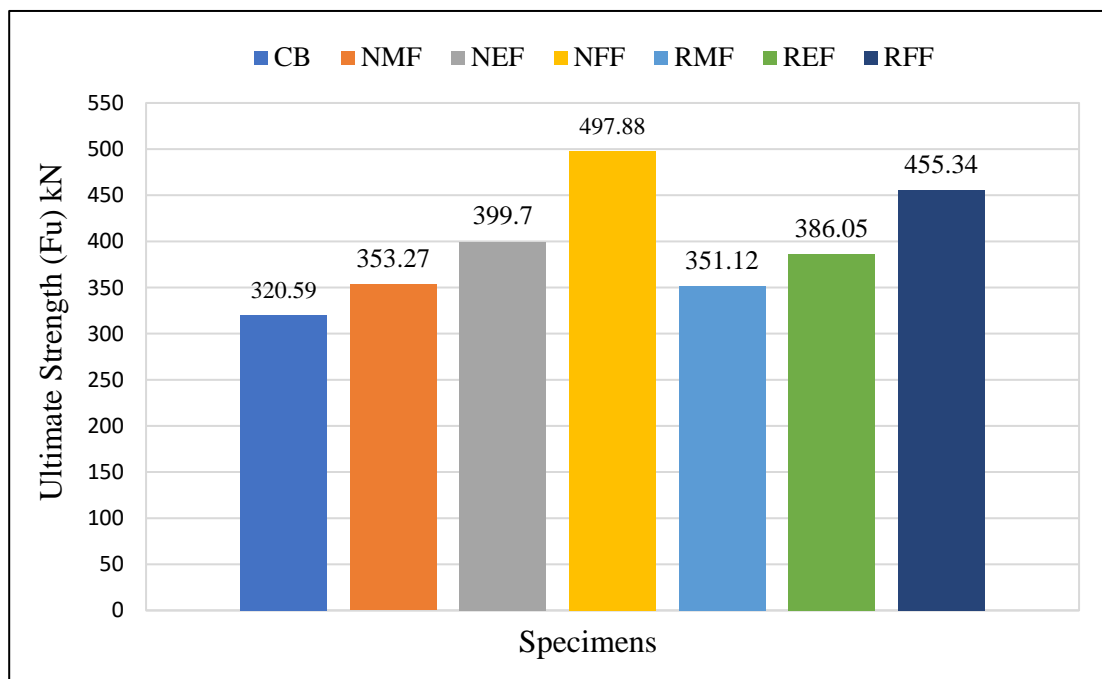


Figure 4- 27: A Comparison in Load Capacity for Tested Beams

Table 4-2: The Ductility Index for The Tested Composite Beams.

No. Group	Specimen	Yielding Displacement	Ultimate displacement (mm)	Ductility index $DI = \Delta u / \Delta y$	Increase in Ductility Ratio $\Delta \%$
Control Beam	CB	5.60	11.78	2.10	-----
Group 1	NMF	5.9	12.14	2.05	N/A
	NEF	6.1	32.06	5.24	149
	NFF	5.2	73	14.03	568
Group 2	RMF	5.75	12.55	2.18	N/A
	REF	6.25	33.42	5.34	154
	RFF	6.30	63.52	10.08	380

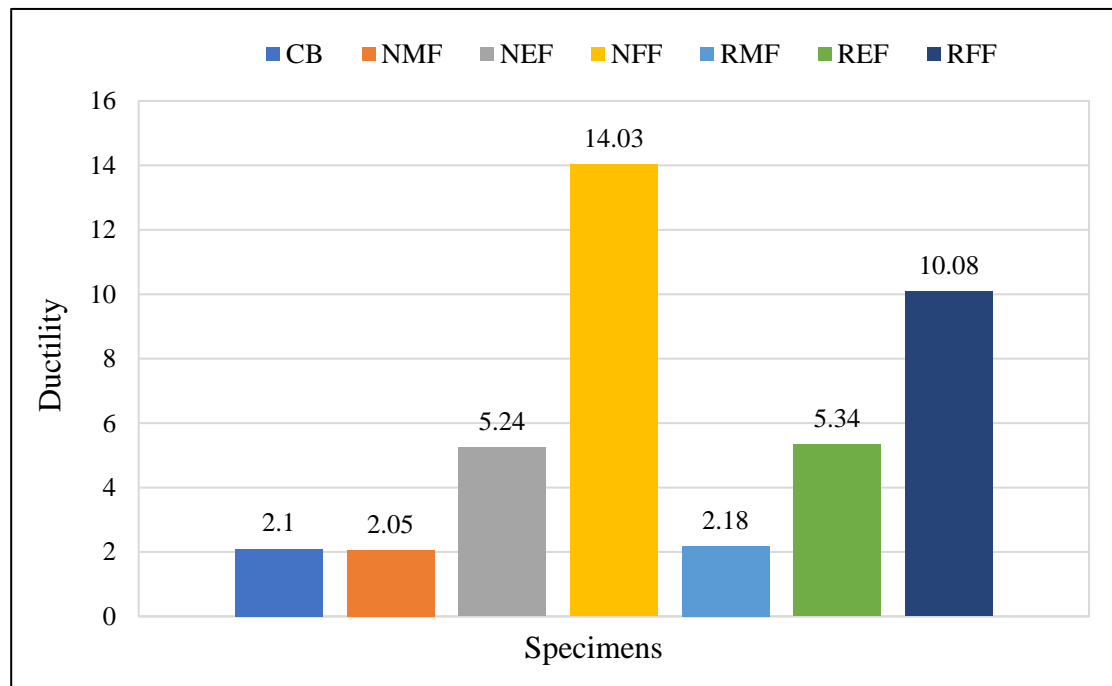


Figure 4- 28: A Comparison in Ductility Factor for Tested Beams.

Table 4-3: The Stiffness For The Tested Composite Beams

No. Group	Specimen	Service Load (FS)	Ultimate displacement at service load (Δy) mm	Stiffens at service load KN/mm $K = \frac{FS}{\Delta y}$	Increase in Stiffness Ratio $\Delta \%$
Control Beam	CB	240.44	5.60	56	-----
Group 1	NMF	264.95	5.90	57.5	2.67
	NEF	299.77	6.10	60.8	8.57
	NFF	373.41	5.20	78.2	39.6
Group 2	RMF	263.34	4.50	58.52	4.5
	REF	289.53	4.71	61.47	9.76
	RFF	341.50	5.65	60.5	8.03

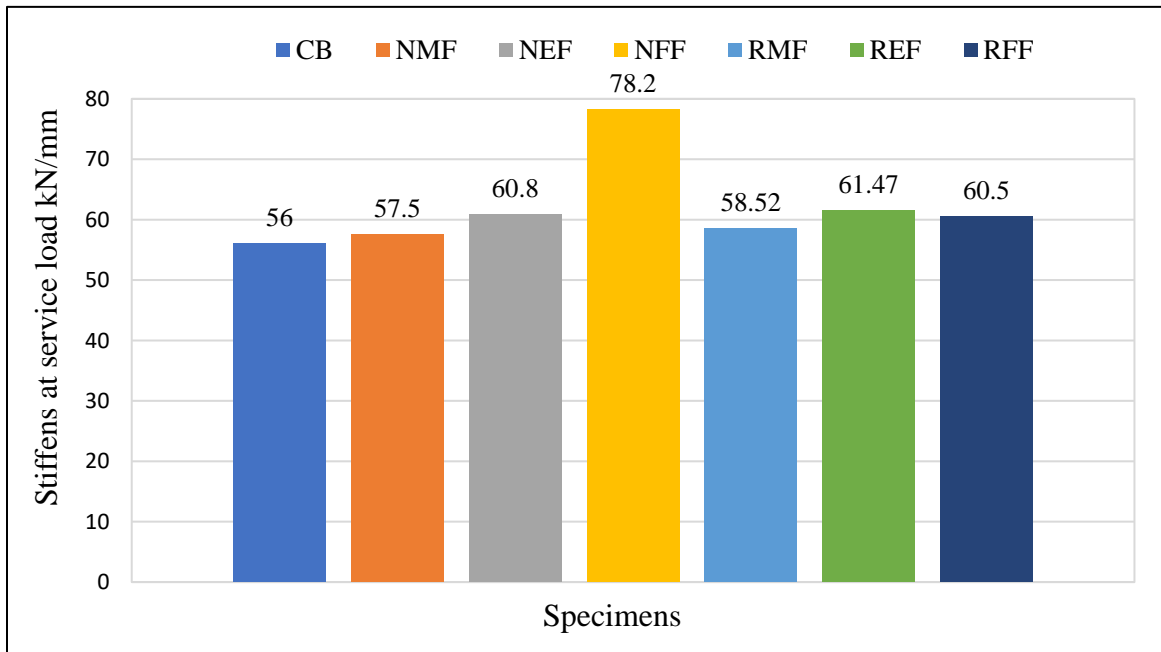


Figure 4- 29:A Comparison in Stiffness Criteria for Tested Beams

4.5. Experimental Work Summary

The following conclusions are drawn from the experimental results of ultimate load, deflection, and failure mode of the specimens studied:

1-Using normal and recycled concrete as fill materials for doubly web sections could increase the maximum load capacity and deflection of the beam if compared to the control double web (hollow beam).

2-Filling side parts of the double web section almost modify the failure mode to flexural failure from web shear failure.

3- The concrete infill materials considerably enhance the region web and reduces the buckling of the double-web beams.

4- The difference in concrete compressive strength has an effect on the capacity, ductility index, and overall flexural and shear behavior of double web beams.

5- The concrete waste material can be used instead of natural gravel to infill the I-doubly web steel beam.

6-The normal and recycled concrete infill had a positive impact on the ultimate shear capacity as it stiffened the web and delayed the shear buckling, thereby increasing the ultimate shear capacity.

7- Concrete filling prevents the local buckling of the steel shell, and it also contributes to the inertia of the section and internal forces, which increases the flexural strength and stiffness of the member.

Chapter Five. FINITE ELEMENT ANALYSIS

CHAPTER FIVE

FINITE ELEMENT ANALYSIS

5.1. Introduction

This chapter intends to construct a model based on experimental results found in chapter four using non-linear finite elements to guarantee that material properties, shape elements, and affinity criteria are acceptable for modelling and response for adoubly web section filled with normal and recycled concrete. Using the validated model and the nonlinear finite element method (ABAQUS/Standard 2021), other variables were also looked at in terms of how they affect the structure.

5.2. Types of Elements

The accuracy of the three-dimensional analysis is determined by the activity of any members constituent elements. For modelling different structural materials, Abaqus includes many elements that may simulate heterogeneous and homogeneous materials. Figure (5-1) shows a three-dimensional element of eight nodes C3D8R (solid) with three degrees of freedom in each node employed in modelling thick steel plates.

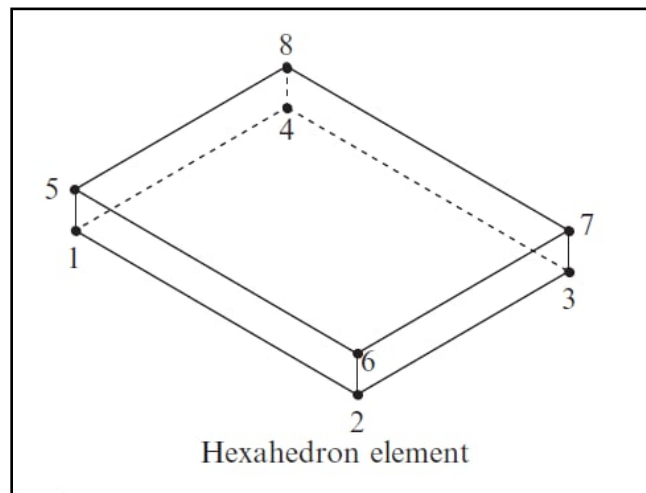


Figure 5-1: Node Solid Element (Ellobody, 2013).

In addition, as described in Figure (5-2), the thin steel plates were modelled using a four-node, three-degree-of-freedom S4R (Shell) element. Table (5-1) provides a summary of the element thicknesses for each specimen portion.

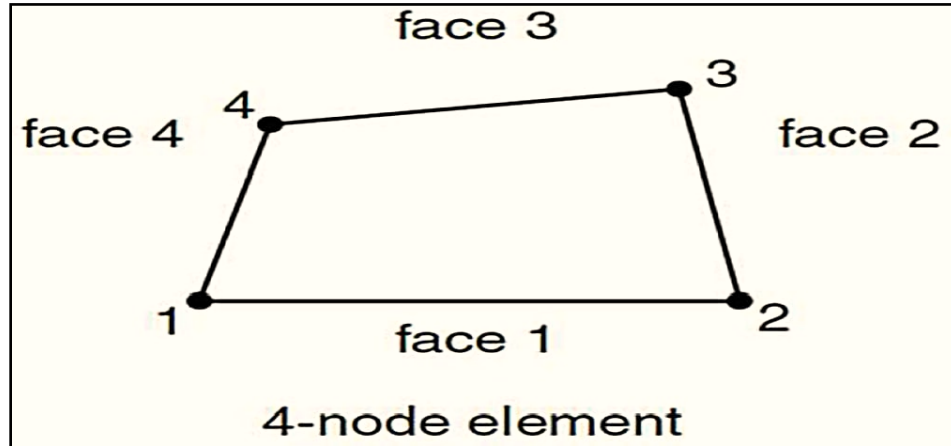


Figure 5-2: Node Shell Element (Ellobody, 2013).

Table 5-1: Thicknesses and Types of Elements.

Part	Thickness (mm)	Element type
Plate Flange	6mm	Shell(S4R)
Plate Web	3mm	Shell(S4R)
Stiffener	6mm	Shell(S4R)
Supports and Loading Plates	----	Solid(C3d8R)
Concrete Block	-----	Solid (C3d8R)

5.3. Description of Finite Element Modelling

5.3.1. Modeling Parts of Specimens

All the double web steel beam in this study consists of the following parts (top and bottom flange and middle web), steel rod, and each part of the steel beam is draw separately and then assembled and combined to obtain a double web steel beam. Figure (5-3) shows the assembly of the parts in the modeling of the samples.

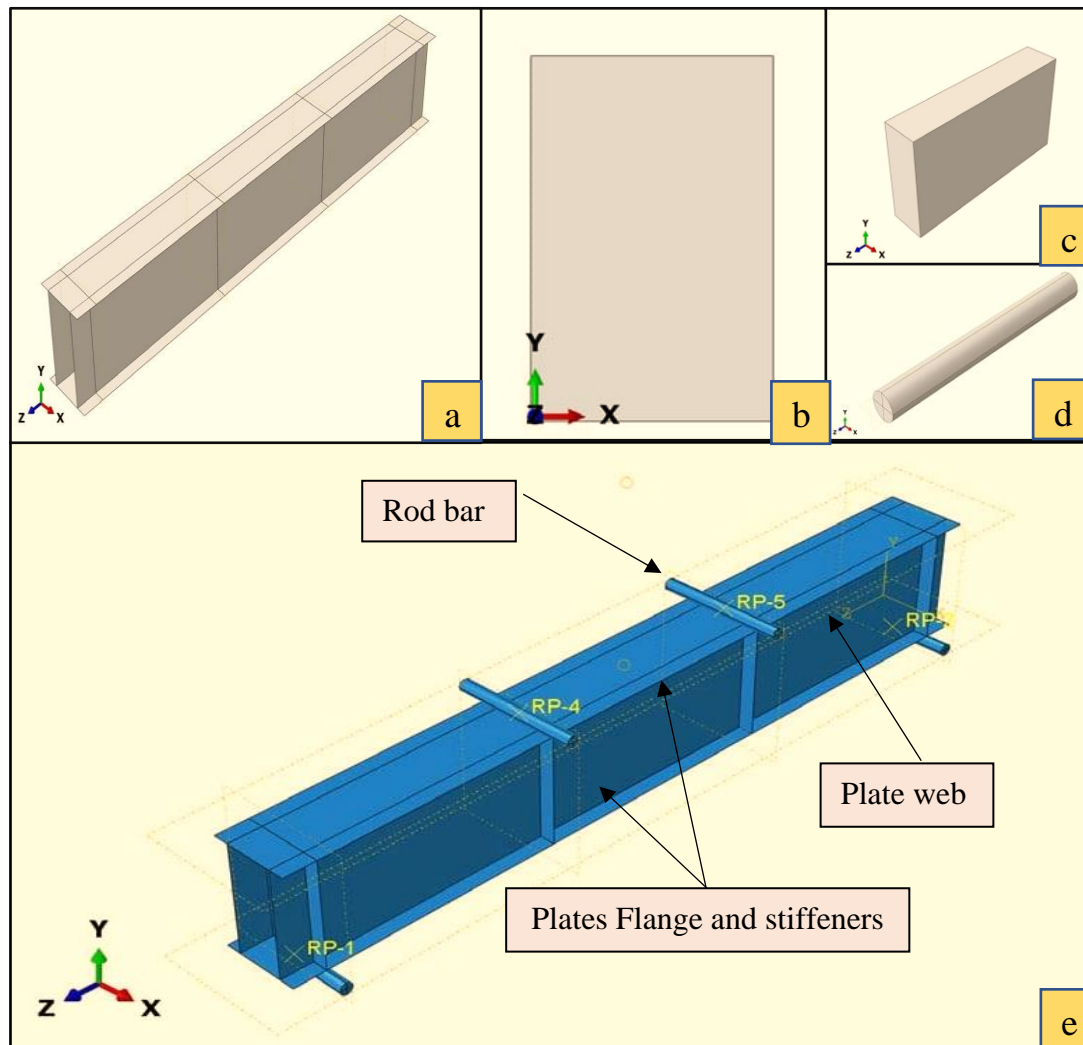


Figure 5-3: Assembling The Over All Parts of Composite Double Web Specimen
 a- double web without Stiffener. b- Stiffener Plate. c- Concrete Block.
 d- steel rod. e- composite double web.

5.4. Materials Properties

5.4.1. Steel Plate Model

The results of the coupon tensile test described in the experimental work chapter were used to model the steel materials used in the paired web sample for all of its components. Steel is a homogeneous material with the same stress and compressive properties in tension and compression. Table (5-2) shows the properties used in material modeling.

Table 5-2: Steel Characteristics Used in The Analysis.

Density (ton/mm ³)		
7.8×10 ⁻⁹		
Elastic zone properties		
Young's Modulus (Es)	Poisson's Ratio(ν s)	
1.9E+5 (MPa)	0.3	
Plastic zone Properties		
Plate thickness(mm)	Yield Stress (MPa)	Plastic Strain (mm/mm)
Flange + Stiffener	279	0.29
Web	293.6	0.29

5.4.2. Concrete Model

The stress-strain curve of unconfined concrete is shown in Figure (5-4), where σ_c is the concrete's unconfined ultimate cylinder compressive strength and ϵ_c is the corresponding strain. In the double web steel sample, the concrete is

confined by the web zone steel tube section, which results in increased ductility and strength of the concrete core compared to unconfined concrete.

In the current study, the stress-strain response of confined concrete proposed by **(Hu et al., 2003)** is adopted in the numerical simulations. This approach has been adopted by other researchers for the simulation of concrete-filled tubular columns, which are eccentrically loaded, leading to non-uniform confining pressure, as occurs in the current scenario **(Ellobody, 2013, Lee et al., 2011)**. Typical uniaxial stress-strain curves of unconfined concrete are shown in Figure(5-4), where f'_{cc} and ϵ'_{cc} are the uniaxial compressive strength and the corresponding strain of confined concrete, respectively. **Mander et al. (1988)** proposed relationships between confined and unconfined concrete strength and strain values, as given by Eqs. (5-1) and (5-2), respectively.

$$f'_{cc} = f'_c + k_1 f_1 \quad (5-1)$$

$$\epsilon'_{cc} = \epsilon'_c \left(1 + k_2 \frac{f_1}{f'_c} \right) \quad (5-2)$$

Values of 4.1 and 20.5 are used for **k1** and **k2**, respectively, based on the study of **(Richart et al., 1928)**. The term ' f_1 ' denotes the confining pressure in the concrete which is determined in the current study based on the empirical relationships presented in Equations (5-3) and (5-4) proposed by **(Hu et al., 2003)**.

$$\frac{f_1}{f_y} = 0.055048 - 0.001885 \left(\frac{B}{t} \right) \quad \left(17 \leq \frac{B}{t} \leq 29.2 \right) \quad (5-3)$$

$$\frac{f_1}{f_y} = 0 \quad \left(29.2 \leq \frac{B}{t} \leq 150 \right) \quad (5-4)$$

B= Overall width.

t=steel thickness

The stress-strain curve of confined concrete, as presented in Figure (5-4), consists of three parts. The first part represents the elastic range to the

proportional limit stress, which can be taken as $0.5 f'_{cc}$ (**Hu et al., 2003**). This part defines in ABAQUS by providing the elastic modulus (E_{cc}) and Poisson's ratio (ν_{cc}) of a specific material. The initial Young's modulus can be reasonably calculated using the empirical equation (5-5) given by (**ACI-318, 2019**), whereas the value of Poisson's ratio of confined concrete is taken as 0.2 (**Ellobody, 2013**).

$$E_{cc} = 4700 \sqrt{f'_{cc}} \quad (5-5)$$

The second part of the stress-strain curve defines the nonlinear behaviour before the concrete reaches its maximum strength, starting from the proportional limit ($0.5 f'_c$) to the maximum confined concrete strength f'_{cc} . The relationship of concrete stress f_c and strain ε in this part of the response was proposed by (**Saenz, 1964**) and is as described by Eqs. (5-6) to (5-8)

$$f_c = \frac{E_{cc} \varepsilon_c}{1 + (R + RE - 2) \left(\frac{\varepsilon_c}{\varepsilon'_{cc}} \right) - (2R - 1) \left(\frac{\varepsilon_c}{\varepsilon'_{cc}} \right)^2 + R \left(\frac{\varepsilon_c}{\varepsilon'_{cc}} \right)^3} \quad (5-6)$$

$$RE = \frac{E_{cc} \varepsilon'_{cc}}{f'_{cc}} \quad (5-7)$$

$$R = \frac{RE(R_\sigma - 1)}{(R_\varepsilon - 1)^2} - \frac{1}{R_\varepsilon} \quad (5-8)$$

Where: R_ε and R_σ were both assumed to be 4.0, in accordance with the recommendations by **Hu and Schnobrich (1989)**.

Finally, the third part of the curve is the descending branch which begins at the maximum confined concrete strength f'_{cc} and decreases linearly until the stress of ($k3 f'_{cc}$) is reached at a corresponding strain of ($11 \varepsilon'_{cc}$). For the

parameter k_3 , Where the value of k_3 can be calculated from the following equations(4-9) and (4-10) proposed by **Hu et al. (2003)**.

$$k_3 = 0.000178 \left(\frac{B}{t}\right)^2 - 0.02492 \left(\frac{B}{t}\right) + 1.2722 \quad 17 \leq B/t \leq 70 \quad (5-9)$$

$$k_3 = 0.4 \quad 70 \leq B/t \leq 150 \quad (5-10)$$

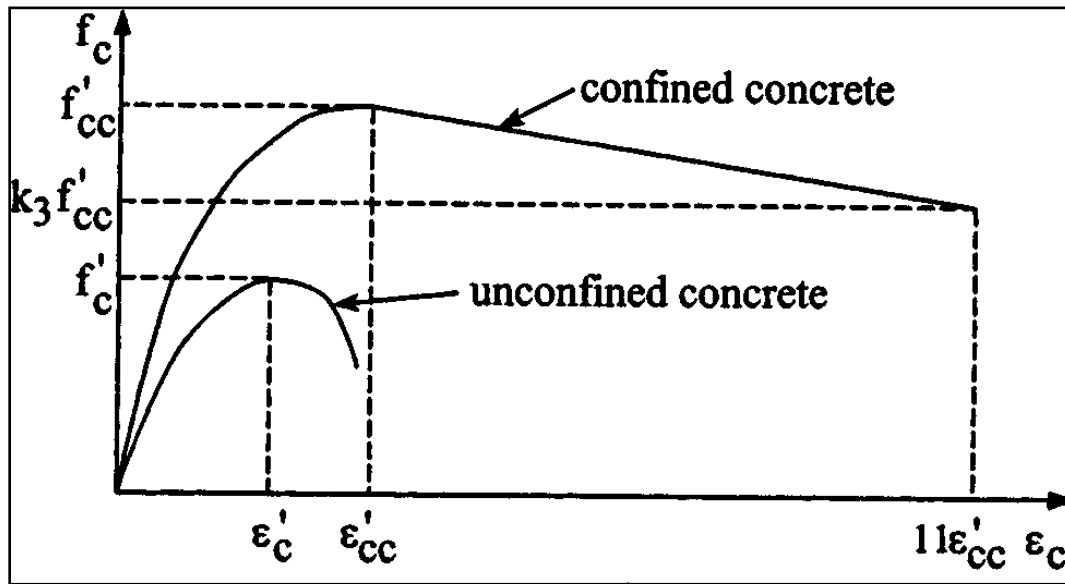


Figure 5-4: Equivalent Uniaxial Stress-Strain Curve for Concrete (**Hu et al., 2003**).

The damage plasticity model provided by ABAQUS is used to simulate the concrete material behavior. The second and third parts of the concrete stress-strain curve were introduced using the damage plasticity model. The tensile and compressive response of concrete is assumed to be characterised by damaged plasticity in this model. It was previously mentioned that the response of concrete under uniaxial compression is linear until it reaches the value of proportional limit stress, whereas it follows a linear elastic relationship until it reaches the failure stress under uniaxial tension.

Other factors in the model that should be carefully determined include potential flow eccentricity (ϵ), which was set to 0.1. And then, there is the (f_{b0}/f_{c0}) ,

which is a ratio of initial equibiaxial compressive yield stress to initial uniaxial compressive yield stress, with a default value of 1.16. Additionally, for any defined value of the pressure invariant at the beginning yield, the ratio of the second stress invariant in the tensile meridian to the compressive meridian. It was created to describe concrete's multi-axial behavior and is about in ABAQUS, the default value is 2/3. Finally, the viscosity parameter (μ) was utilized at 0. Summary Table (5-3) shows the parameters used in concrete damage plasticity for normal and recycled concrete.

Table 5-3: Concrete Damage Plasticity Parameters

Parameter	Selected value
ψ	36°
ϵ	0.1
f_{bo} / f_{co}	1.16
K	2/3
μ	0

The behavior and properties of the material concrete used in this study are shown in **Appendix B**.

5.5. Finite Element Modeling Interaction

After the parts are assembled and their properties defined, they must be connected together to operate a composite system. The contact between the steel section and the concrete in-filled was modelled using the contact algorithm option available in ABAQUS. To introduce the contact algorithm, ABAQUS requires the master and slave surfaces to be specified. It is necessary to follow the rules in the selection of these surfaces, which are the slave surfaces should be the more finely meshed surface and the softer underlying material. The master surface within this model is introduced as the stainless steel surface confining the concrete infill that is the slave surface. The contact

interaction controls the normal and tangential stress behavior of surfaces. In the normal direction, the default ABAQUS option of hard contact was used, whereas, in the tangential direction, the isotropic penalty formulation was used throughout this study. The penalty model requires the definition of the coefficient of friction, which is taken as 0.6.

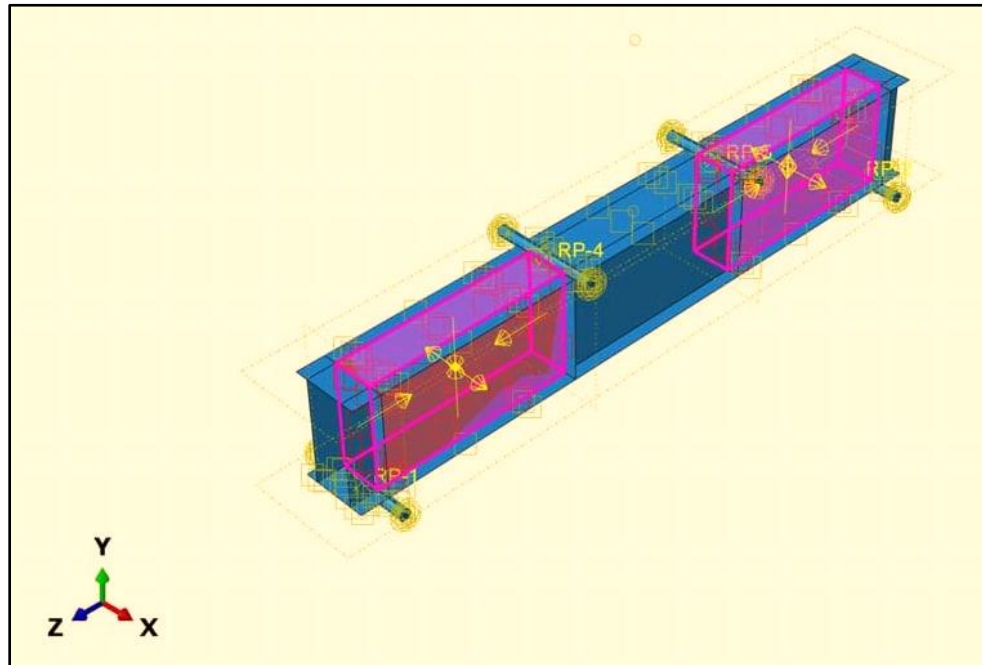


Figure 5-5: Contact type Between The Steel Section and Concrete.

5.6. Residual Stresses and Initial Geometric Imperfections

The effect of the residual stress pattern was taken in this study as a result of welding and engineering defects during the manufacture and welding of models by means of standard pre-processing tools using the PREDEFINED FIELDS option available in ABAQUS library. Depended on the study (Truong et al., 2019) where the Figure (5-6) shows the residual stress distribution of welded I-type cross-section, and Figure (5-7) shows the residual stress distribution of welded I-double web.

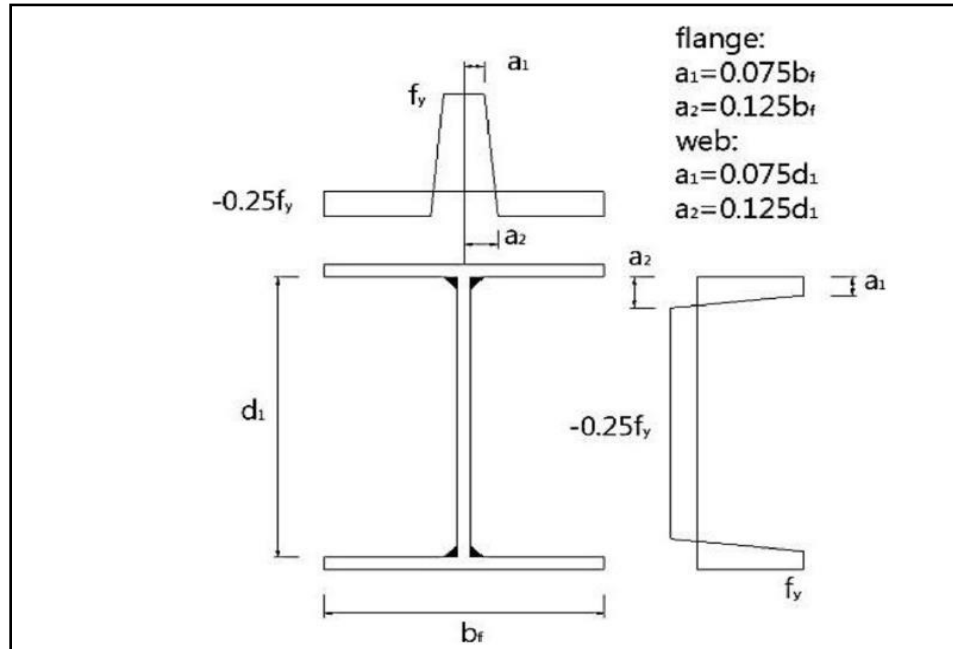


Figure 5-6: Residual Stress Distribution of Welded I-Type Cross-Section (Truong et al., 2019).

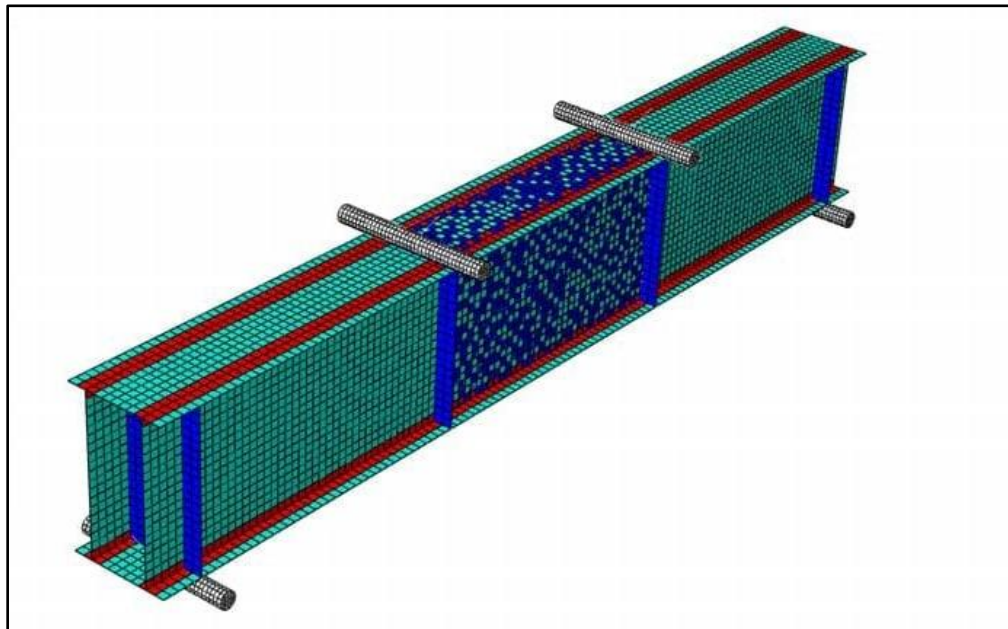


Figure 5-7: Residual Stress Distribution Of Welded I-Double Web.

5.7. Loading and Boundary Conditions

In the numerical study, loads were applied two-point on a double web with/without concrete. Two steel rods are located on the upper edge at a

distance of one-third of the length of the span from the support to transfer the loads to the tested beam, as shown in Figure (5-8).

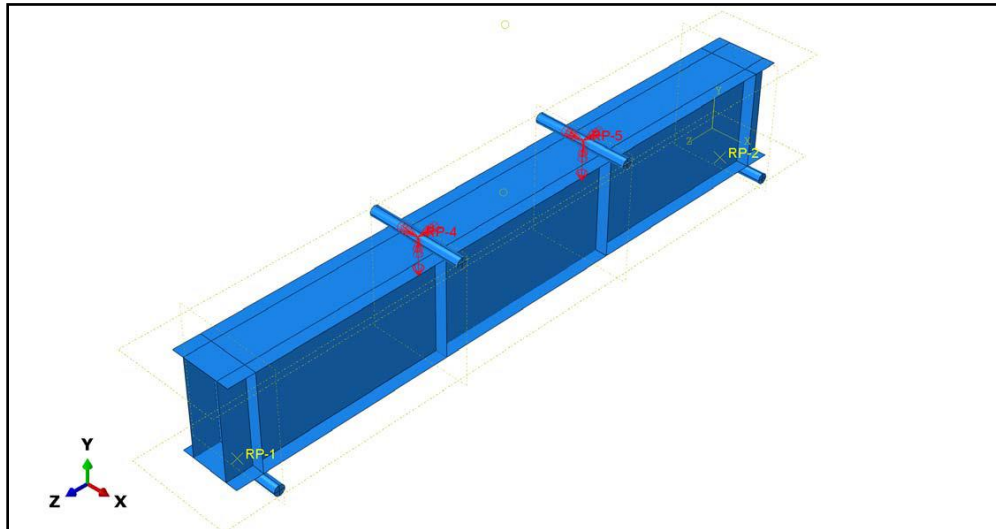


Figure 5- 8: Applied Load on I-Double Web Beam.

To achieve the appropriate solution, all-composite models were constrained by displacement of the boundary condition. At pin support, all models were constrained in the z-direction, y-direction, and x-direction ($U_z = U_y = U_x = 0$), while at roller support, all models were constrained in the x-direction and y-direction ($U_x = U_y = 0$).

5.8. Mesh Sensitive

In the finite element model, the element size selection is very important. After doing the necessary tests of different element sizes, the element size that gives the required precision was chosen. When specimens are divided into an adequate number of elements, the result has a strong convergence, which is evident when the reduced element size has minimal effect on the outcome. The mesh size of the element and the modeling type influenced the results of the analysis, including the displacement-time curve. The precision of the finite element solutions is enhanced by the tiny element size. In addition, as

illustrated in Figure (5-9). Various element sizes (10, 12, 15, 20, and 25 mm) were applied in the examination of steel convergence. As the element size decreased, the displacement increased closer, as indicated by the element size results, As displayed in Figure (5-10). The element size of 10 mm yielded the displacement values closest to the experimental results of the control beam for the remaining tested beams.

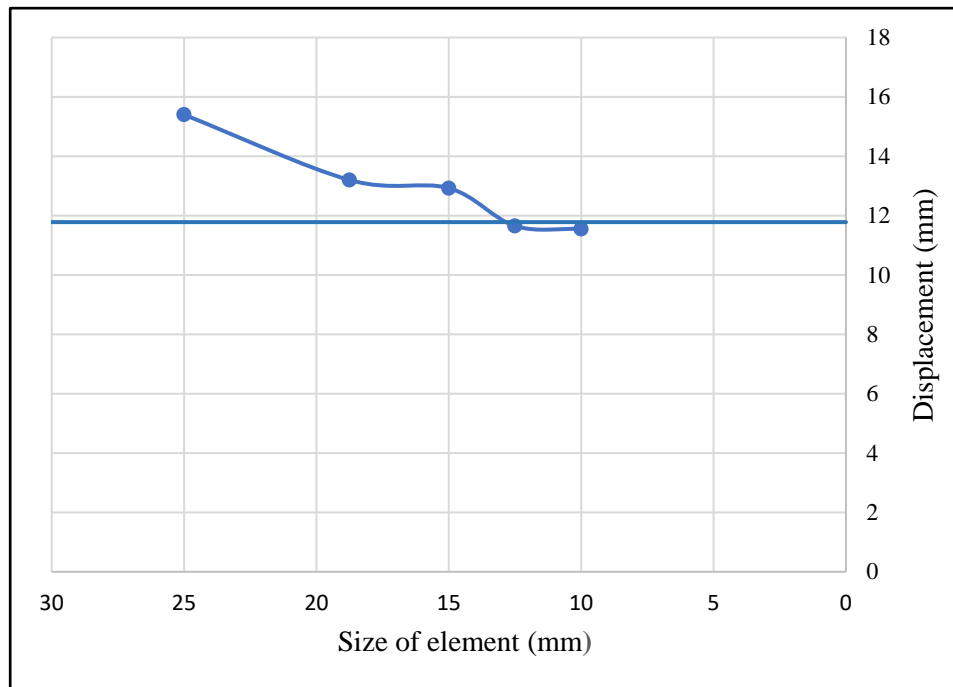
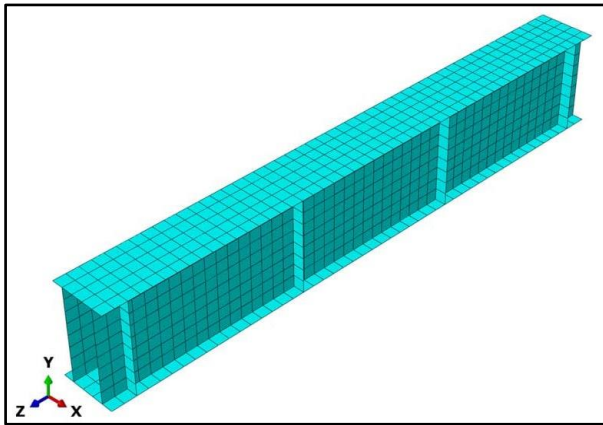
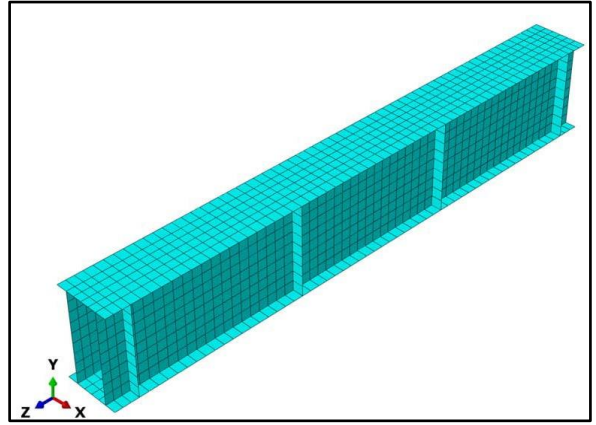


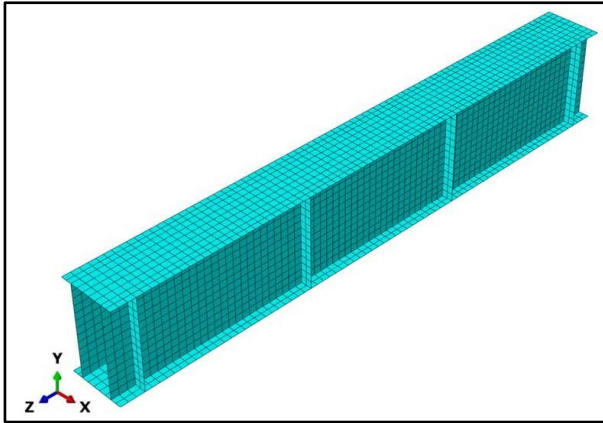
Figure 5- 9: Convergence Study Analysis.



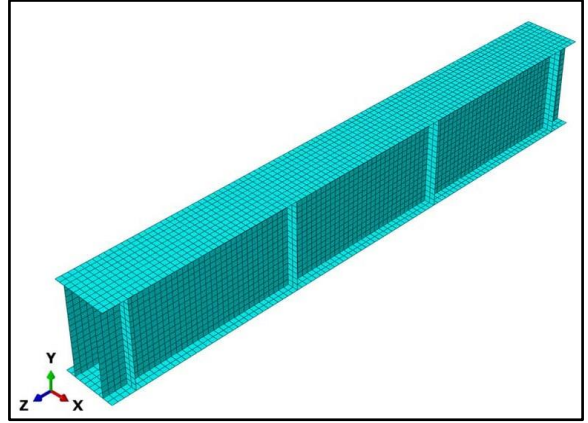
Status No.1: Element size 25 mm



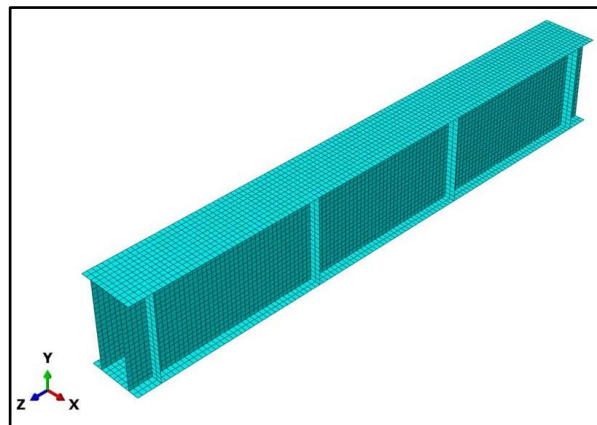
Status No.2: Element size t 20 mm



Status No.3: Element size 15 mm



Status No.4: Element size 12 mm



Status No.5: Element size 10 mm

Figure 5-10: Finite Element Mesh Density.

5.9. Analysis procedure

Because of the complex interaction between different components in a composite double web beam, convergence is always very difficult to achieve if using the General Static approach in ABAQUS. Instead, the Dynamic Implicit approach was used to accelerate convergence in this study. Since the simulation is for static tests only, there is a need to ensure that the dynamic effects are negligible in the FE analysis by comparing the kinetic energy (KE) of the whole model with the internal energy (IE) of the whole model. It was found that KE was less than 5% of IE in all cases. Therefore, it can be concluded that any dynamic effects resulting from the analysis can be ignored according to the ABAQUS User's Manual Version 6.14 (Systemes, 2014).

5.10. Comparative Study between FEM and Experimental Results

This section compares experimental and finite element results in terms of ultimate capacity, maximum displacement, failure mode, and load displacement for all tested composite beams. The comparison between the numerical analysis by ABAQUS and the experimental data presented in chapter four demonstrated the validity of the numerical analysis.

5.10.1. Result of Control Beam (CB)

A 1.2-meter-long double steel beam (control beam) was used without concrete. The ABAQUS software used and found a good convergence in the load, displacement, and failure shapes, with the percentage difference between the experimental results and the numerical values of load and displacement being roughly 2.09 % and 3.98 %, respectively. Figure (5-11) displays numerical and experimental load-deflection curves for CB. As for the failure mode, it was similar to the practical shear buckling in the web, as shown in Figure (5-12) experimental and numerical failure shape for CB.

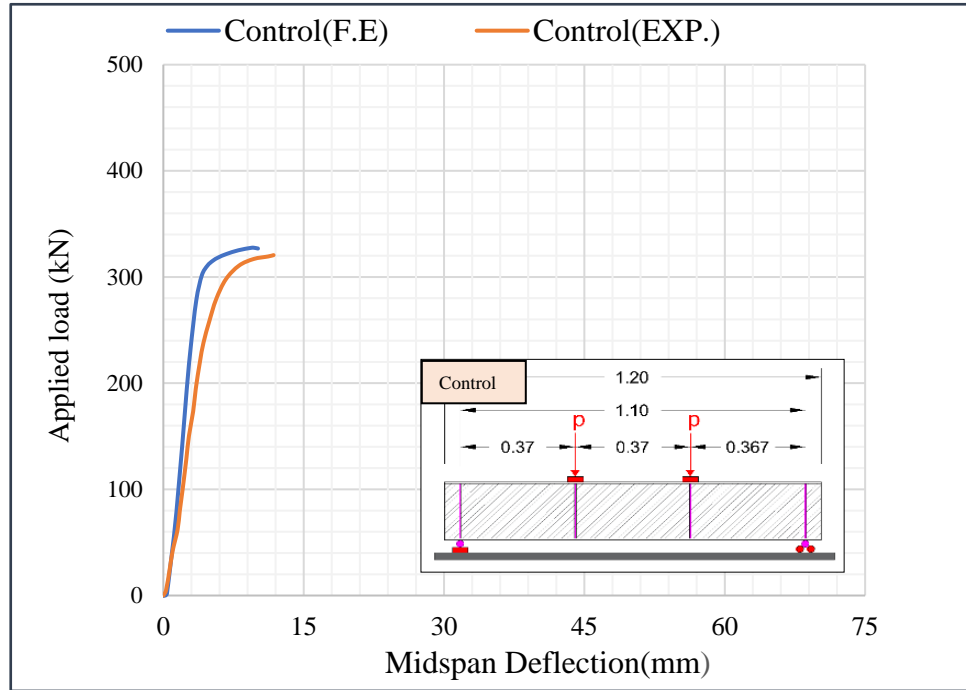


Figure 5-11: Numerical and Experimental load-deflection curves for CB.

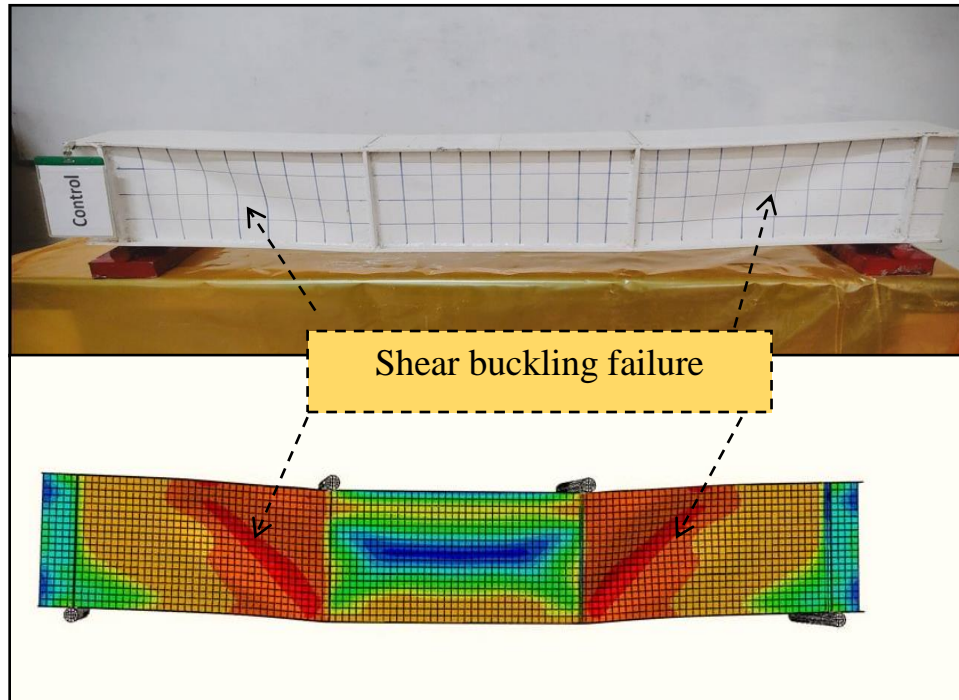


Figure 5-12: Experimental and Numerical Failure Shape for CB.

5.10.2. Result of Beam (NMF)

This specimen contains normal concrete in the middle zone of the specimen. From load-deflection curve for these double web specimen obtained by finite element analysis and experimental work is presented in Figure (5-13). The ultimate load capacity increased by about 1.4 %, and the maximum deflection increased by about 4.6 % for NMF compared with the ultimate experimental load and maximum deflection of this double web specimen. The failure mode was similar to the control beam, as shown in Figure(5-14). Concrete filler prevents local buckling in the middle area and thus increases the flexural strength and stiffness of the specimen.

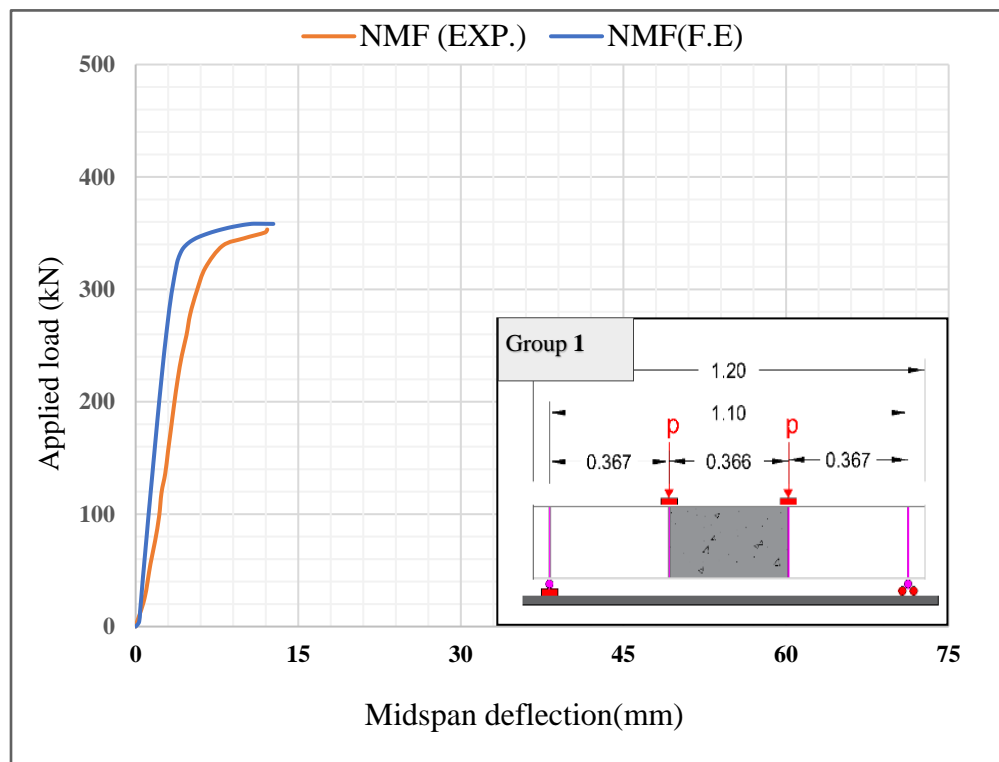


Figure 5-13: Numerical and Experimental Load-Deflection Curves for NMF.

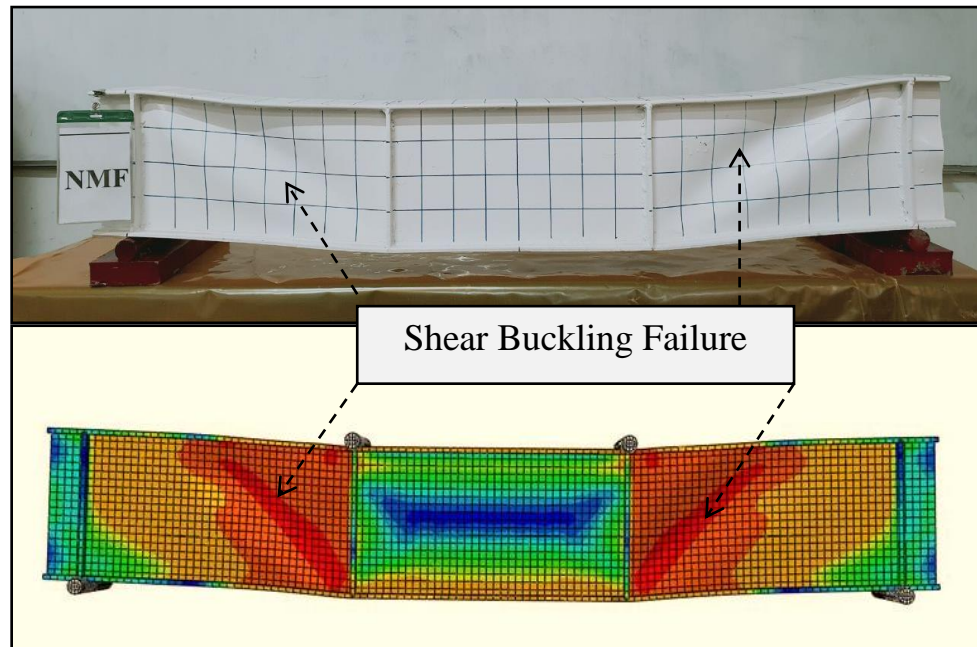


Figure 5-14: Experimental and Numerical Failure Shape for NMF.

5.10.3. Result of Double Web Beam (NEF)

Figure (5-15) show the load-deflection response for a double web filled with normal concrete on both sides, obtained from the finite element analysis and experimental work, respectively. The ultimate load capacity obtained from the finite element is convergent compared with the experimental results. The ultimate load capacity obtained by the finite element is convergent and increased about 5.50 % compared with the experimental results, and the maximum deflection decreased about 5.09 % compared with the experimental maximum deflection of this beam. The failure mode was top flange and shear buckling because there is no concrete in the middle zone, the beam is more susceptible to buckling in this region as shown in the Figure (5-16).

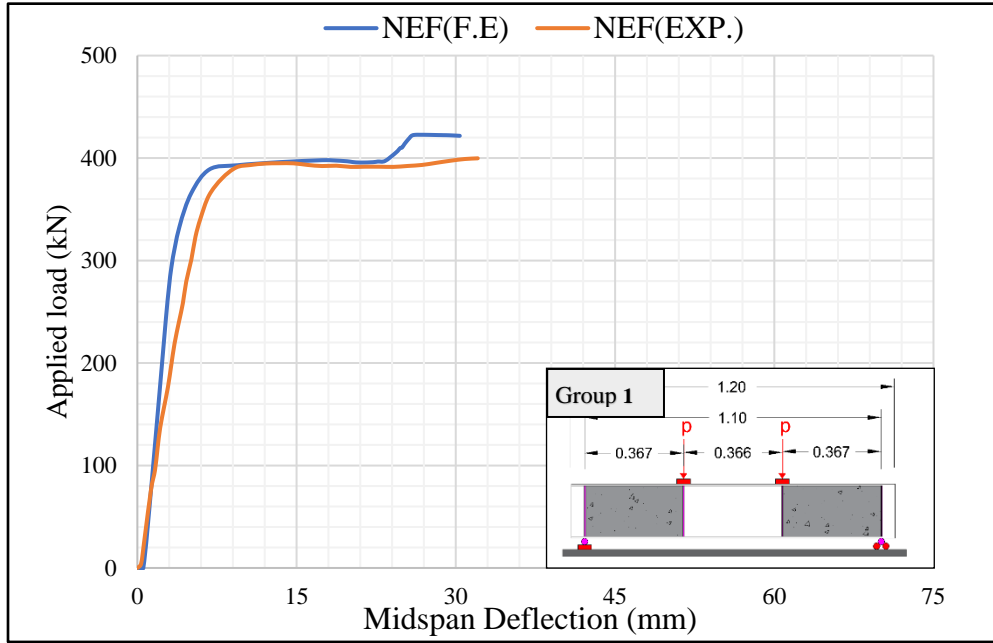


Figure 5- 15: Experimental and Numerical Failure Shape for NEF.

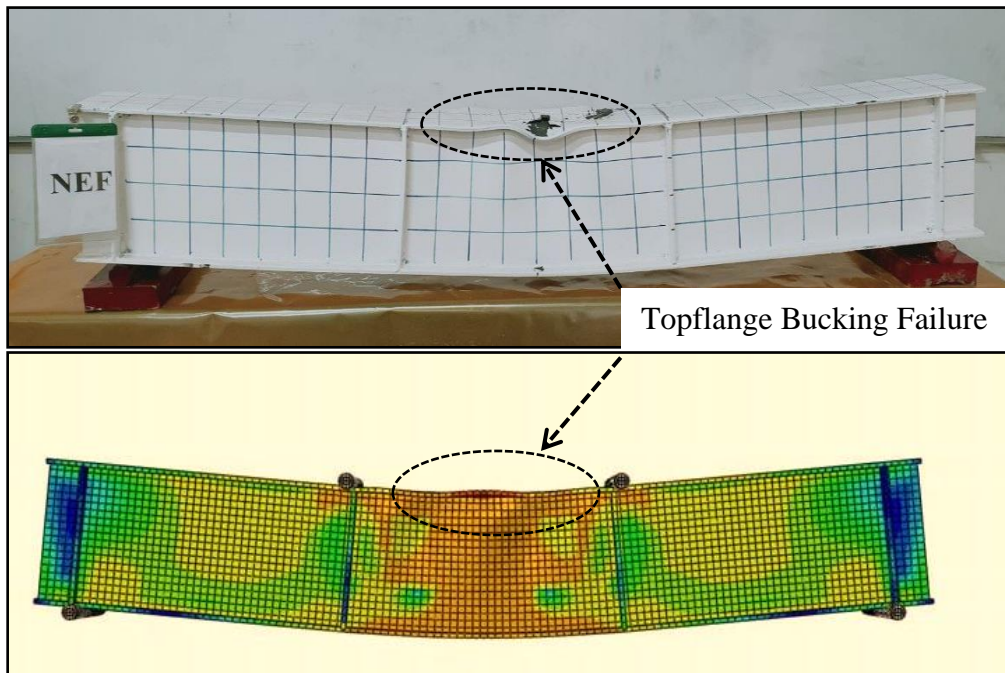


Figure 5- 16: Experimental and Numerical Failure Shape for NEF.

5.10.4. Result of Double Web Beam (NFF)

The failure mode of the specimen was Flexural because of the presence of concrete in the middle and sides of the double web beam, as illustrated in Figure (5-18). The normal concrete filling materials improved the flexural behavior of the double web beam significantly. The finite element showed that the ultimate load capacity was 2.09 % higher than the experimental results, while the maximum deflection was 5.62 % lower than the experimental maximum displacement of this beam as shown in Figure (5-17).

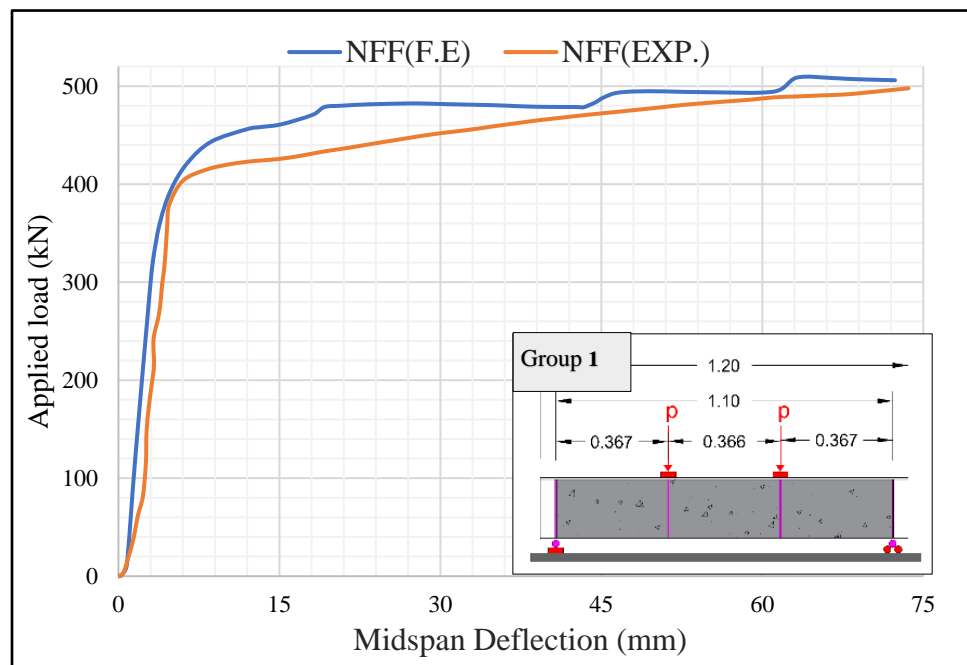


Figure 5-17: Numerical and Experimental Load-Deflection Curves for NFF.

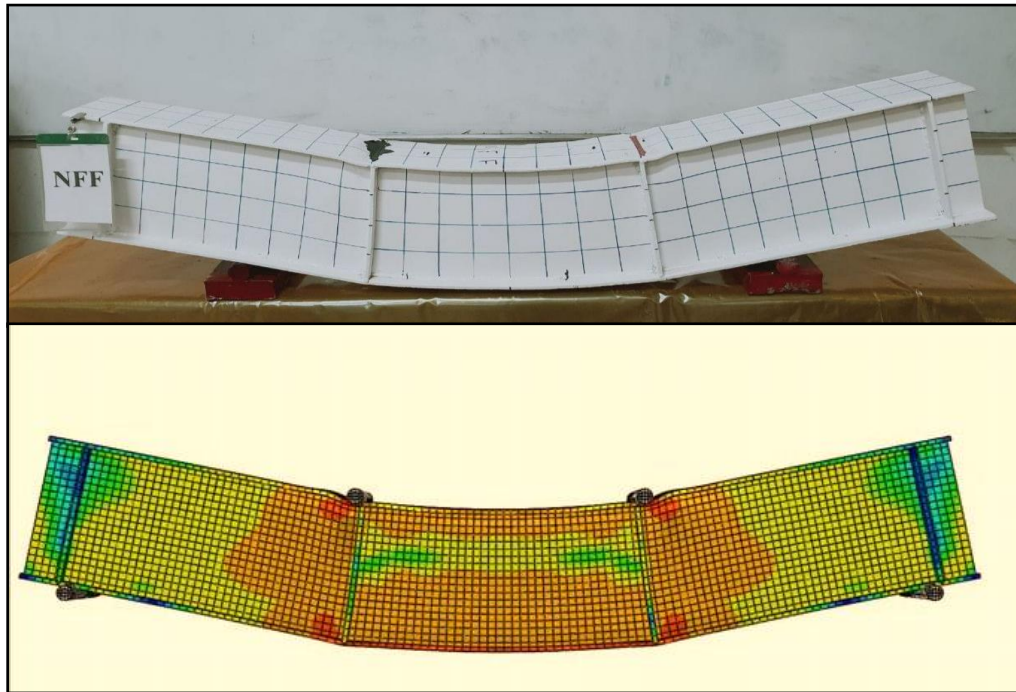


Figure 5-18: Experimental and Numerical Failure Shape for NFF.

5.10.5. Result of Double Web Beam (RMF).

From load-deflection curve for this double web specimen obtained by finite element analysis and experimental work is presented in Figure (5-19). The ultimate load capacity increased by about 1 %, and the maximum deflection decreased by about 5.65 % for RMF compared with the ultimate experimental load and maximum deflection of this double web specimen. This specimen contains recycled aggregate concrete in the middle zone of the specimen. The failure mode was a shear buckling failure, as shown in Figure (5-20).

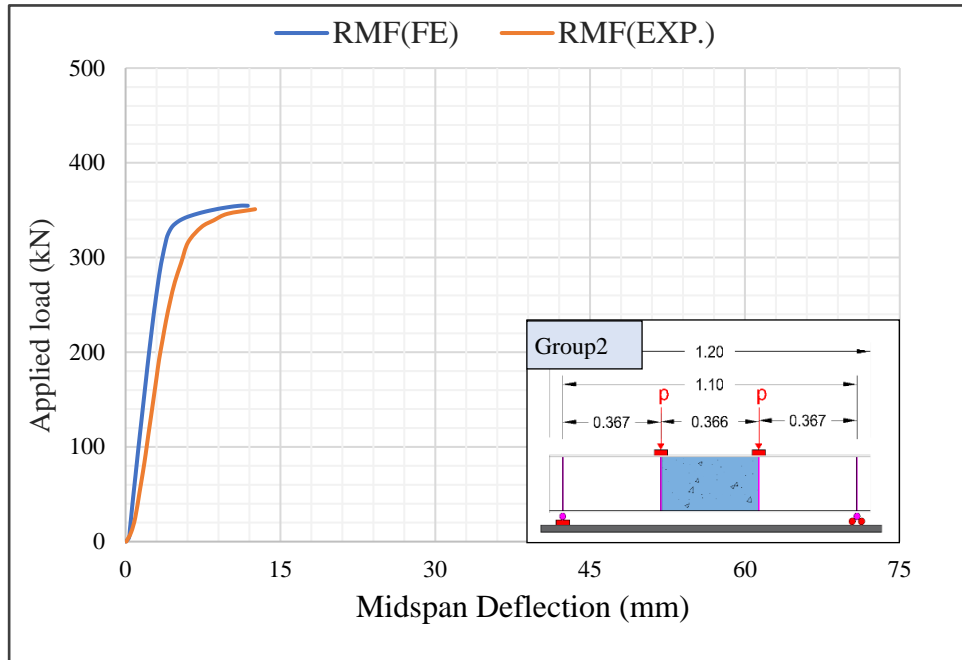


Figure 5-19: Experimental and Numerical Failure Shape for RMF.

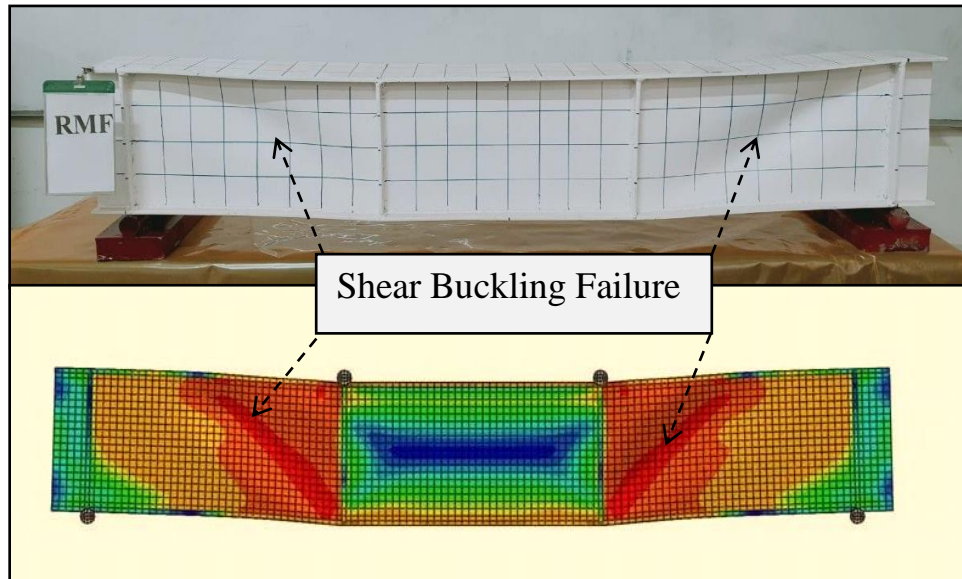


Figure 5-20: Experimental and Numerical Failure Shape for RMF.

5.10.6. Result of Double Web Beam (REF).

Figures (5-21) depict the load-deflection response for a double web filled on both sides with recycled aggregate concrete, as determined by finite element analysis and experimental investigation, respectively. The ultimate load capacity calculated by the finite element method converges with experimental data. The ultimate load capacity determined by the finite element method is convergent and increased by about 3.78 % compared to the experimental data, while the maximum deflection of this beam increased by approximately 7.66 % compared to the experimental maximum deflection. The failure mechanism was top flange and shear buckling, as indicated in Figure (5-22). Since there is no concrete in the intermediate zone, the beam is more prone to buckling in this location.

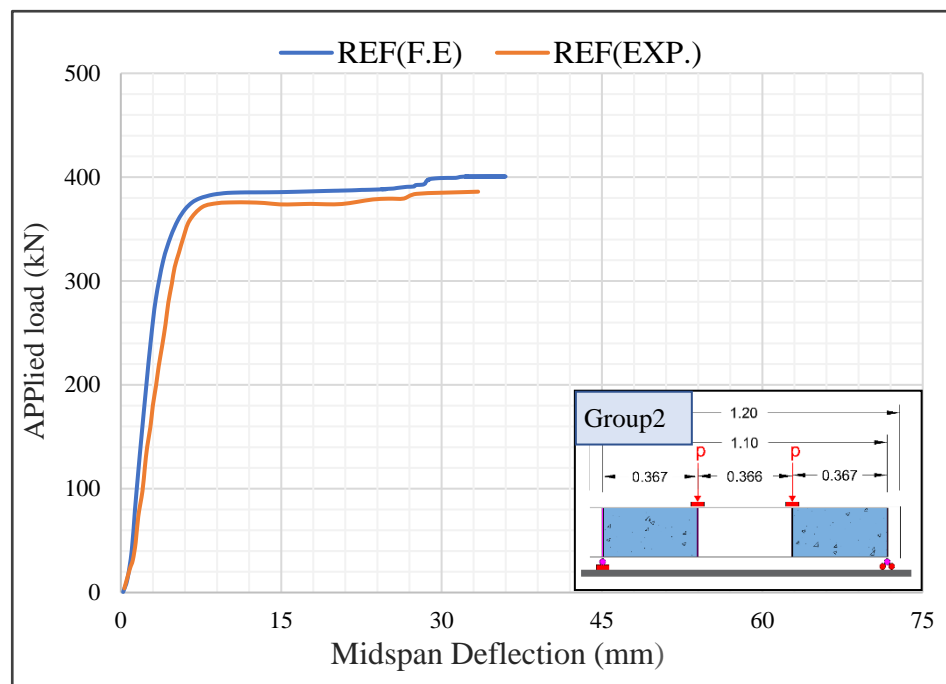


Figure 5-21: Numerical and Experimental Load-Deflection Curves for REF.

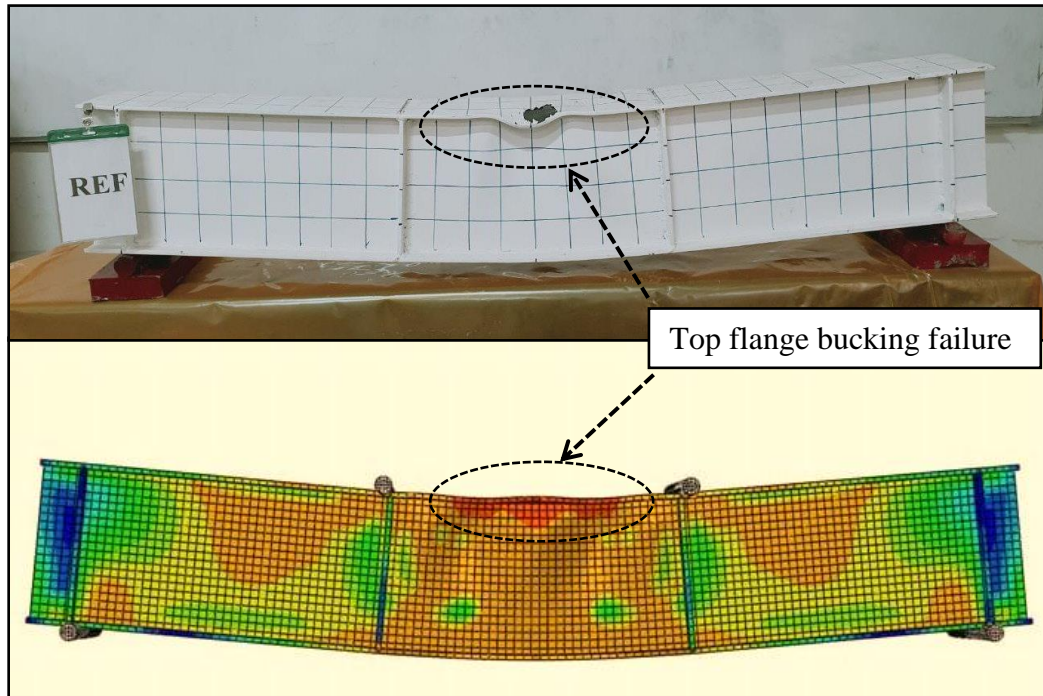


Figure 5-22: Experimental and Numerical Failure Shape for REF.

5.10.7. Result of Double Web Beam (RFF)

A double steel beam filled with recycled concrete was studied by finite element. It found convergence in the forms of load, displacement and failure, where the percentage difference between the experimental results and the numerical values of the load and displacement was about 5.27 % and 7.90 %, respectively. Figure (5-23) presents the numerical and empirical load-deflection curves for RFF. As for the failure mode, it was similar to the practical bending because of the presence of concrete in the middle and sides of the double web beam.

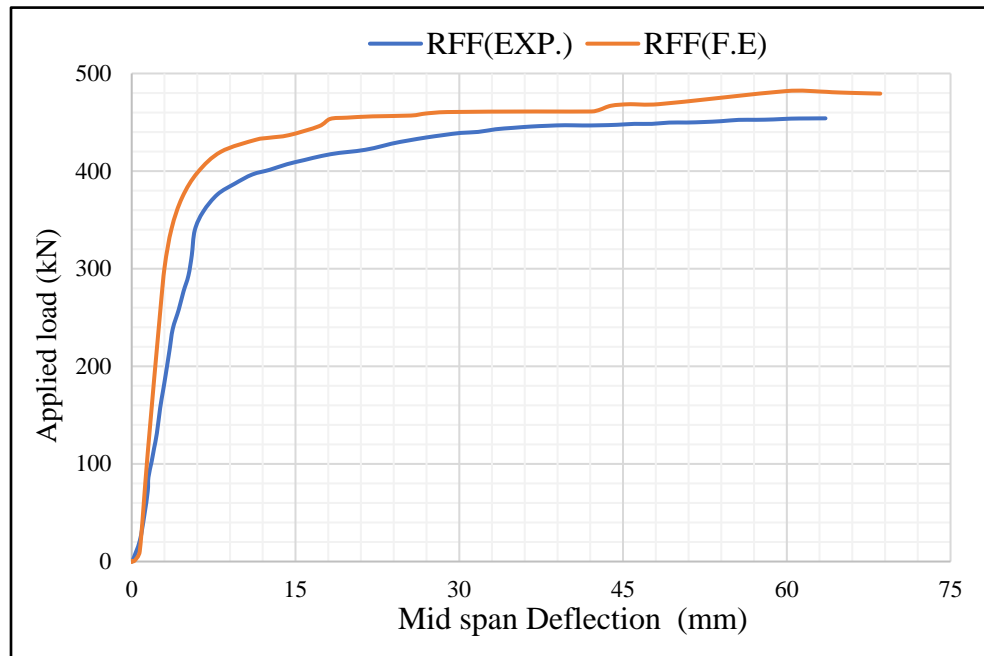


Figure 5-23: Numerical and Experimental Load-Deflection Curves for RFF.

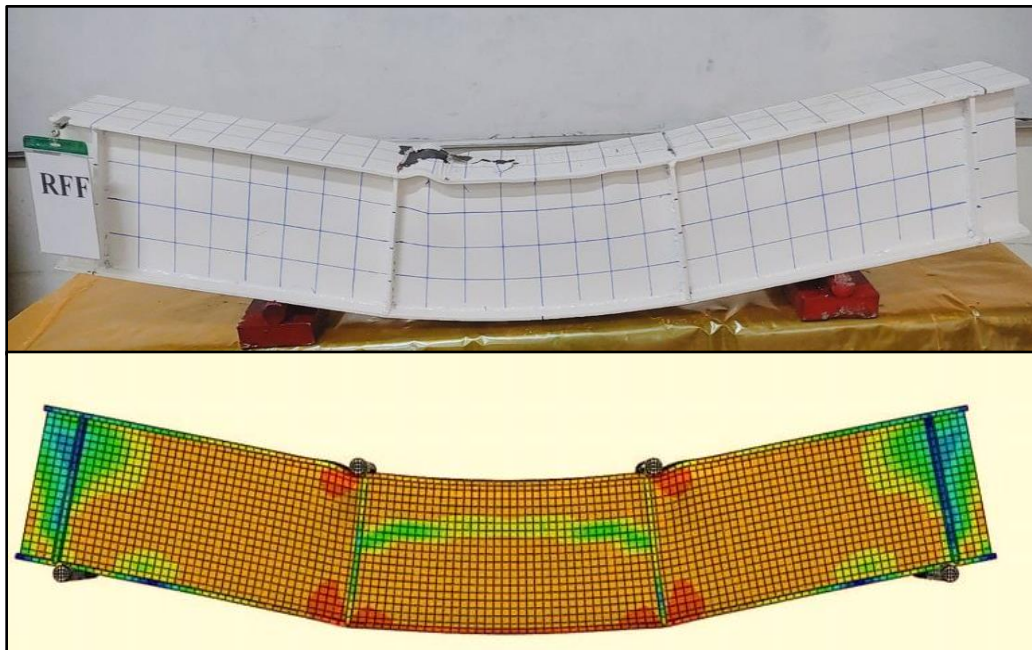


Figure 5-24: Experimental and Numerical Failure Shape for (RFF).

5.11. Summary of Finite Element Results

The results obtained from practical examinations and theoretical analysis using Finite Elements compared to the experimental and numerical results, as shown in Table (5-4).

Table 5-4: Experimental and Numerical Results for Tested Composite Beams

Group No.	Specimen symbol	Ultimate load (Pu) kN		Difference percentage	Deflection (Δ) mm		Difference percentage
		EXP	FEA		EXP	FEA	
Control Beam	CB	EXP	320.1	2.09 %	EXP	11.78	-3.98 %
		FEA	326.80		FEA	11.31	
Group 1	NMF	EXP	353.27	1.4%	EXP	12.14	4.6%
		FEA	358.23		FEA	12.70	
	NEF	EXP	399.7	5.50%	EXP	32.0	-5.09%
		FEA	421.71		FEA	30.37	
	NFF	EXP	497.88	2.09%	EXP	73.62	-5.62%
		FEA	508.29		FEA	69.48	
Group 2	RMF	EXP	351.12	1%	EXP	12.55	-5.65
		FEA	354.65		FEA	11.84	
	REF	EXP	386.05	3.78 %	EXP	33.42	7.66%
		FEA	400.66		FEA	35.98	
	RFF	EXP	455.34	5.27%	EXP	63.54	7.90%
		FEA	479.38		FEA	68.56	

The results showed the finite element of modeling an I-double web steel beam shown in Table (5-4). There is a good convergence in terms of performance, load, and displacement with the practical results described in the fourth chapter of this study, The maximum difference in results varied between (1 % to 5.50 %) as an increase in the ultimate load. At the same time, the difference in the maximum deflection at mid-span varies between 3.98 % as a reduction to 7.90 % as an increase.

5.12. Specimens Stress Distribution

This section will present the stress by finite element / ABAQUS for the samples tested in the practical programme. Where Figures (5-25) to (5-31) show the stress distribution for I-double web steel models, it has been observed that buckling occurs in areas not filled with normal and recycled concrete, because concrete prevents local buckling of steel, and also contributes to improved inertia of the section and internal forces, which increases the flexural strength and rigidity of the member. It was observed that the maximum stresses of steel occur in regions where buckling occurs. For samples filled of the middle, the stresses were concentrated on the side of the sample in the web region; for samples filled with sides, the stresses were concentrated in the middle area of the web; and for samples filled completely, the stresses were concentrated under points load. And it was observed that the maximum stresses of concrete occur in the areas under the load points at the edges of the concrete block as a result of the confinement provided by the steel to the concrete.

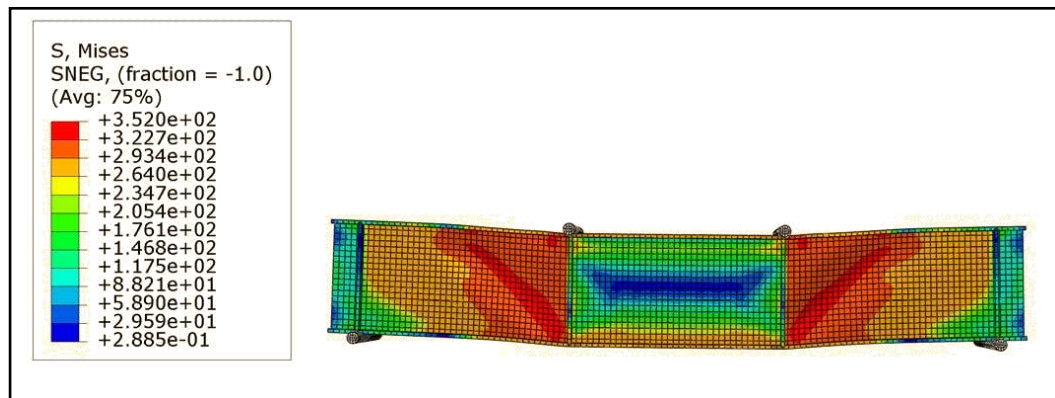


Figure 5- 25: Stress Distribution for Control Specimen at Ultimate Stage.

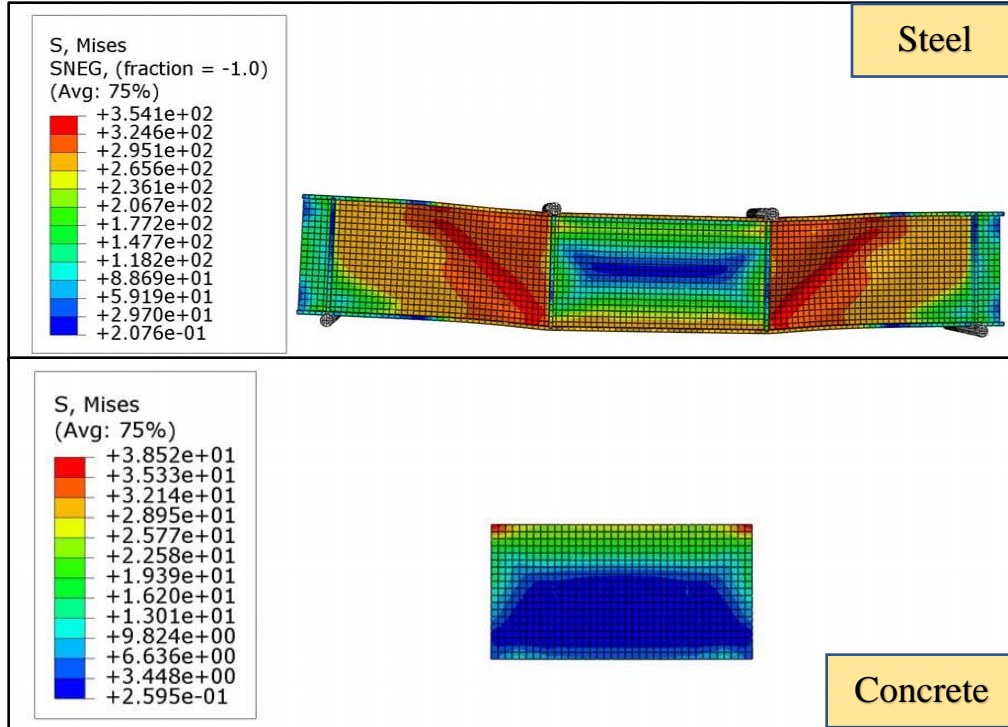


Figure 5- 26: Stress Distribution for NMF Specimen at Ultimate Stage.

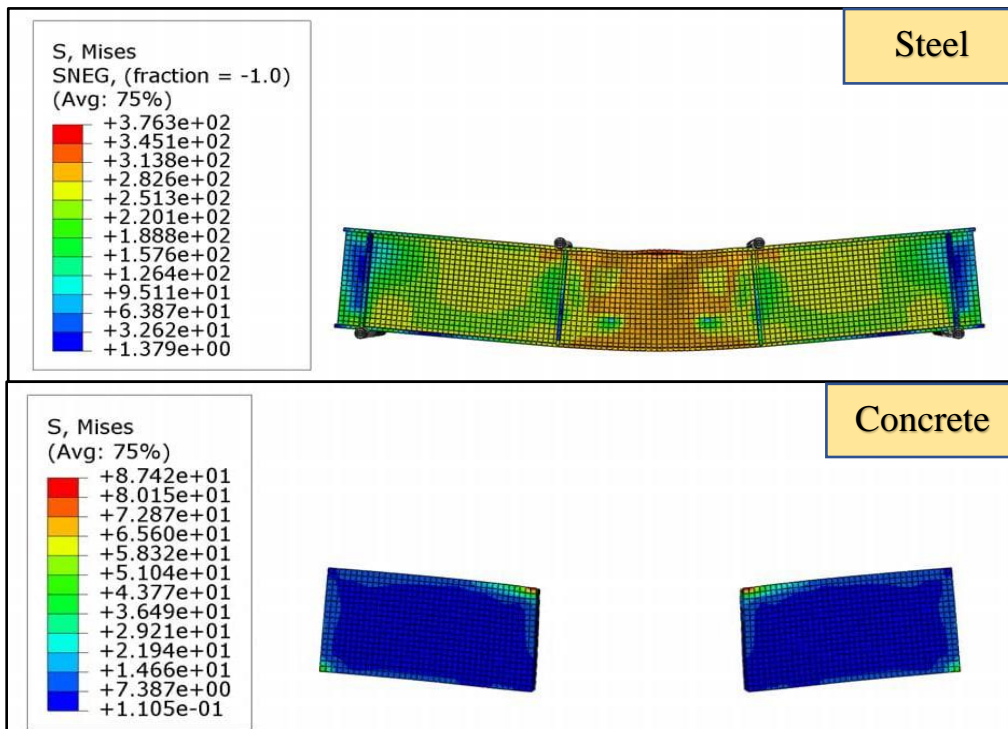


Figure 5- 27: Stress Distribution at Ultimate Load for NEF Specimen.

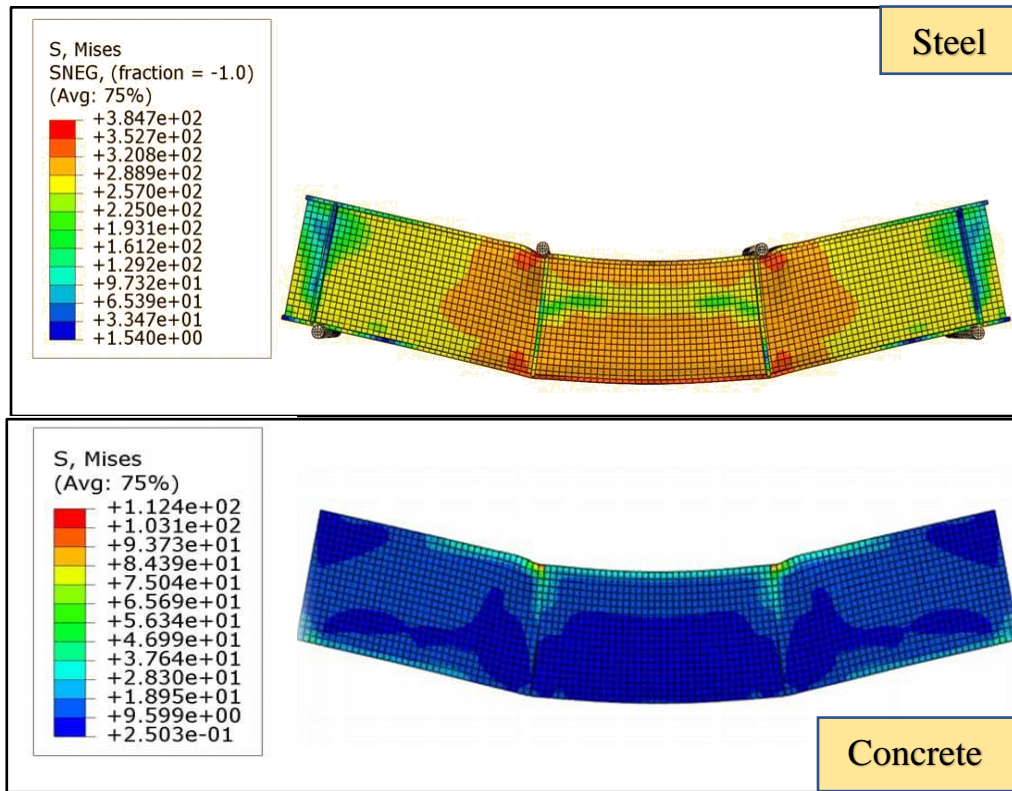


Figure 5-28: Stress Distribution at Ultimate Load for NEF Specimen.

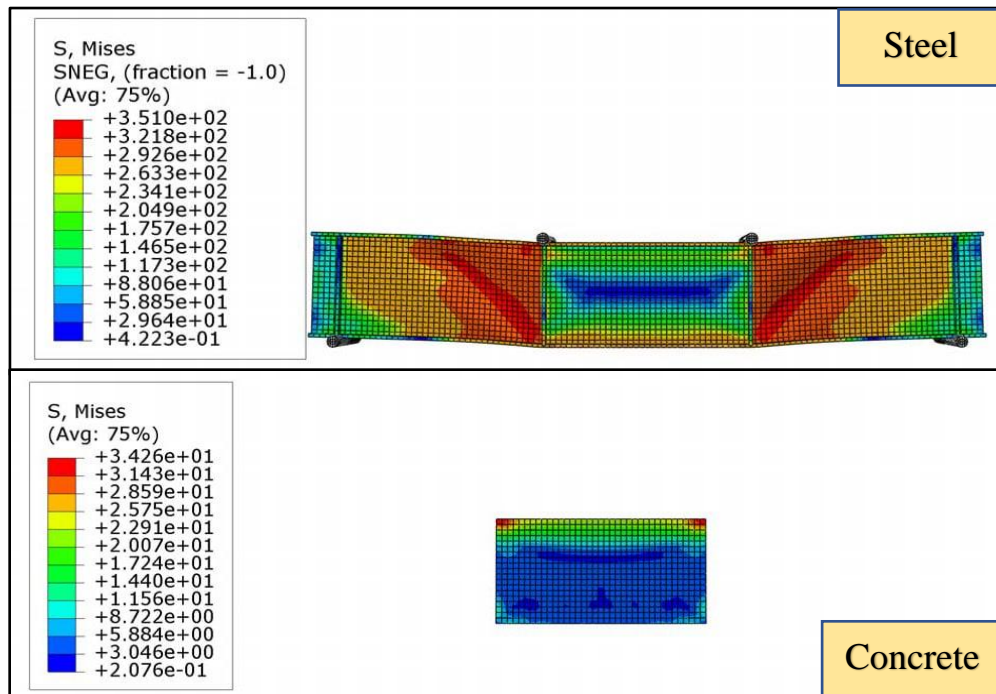


Figure 5- 29: Stress Distribution for RMF Specimen at Ultimate Stage.

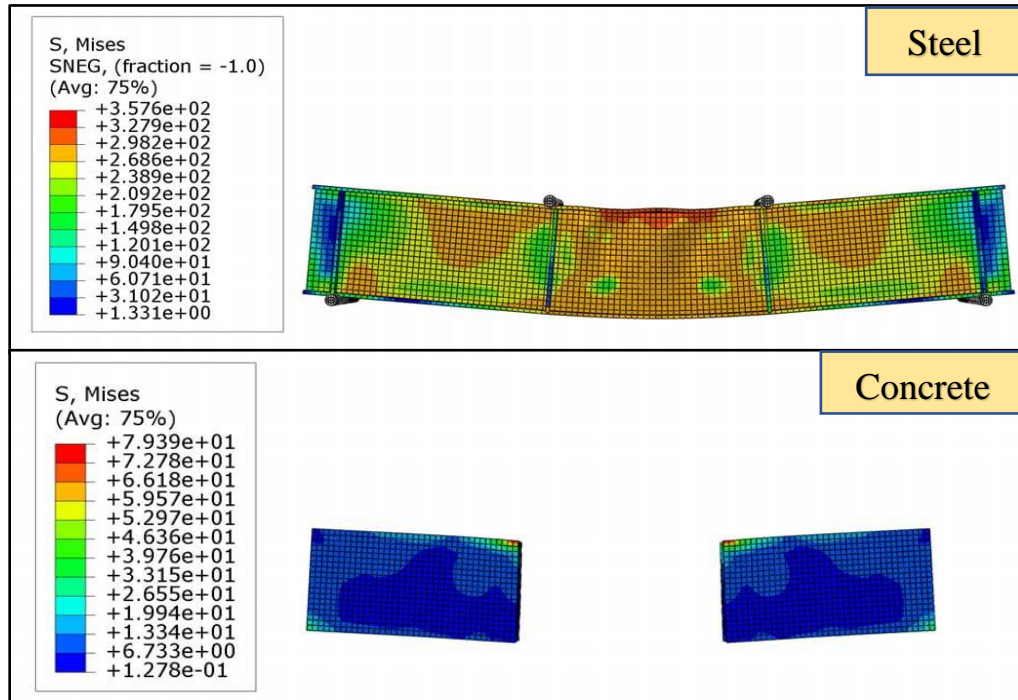


Figure 5- 30: Stress Distribution at Ultimate Load for REF Specimen.

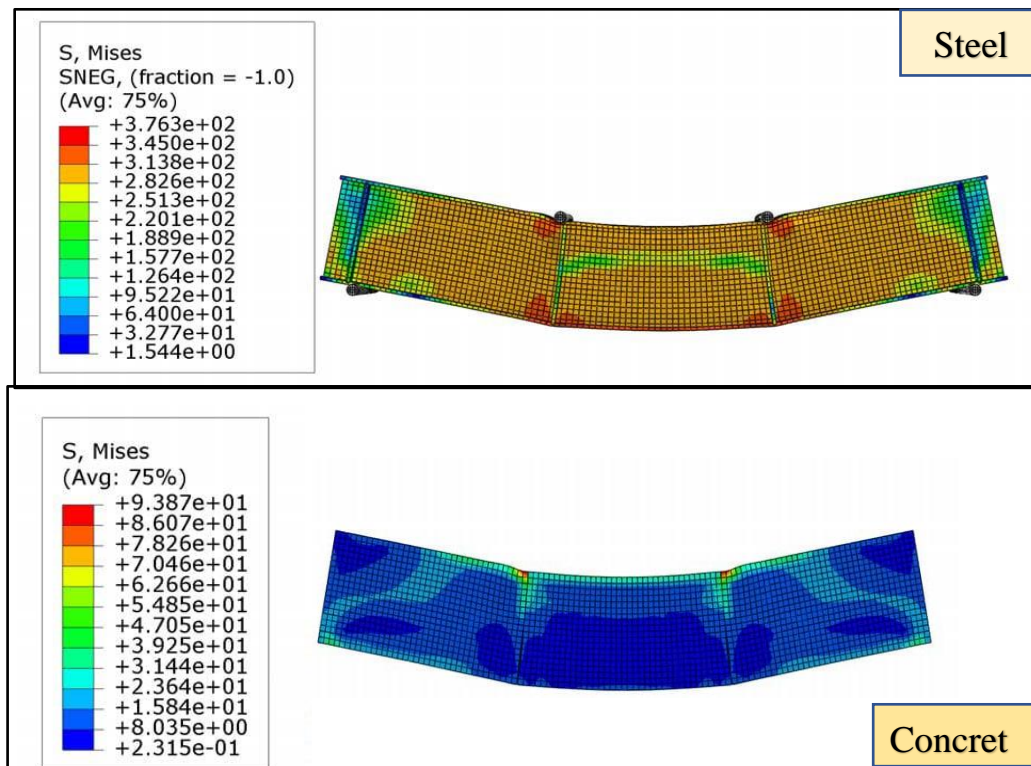


Figure 5-31: Stress Distribution at Ultimate Load for RFF Specimen.

5.13. Strain Behavior of Composite Double Web Beams

After studying the load-deflection curve and modes failure, and the stress distribution mechanism for the filled and unfilled double web samples with concrete, the plastic strain will study in the failure areas of the samples and a distribution mechanism on the depth of the section. The results of the plastic strain along the depth of each composite beam at the ultimate.

The plastic strains are recorded along the depth at a side-span for the NMF and RMF specimens shown in Figures (5-32) and (5-35), and the maximum compression strain steel at depth 82.63 mm was 0.023 and at depth 78 mm was 0.023 for the NMF and RMF samples, respectively. It was observed that there was an increase in plastic strain due to the presence of concrete in the central region of the web, when compared with the control shown in Figure (5-32).

Figures (5-34) and (5-37) depict the plastic strains along the depth at a mid-span for the NEF and REF specimens, and the maximum tension strain steel at top flange for the NEF and REF specimens was 0.054 and 0.051, respectively. It was observed that the plastic stress in top flange of the NEF and REF samples was increased, due to the presence of concrete on both sides of the double web samples, making these areas more stiffness. If compared to the reference beam.

The plastic strains along the depth at the midspan for the NFF and RFF specimens are depicted in Figures (5-35) and (5-38), and the maximum tension strain steel at the top for the NFF and RFF samples was 0.044 and 0.041, respectively. The presence of concrete along the samples led to an increase in plastic strain, which makes these samples have a high ductility index, as mentioned earlier in the fourth chapter. If compared to the reference beam.

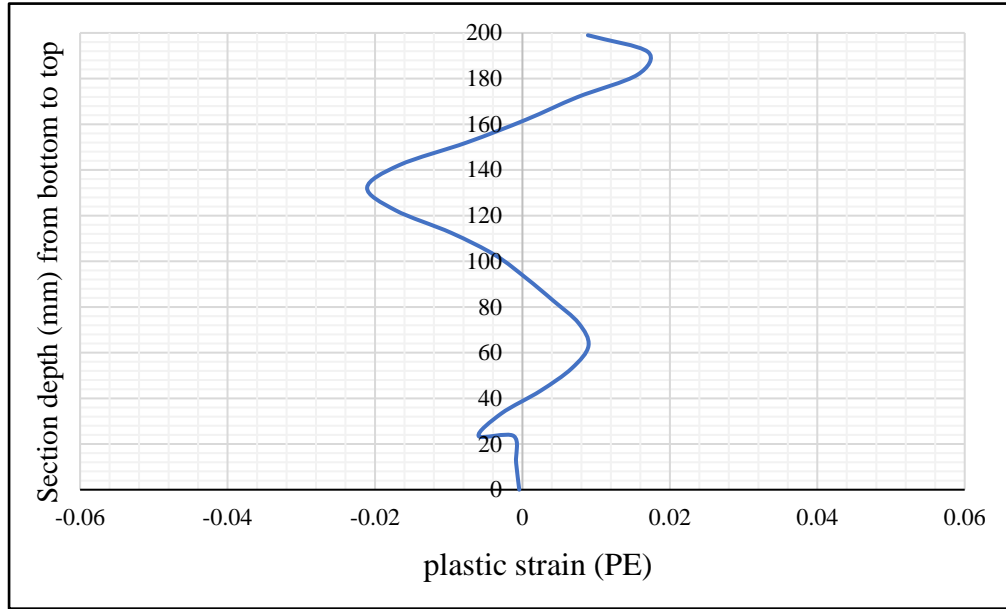


Figure 5- 32: Plastic Strain (PE22) at Side-Span Section of Control.

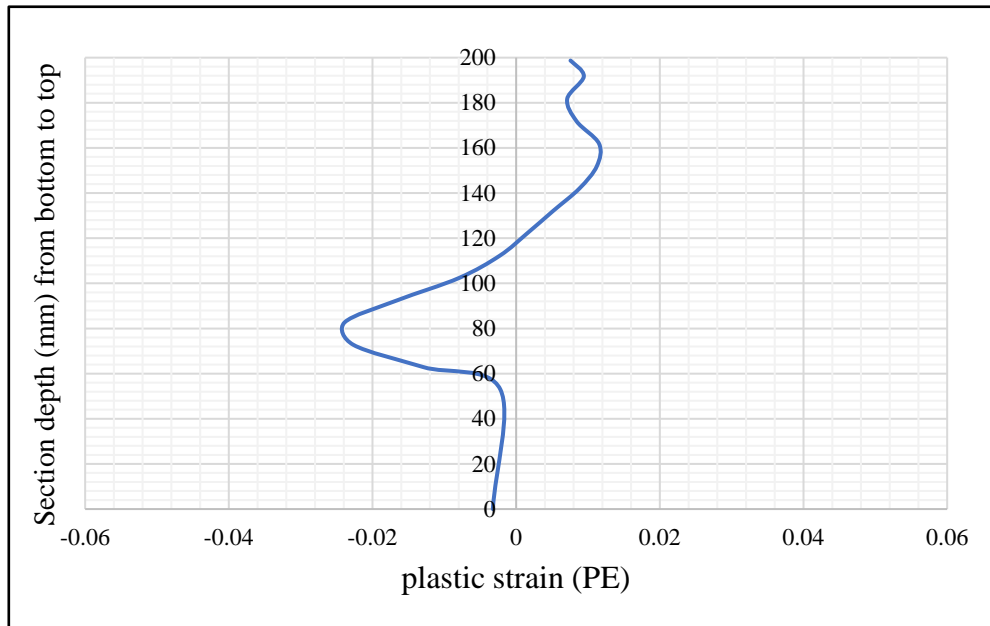


Figure 5- 33: Plastic Strain (PE22) at Side-Span Section of NMF.

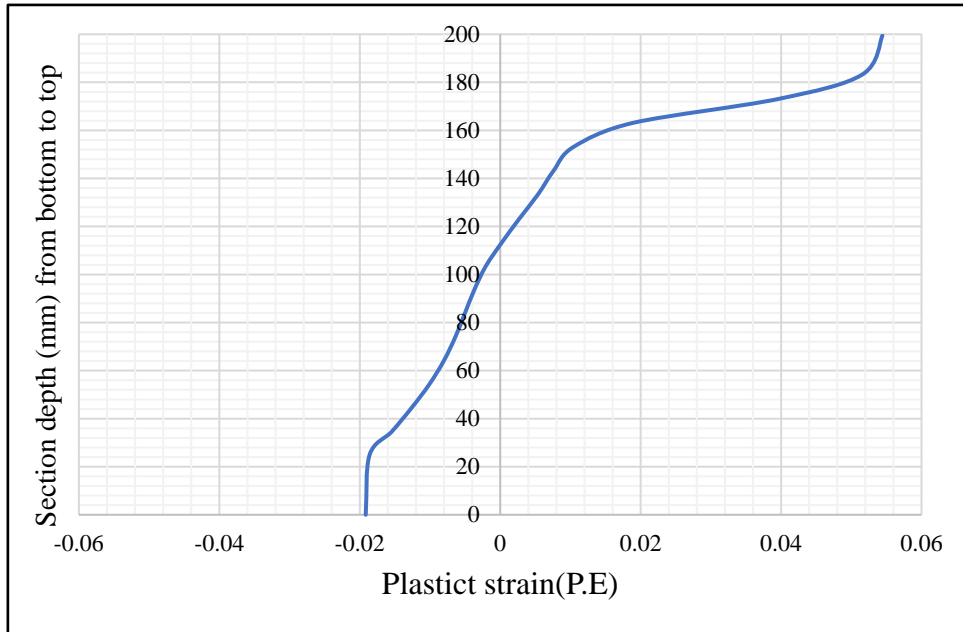


Figure 5- 34: Plastic Strain (PE22) at Mid-span Section of NEF.

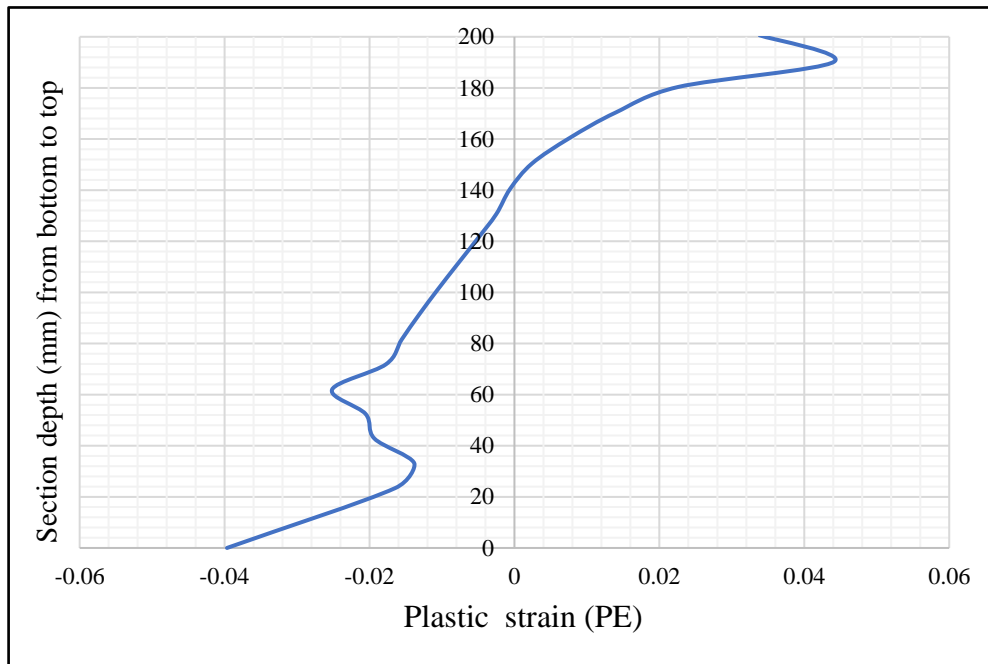


Figure 5- 35: Plastic Strain (PE22) at Mid-Span Section of NFF.

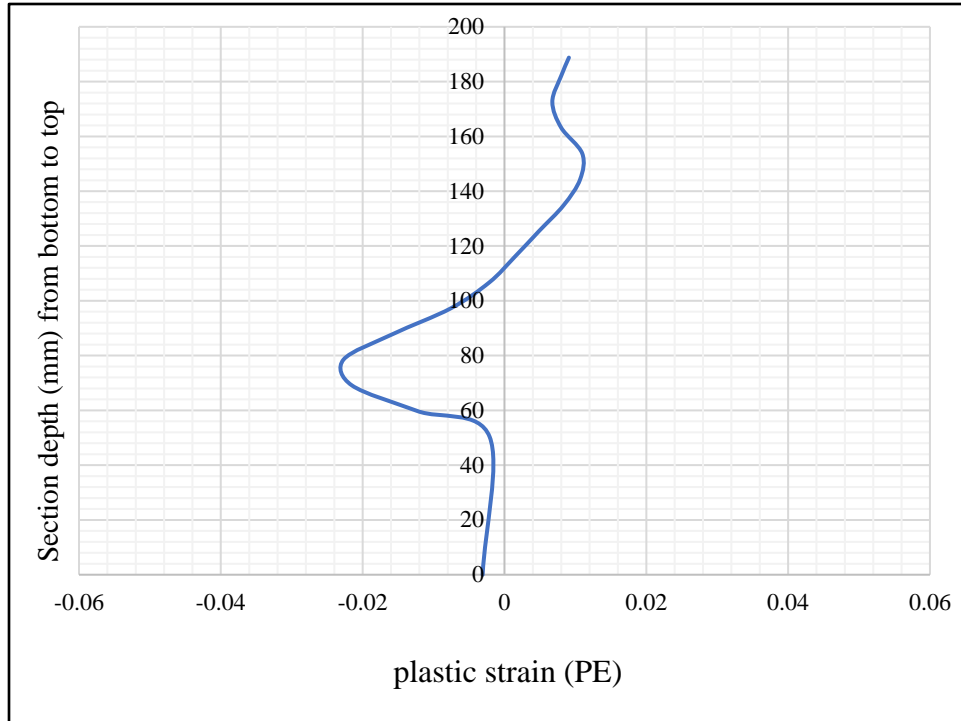


Figure 5- 36: Plastic Strain (PE22) at Side-Span Section of RMF.

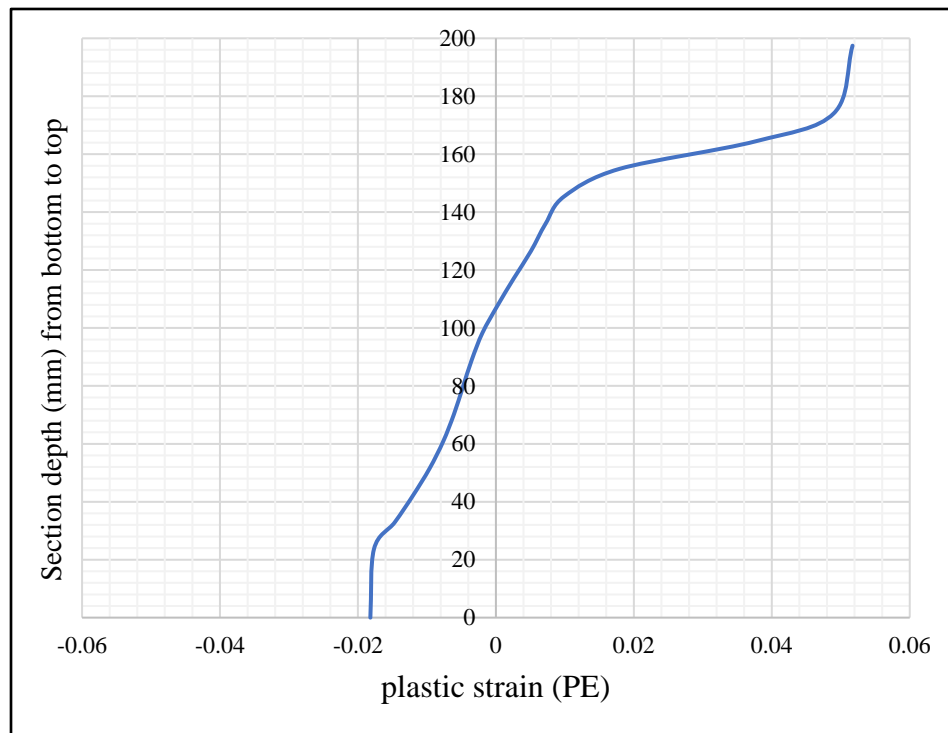


Figure 5- 37: Plastic Strain(PE22) at Mid-Span Section of REF.

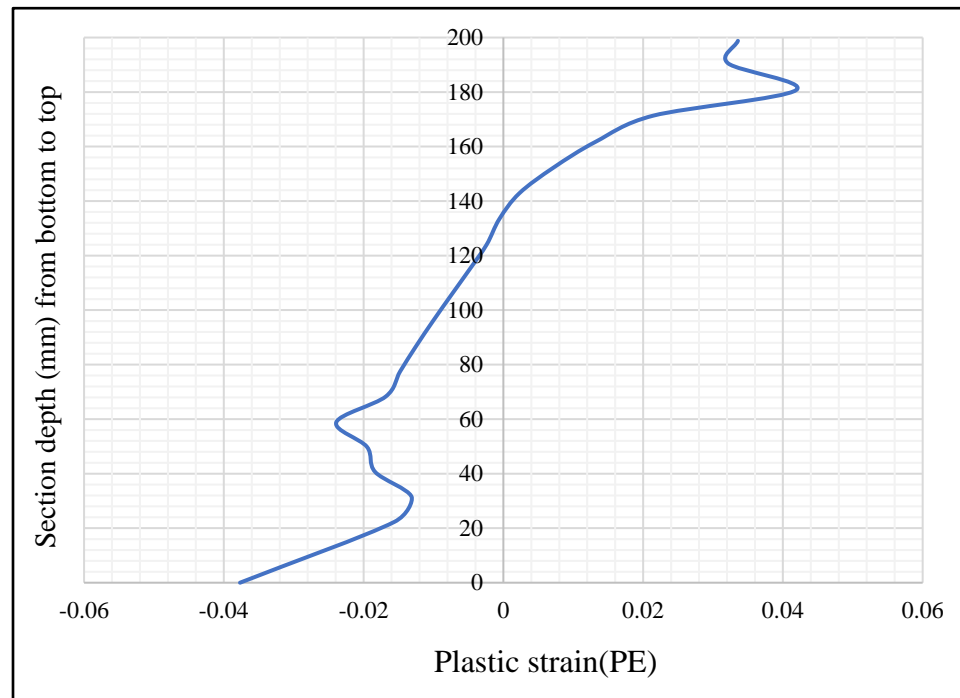


Figure 5- 38: Plastic Strain (PE22) at Mid-Span Section of RFF.

5.14. Parametric Study

Several vital parameters have been proposed to study their effect on the behavior of double web sections under two loads, and they can be summarized as follows:

5.14.1. Effect of Concrete Compressive Strength

The effect of changing the compressive strength of normal concrete on the load-deflection curves, load capacity, and deflection of doubly web beam (DWB) for NEF specimen was studied. The tested concrete compression strengths were 20 MPa and 25 MPa, with all other variables, such as steel characteristics, held constant. Where it was observed that the presence of concrete on both sides of the specimen contributed to the increase in the ultimate capacity of the form, and the percentage of increase was 10.33 % and 4.21 % for compressive strengths 25 MPa and 20 MPa, respectively, as shown in Figure (5-38) illustrates the load deflection for NEF specimen with/without

concrete. Table (5-5) shows that the maximum load capacity of a double web steel beam increases as its compressive strength increases.

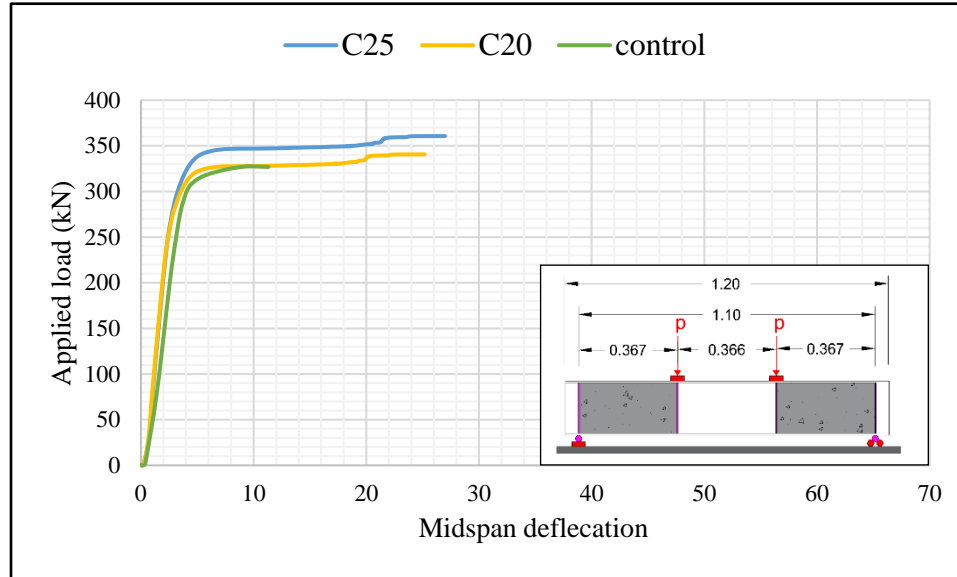


Figure 5-39: Impact of The Compressive Strength on The Load-Deflection for NEF.

Table 5-5: Effect of Compressive Strength on Ultimate Load and Maximum Deflection.

Beam symbol	Compressive strength (MPa)	Ultimate load (KN)	Increment Ratio	Max. Deflection (mm)
control	-----	326.8	----	11.31
NEF	f 'c -25	360.59	10.33%	26.98
NEF	f 'c -20	340.55	4.21%	25.18

5.14.2. Effect of yield strength of steel on the flexural behaviour

Figure (5-34) shows the load-displacement curves of the control beam but with the different yield strength of web steel yield, with all other variables

held constant, such as the properties of flanged steel. Where the yield strength f_y was 310,350 N/mm², it was observed that the ultimate capacity of double web steel increased as the yield stresses of the web increased by 5.5 % and 11.11 %, respectively, as shown in Table (5-6). The ultimate bending capacity is proportional to the steel yield strength. The steel strength makes almost no contribution to the stiffness of the member in the elastic stage, which is expected as Young's modulus value remains constant.

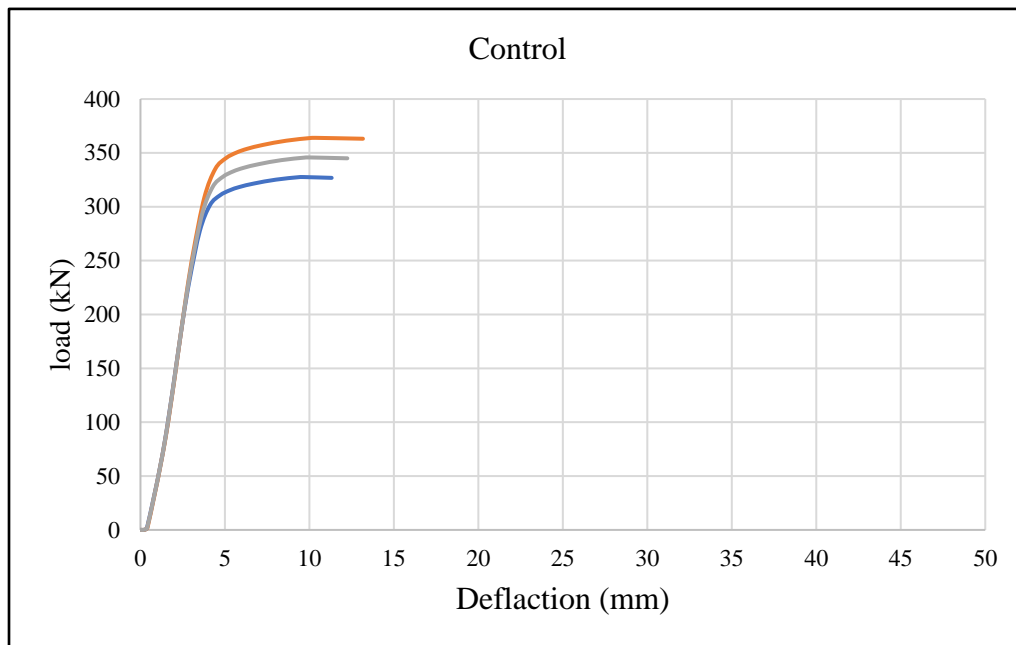


Figure 5- 40: Deflection at Mid-Span with Different Yielding Strength of Steel.

Table 5- 6: Effect of Yield Stress on Ultimate Load and Maximum Deflection.

yield stress	Ultimate load (kN)	Increment Ratio	Max.Deflection(mm)
$F_y = 294.6$	326.8	-----	11.31
$F_y = 310$	344.96	5.5%	12.24
$F_y = 350$	363.12	11.11%	13.16

Chapter Six. CONCLUSIONS AND RECOMMENDATIONS

CHAPTER SIX

CONCLUSIONS AND RECOMMENDATIONS

6.1. Introduction

The behavior of steel double web filled with different types of concrete (normal and recycled) under static load. The work included experimental work and numerical study. The first one was a complicated beam test, and the last one used a non-linear finite element (ABAQUS, 2021) to predict how different cases would behave in general. The conclusions drawn from the experimental and numerical results are illustrated in this chapter, and the recommendation for future research.

6.2. Conclusions

This part presented the main conclusions noticed for each stage of the work (experimental and numerical results obtained) for the composite beams filled with normal concrete and recycled concrete.

6.2.1. Experimental Conclusions

1. The normal and recycled concrete infill had a positive impact on the ultimate shear capacity as it stiffened the web and delayed the shear buckling, thereby increasing the ultimate shear capacity of double web steel.
2. The location of concrete in the double web section has a remarkable effect on the ultimate strength of the beams. When compared to the control beam, the increases in group one were (10 %, 24 %, and 55 %) respectively, when normal concrete was in the middle zone of the web, the edges zone, both the middle and edges zones. while the increases were (9.52 %, 20.4 %, and

42.03 %) respectively, when recycled aggregate concrete was in the middle zone of the web, the edges zone, both the middle and edges zones.

3. Failure type changed from shear buckling failure to flexural failure for all double web beams filled with concrete at the edges.
4. The ductility of specimen filled normal concrete full double web showed increased by about (568 %) while the ductility of specimen filled recycled concrete full double web showed increased by about (380 %), respectively, when compared to control beam.
5. The stiffness of specimen filled normal concrete full double web showed increased by about (39.6 %) while the stiffness of specimen filled recycled concrete full double web showed increased by about (8.03 %), respectively, when compared to double web hollow.
6. The use of different types of concrete in the webs of composite beams led to improved performance compared with the control beam.
7. When adding concrete in the middle or edge sections of the specimens or the whole specimen, the self-loads will increase. At the same time, the structural behavior and failure mode were improved, and the ultimate capacity of the composite specimen was increased by a higher rate if compared to the hollow specimen.
8. In composite specimens, the ultimate capacity and overall flexural performance of double web beams are affected by site differences in concrete.
9. RAC prevents the local buckling of the double web, and it also contributes to the inertia of the double web, which increases the flexural strength and stiffness of the member.

6.2.2. Numerical Conclusions

1. The ABAQUS software analysis created models predict the actual performance of the I-double web for maximum load, load-displacement curves, and failure mode.
2. The behavior of the plastic strain distribution is non-linear for composite double web beams.
3. The ultimate load capacity of NEF increased as the compressive strength increased. When the compressive strength was 25 MPa and 20 MPa, the increase was 10.33 % and 4.21 %, respectively, if compared with the control beam.
4. The ultimate load capacity of the control beam increased as the yield stress of the web increased. When the yield stress was 310 MPa and 350 MPa, the increase was 5.5 % and 11.11 %, respectively.

6.2.3. Recommendations for Future Studies

Based on the work conducted in this research, a number of areas which would benefit from more research in the future have been identified. These are summarised hereafter:

- 1-Behavior of steel double web filled steel beams under torsion.
- 2-Deriving equations to determine the ultimate load capacity and maximum deflection for composite doubly web beam based on part filled and properties materials.
- 3- Investigating the temperature effect on the behaviour of steel double web filled steel beams.
- 4-Experimental tests on composite steel double web filled steel beams can be done under impact or repeated load.

References

- ABDALLA, S. H. 2012. Behavior of Concrete Filled Steel Tube (CFST) Under Different Loading Conditions.
- ABED, F., ABDELMAGEED, Y. & ALHOUBI, Y. 2021. Effect of different cross-sections and concrete types on the flexural behavior of CFSTs. *Composite Structures*, 276, 114570.
- ABED, F. H., NAZZAL, M. D., ATTOM, M. F., EL-EMAM, M. E. & ELMESSALAMI, N. 2018. Use of treated wastewater in the construction of base course layers for sustainable pavement structures. *Journal of Materials in Civil Engineering*, 30, 04018140.
- ABED, F. H., NAZZAL, M. D., ATTOM, M. F., EL-EMAM, M. E., ELMESSALAMI, N. & AL-DABAGH, S. The use of wastewater in construction of base course layers in pavement structures. *International Congress and Exhibition" Sustainable Civil Infrastructures: Innovative Infrastructure Geotechnology"*, 2017. Springer, 31-37.
- ACI-318 2019. Building code Requirements for structural concrete and commentary.
- ACI 211.1-91. Standard Practice for Selecting Proportions for Normal, Heavyweight, and Mass Concrete. American Concrete Institute.
- ADLURI, S. 2013. Structural steel design, composite beams”, a project report, Memorial University, Newfound and Labrador, Canada, Faculty of Engineering & applied science.
- AISC-LRFD-360 2016. Specification for Structural Steel Buildings.
- AL-OBAIDI, S., SALIM, T. & HEMZAH, S. A. 2018. Flexural behavior of concrete filled steel tube composite with different concrete compressive strength. *International Journal of Civil Engineering and Technology*, 9, 824-832.
- AL-ZAND, A. W., HOSSEINPOUR, E. & TAWFEEQ, W. M. 2017. The effects of filling the rectangular hollow steel tube beam with concrete: an experimental case study. *Journal of Civil Engineering Researchers*, 1, 23-30.
- AL ZAND, A. W., ALI, M. M., AL-AMERI, R., BADARUZZAMAN, W. H. W., TAWFEEQ, W. M., HOSSEINPOUR, E. & YASEEN, Z. M. 2021.

- Flexural Strength of Internally Stiffened Tubular Steel Beam Filled with Recycled Concrete Materials. *Materials*, 14, 6334.
- ASTM A370. Standard test methods and definitions for mechanical testing of steel products. ASTM International.
- ASTM C33-03. Standard Specification for Concrete Aggregates.
- ASTM C39-05. Standard Test Method for Compressive Strength of Cylindrical Concrete Specimens.
- ASTM C78-02. Standard Test Method for Flexural Strength of Concrete (Using Simple Beam with Third-Point Loading).
- ASTM C496-11. Standard test method for splitting tensile strength of cylindrical concrete specimens.
- ATTOM, M., ABED, F., ELEMAM, M., NAZAL, M. & ELMESSALAMI, N. 2016. The effect of treated waste-water on compaction and compression of fine soil. *International Journal of Civil and Environmental Engineering*, 10, 1122-1126.
- BAIRAGI, N., RAVANDE, K. & PAREEK, V. 1993. Behaviour of concrete with different proportions of natural and recycled aggregates. *Resources, conservation and recycling*, 9, 109-126.
- BEHERA, M., BHATTACHARYYA, S., MINOCHA, A., DEOLIYA, R. & MAITI, S. 2014. Recycled aggregate from C&D waste & its use in concrete—A breakthrough towards sustainability in construction sector: A review. *Construction and building materials*, 68, 501-516.
- CHEN, Y., WANG, K., FENG, R., HE, K. & WANG, L. 2017. Flexural behaviour of concrete-filled stainless steel CHS subjected to static loading. *Journal of Constructional Steel Research*, 139, 30-43.
- DE OLIVEIRA, W. L. A., DE NARDIN, S., DE CRESCE EL, A. L. H. & EL DEBS, M. K. 2009. Influence of concrete strength and length/diameter on the axial capacity of CFT columns. *Journal of Constructional Steel Research*, 65, 2103-2110.
- EL-EMAM, M., ATTOM, M., ABED, F., ELMESSALAMI, N., JOUDEH, H., ASKARPOOR, A., NOUNOU, W. & ALIMAM, A. 2016. Potential of Using Recycled Aggregate with Treated Wastewater as Road Base Material. *International Proceedings of Chemical, Biological and Environmental Engineering*, 92, 103-107.

- ELLOBODY, E. 2013. Numerical modelling of fibre reinforced concrete-filled stainless steel tubular columns. *Thin-Walled Structures*, 63, 1-12.
- GHANNAM, S. 2016. Flexural strength of concrete-filled Steel tubular beam with partial replacement of coarse aggregate by granite. *International Journal of Civil Engineering and Technology*, 7.
- HAN, L.-H., LI, W. & BJORHOVDE, R. 2014. Developments and advanced applications of concrete-filled steel tubular (CFST) structures: Members. *Journal of constructional steel research*, 100, 211-228.
- HANSEN, T. C. 1992. *Recycling of demolished concrete and masonry*, CRC Press.
- HU, H.-T., HUANG, C.-S., WU, M.-H. & WU, Y.-M. 2003. Nonlinear analysis of axially loaded concrete-filled tube columns with confinement effect. *Journal of Structural Engineering-ASCE*, 129, 1322-1329.
- IQS No.5/2019. "Portland Cement", The central organization for standardization and quality control, Baghdad.
- IQS No.1703/1992. Iraqi Standard (Materials Specification & Construction Works).
- IQS No. 45/1984. Aggregate from Natural Sources for Concrete and Construction.
- JAVED, M. F., SULONG, N. R., MEMON, S. A., REHMAN, S. K. U. & KHAN, N. B. 2017. FE modelling of the flexural behaviour of square and rectangular steel tubes filled with normal and high strength concrete. *Thin-walled structures*, 119, 470-481.
- JOHNSON, R. P. 1994. *Composite Structure of Steel and Concrete*. 1.
- KOU, S.-C. & POON, C.-S. 2013. Long-term mechanical and durability properties of recycled aggregate concrete prepared with the incorporation of fly ash. *Cement and Concrete Composites*, 37, 12-19.
- KOVAC, B. 2010. Structural response of circular concrete filled tube piers in integral bridges. *Universitat Politècnica de Catalunya*.
- LEE, S.-H., UY, B., KIM, S.-H., CHOI, Y.-H. & CHOI, S.-M. 2011. Behavior of high-strength circular concrete-filled steel tubular (CFST) column under eccentric loading. *Journal of Constructional Steel Research*, 67, 1-13.

- LIN, H. 2004. Flexural Behaviour of Concrete-Filled Steel Tube. *Journal of Constructional Steel Research*, 60, 313-337.
- MANDER, J. B., PRIESTLEY, M. J. & PARK, R. 1988. Theoretical stress-strain model for confined concrete. *Journal of structural engineering*, 114, 1804-1826.
- MATSUMURA, T., HOSAKA, T., HIRAOKA, C. & NISHIUMI, K. Practical application of composite bridge for Shinkansen using CFT. IABSE Symposium Report, 2003. International Association for Bridge and Structural Engineering, 149-155.
- PEREIRA, P., EVANGELISTA, L. & DE BRITO, J. 2012. The effect of superplasticizers on the mechanical performance of concrete made with fine recycled concrete aggregates. *Cement and concrete composites*, 34, 1044-1052.
- RICHART, F. E., BRANDTZÆG, A. & BROWN, R. L. 1928. A study of the failure of concrete under combined compressive stresses. University of Illinois at Urbana Champaign, College of Engineering
- ROEDER, C. W., LEHMAN, D. E. & BISHOP, E. 2010. Strength and stiffness of circular concrete-filled tubes. *Journal of structural engineering*, 136, 1545-1553.
- ROLA, E.-N., MU'TASIM, A.-J., YASSER, H. & MA'EN, A.-J. 2021. Behavior of light-gauge steel beams filled with recycled concrete. *Magazine of Civil Engineering*, 10102.
- SAENZ, L. P. 1964. Discussion of "Equation for the Stress-Strain Curve of Concrete" by Desayi and Krishana. *Proceedings of ACI*, 61, 1229-1235.
- SHALLAL, M. A. Flexural behavior of concrete-filled steel tubular beam. 2018 International Conference on Advance of Sustainable Engineering and its Application (ICASEA), 2018. IEEE, 153-158.
- SHANMUGAM, N. E. & LAKSHMI, B. 2001. State of the art report on steel-concrete composite columns. *Journal of constructional steel research*, 57, 1041-1080.
- SUSANTHA, K., GE, H. & USAMI, T. 2001. Uniaxial stress-strain relationship of concrete confined by various shaped steel tubes. *Engineering Structures*, 23, 1331-1347.

- SYSTEMES, D. 2014. ABAQUS/CAE User's Manual, Version 6.14. Providence, RI: Dassault Systemes Simulia Corp.
- T SIVA NAGA, A. & MADHURI, N. M. 2017. Flexural behaviour of concretefilled steel tube beams. Anveshana's International Journal of Research in engineering and applied sciences, 2, 2455-6300.
- TRUONG, V.-H., PAPAZAFEIROPOULOS, G., PHAM, V.-T. & VU, Q.-V. Effect of multiple longitudinal stiffeners on ultimate strength of steel plate girders. Structures, 2019. Elsevier, 366-382.
- WANG, W.-D., XIAN, W., HOU, C. & SHI, Y.-L. Experimental investigation and FE modelling of the flexural performance of square and rectangular SRCFST members. Structures, 2020. Elsevier, 2411-2425.

Appendix-A-

Analysis of Control Beam

Using the LRFD process to theoretically assess moment ability and shear according to the limitations of the built-up portion of (AISC-LRFD-360, 2016). The cross-section of the chosen beams, as well as their parameters, are defined in Figure (A-1).

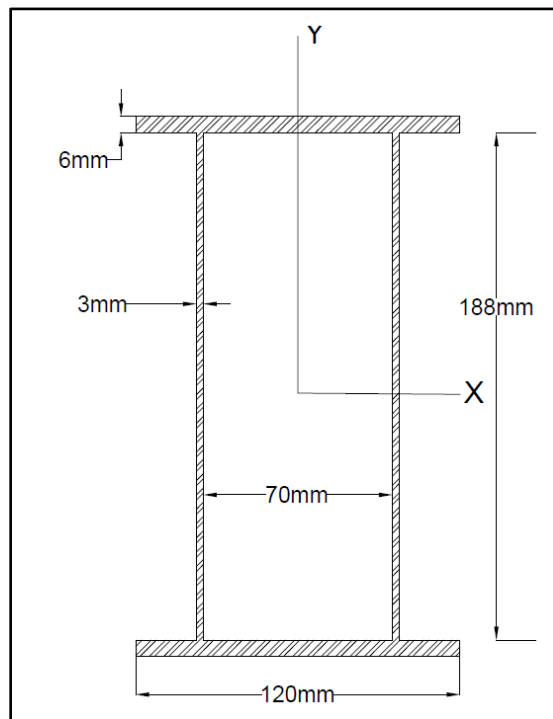


Figure A-1: Typical Cross-Section of The Steel Beam Double Web.

❖ Classification of Shapes

Check Section from AISC Manual Table B4.1

$$E = 190,000 \text{ MPa}$$

$$\text{For Flange } F_y = 279 \text{ Mpa}$$

$$b_f = 23.75 \text{ mm}$$

$$t_f = 6 \text{ mm}$$

$$\lambda_f = \frac{b_f}{t_f} = \frac{23.75}{6} = 3.95 \text{ unit less}$$

$$\lambda_p = 0.38 \sqrt{\frac{E}{f_y}} = 0.38 \sqrt{\frac{190,000}{279}} = 9.91$$

$\lambda_f < \lambda_p \therefore$ Flange is compact.

For web $F_y = 293.6 \text{ Mpa}$

$$h_w = 188 \text{ mm}$$

$$t_w = 2.5 \text{ mm}$$

$$\lambda_w = \frac{h_w}{t_w} = \frac{188}{2.5} = 75.2 \text{ unit less}$$

$$\lambda_{pw} = 3.76 \sqrt{\frac{E}{f_y}} = 3.76 \sqrt{\frac{190,000}{293.6}} = 95.65$$

$\lambda_w < \lambda_{pw} \therefore$ Web is compact

$$I_x = \left(\frac{bh^3}{12} + Ad^2 \right) \text{ flange} + \left(\frac{bh^3}{12} \right) \text{ web}$$

$$I_x = \left[\frac{120 * 6^3}{12} + (6 * 120) * (97)^2 \right] * 2 + \left[\frac{188^3 * 3}{12} \right] * 2$$

$$I_x = 1.68 * 10^7 \text{ mm}^4$$

$$A_g = (6 * 2 * 120) + (188 * 3 * 2) = 2568 \text{ mm}^2$$

$$r_x = \sqrt{\frac{I}{A}} = \sqrt{\frac{1.68 * 10^7}{2568}} \Rightarrow \Rightarrow \Rightarrow r = 80.8 \text{ mm}$$

$$C = 100 \text{ mm}$$

$$\text{Elastic Section Modulus } S = \frac{I}{C} = \frac{1.68 * 10^7}{100}$$

$$S = 1.68 * 10^5 \text{ mm}^3$$

$$F_y = 279 \text{ MPa}$$

$$M_y = F_y * S = 279 * 1.68 * 10^5 = 46.87 \text{ kN.m}$$

$$\text{Centroid } (\bar{y}) = \frac{(6*120*3) + (2*3*120*100)}{(6*120) + (2*3*94)} = 57.75 \text{ mm}$$

$$a = 2\bar{y} = 2 * 57.75 = 115.51 \text{ mm}$$

$$Z = \frac{A}{2} a = \frac{2568}{2} * 115.51 = 148314.84 \text{ mm}^3$$

$$M_p = F_y * Z = 279 * 148314.84 = 41379840.36 \text{ N.mm} = 41.37 \text{ Kn.m}$$

$$M = \frac{p}{2} * 0.367 \approx 0.184 p$$

P form flexure

$$M_n = 0.184 p$$

$$M_n \text{ ext} = M \text{ int}$$

$$41.37 = 0.184 p$$

$$\text{P flexure} = 224.83 \text{ KN}$$

P from Shear

$$V_n = 0.6 f_y A_w C_v$$

$$f_y = 293.6 \text{ MPa}, C_v = 1$$

$$A_w = dtw = 200 * (3 * 2) = 1200 \text{ mm}^2$$

$$k_v = 5 + \frac{5}{\left(\frac{a}{h}\right)^2} = 134$$

$$\frac{h}{tw} = \frac{188}{3} = 62.66$$

$$1.10 \sqrt{k_v \frac{E}{f_y}} = 1.10 \sqrt{134 * \frac{190000}{293.6}} = 323.9 > \frac{h}{tw} \therefore \text{case (2)}$$

$$\Rightarrow C_v = 1$$

$$V_n = 0.6 F_y * A_w * C_v$$

$$V_u = 0.6 * 293.6 * 1000 * 1$$

$$V_{n \text{ int}} = 176.160 \text{ kN}$$

$$V_{n \text{ ext}} = \frac{p}{2}$$

$$V_{n \text{ int}} = V_{n \text{ ext}}$$

$$176.16 = \frac{p}{2}$$

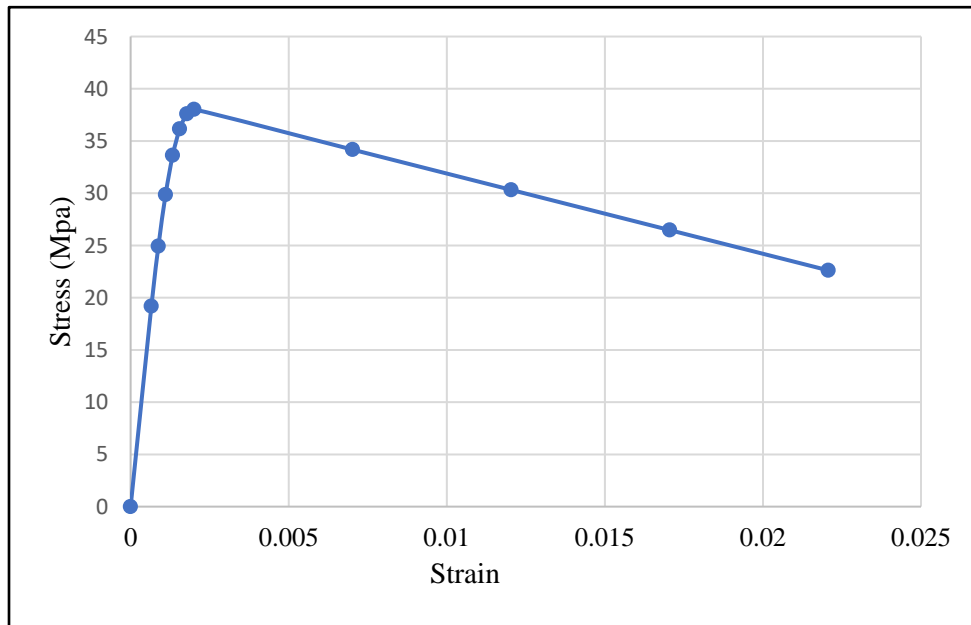
$$\mathbf{P \text{ Shear} = 352.32 \text{ kN}}$$

Appendix-B-

Materials Properties Used in ABAQUS

Table B- 1: Data Stress-Strain Relationship Used in This Research for C38.

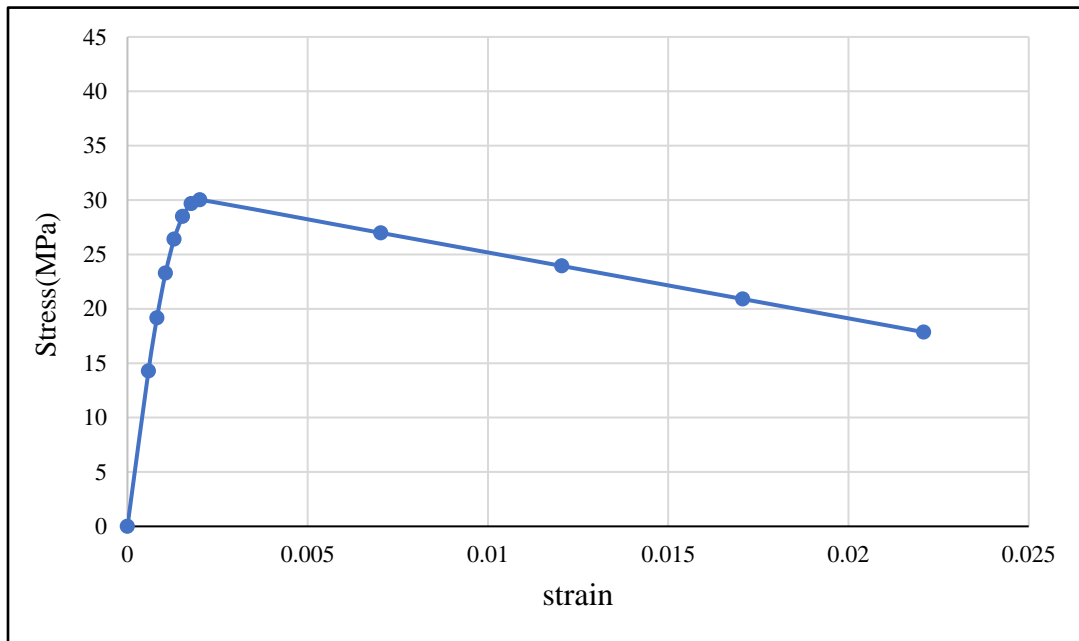
Stress (MPa)	Strain
0	0
19.17592007	0.000655998
24.9312734	0.000878809
29.86118929	0.001105671
33.62445708	0.001331183
36.15999184	0.001553995
37.59364112	0.001780857
38.02420376	0.002006369
34.17227626	0.007022293
30.32034876	0.012038216
26.46842126	0.01705414
22.61649376	0.022070064



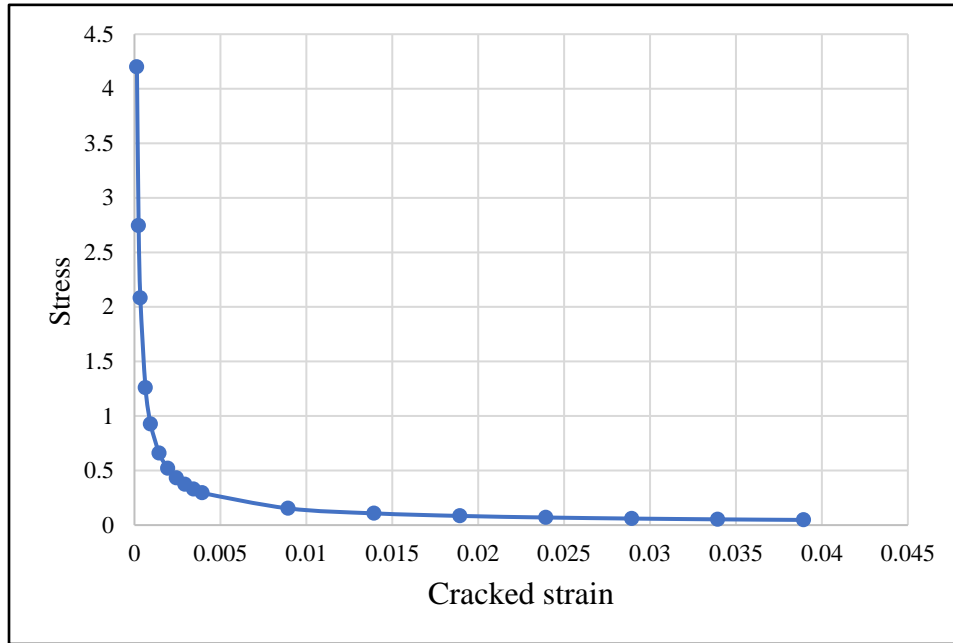
Figuer B-1: Stress Inelastic Strain for Noromal Concrete in Compression Used in This Research.

Table B- 2: Data Stress-Strain Relationship Used in This Research for C30.

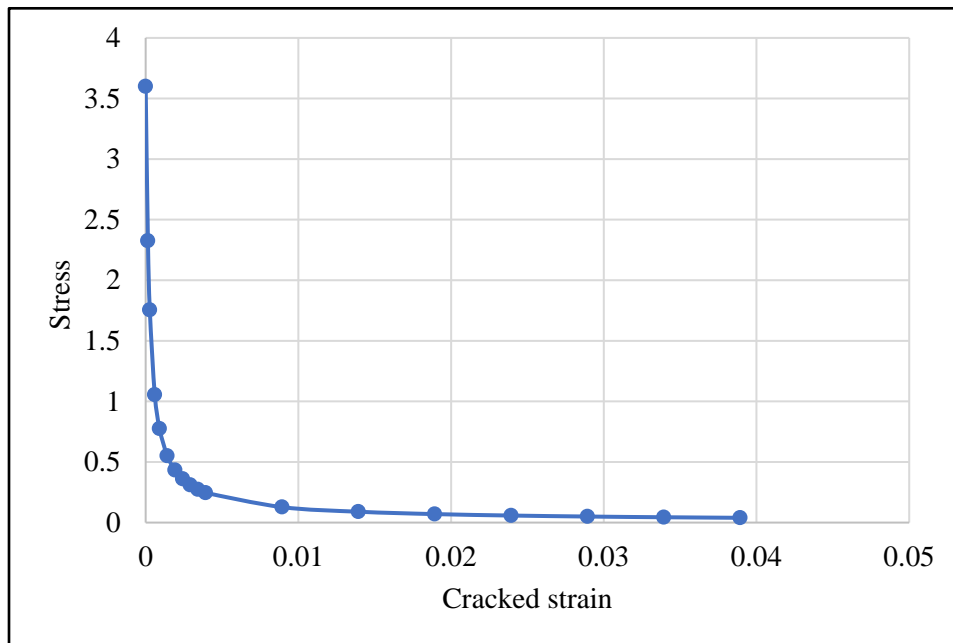
Stress (MPa)	Strain
0	0
14.28248	0.000583
19.1656	0.000818
23.28874	0.001057
26.40611	0.001295
28.49429	0.001531
29.67124	0.00177
30.0242	0.002008
26.98269	0.007028
23.94118	0.012048
20.89967	0.017069
17.85816	0.022089



Figuer B-3: Stress Inelastic Strain for Recycled Concrete in Compression in Used in This Research



Figuer B- 4: Stress Cracking Strain for Noromal Concrete in Tension



Figuer B- 5: Stress Cracking Strain for Recycled Concrete in Tension

الملخص

يهدف هذا البحث إلى التحقق من السلوك الإنشائي لعينة الوتر المزوج المملوء بالخرسانة المختلفة المصنوعة من الركام الطبيعي (NA) والركام الخرساني المعاد تدويره (RCA). يتم تحقيق الهدف من خلال تنفيذ العمل المختبري والعددي.

يتضمن العمل المختبري تهيئة سبع نماذج تم اختبارها تحت حملين مركزيين ومتناظرين بالخصائص (منها طول العتب ، المقطع العرضي ، ظروف الاسناد). كان سمك وعرض صفائح الشفة لاعتاب الفولاذ 120 ملم و 6 ملم على التوالي ، بينما كان سمك ألواح الويب 3 ملم. كل عينات العتب لديها 1100 مم بين الاسناد. يتم تصنيف الاعتاب إلى مجموعتين ، بالإضافة إلى عتب واحد بدون خرسانة كنموذج مرجعي. اشتملت المجموعة الأولى على ثلاث اعتاب مملوءة بالخرسانة العادية ، بينما احتوت المجموعة الثانية على ثلاثة اعتاب مملوءة بالخرسانة المعاد تدويرها. كانت المتغيرات المدروسة هي نوع ومواقع الخرسانة في عتب مزدوج من الوتر.

أظهرت النتائج المختبرية للمجموعة الأولى من الاعتاب أن الخرسانة العادية المملوءة في منطقة الويب تسبب في زيادة الحمل النهائي بنسبة (10.19% إلى 55.30%). علاوة على ذلك ، كانت الزيادة القصوى في مؤشر ليونة النموذج (المملوء كلياً بالخرسانة الاعتيادية) حوالي 568% وزيادة صلابة من (2.6% إلى 39%) إذا ما قورنت بشعاع المرجعي. بينما اظهرت المجموعة الثانية من الاعتاب التي ملأت خرسانة المعاد تدويرها في منطقة الويب في زيادة الحمل النهائي بنسبة (9.52% إلى 42.03%) بالإضافة إلى الزيادة القصوى في مؤشر ليونة النموذج (المملوء كلياً بالخرسانة المعاد تدويرها) زادت بنسبة (380%) وزادت في صلابتها من (4.5 إلى 8.03%) بالمقارنة مع شعاع المرجعي.

تضمن العمل العددي استخدام نموذج غير خطي لتحليل العناصر المحدودة بواسطة حزمة برامج ABAQUS (2021) لإجراء التحقيق العددي لوترة مزدوجة مملوءة بأنواع مختلفة من الخرسانة العادية والمعاد تدويرها ، وكان هناك تقارب جيد بين النتائج التجريبية والرقمية فيما يتعلق بالحمل النهائي ، وأقصى انحراف ، ومنحنيات انحراف الحمل ، ووضع الفشل. وجد أن متوسط الفرق في الحمل النهائي والحد الأقصى للانحراف يساوي 5.50% و 7.90% على التوالي ، مما يضمن صلاحية العمل العددي. كما تم فحص دراستين بارامتريتين لمتغيرات مختلفة عددياً (تأثير مقاومة الانضغاط للخرسانة وإجهاد الخضوع الفولاذ). كانت نتيجة الدراسات البارامترية زيادة إجهاد الخضوع لنموذج التحكم 310 ميغا باسكال و 350 ميغا باسكال ، وكانت الزيادة 5.5% و 11.11% على التوالي ، وكانت زيادة مقاومة الانضغاط للعارضة المملوءة بالخرسانة العادية في الجوانب 25 ميغا باسكال و 20 ميغا باسكال ، كانت الزيادة 10.33% و 4.21% على التوالي ، إذا ما قورنت بالنموذج التحكم.



جمهورية العراق

وزارة التعليم العالي و البحث العلمي

جامعة كربلاء

كلية الهندسة

قسم الهندسة المدنية

تصرف الاعتاب الفولاذية مزدوجة الوترة والمملوءة بالخرسانة

رسالة مقدمة الى مجلس كلية الهندسة/ جامعة كربلاء وهي جزء من متطلبات نيل درجة الماجستير

في علوم الهندسة المدنية

عباس جلال كعيشيش

بكالوريوس في الهندسة المدنية - 2019

بأشراف

أ.د سجاد عامر حمزة

أ.م.د بهاء حسين محمد

شباط , 2023 م

رجب , 1444 هـ